Master Thesis, Department of Geosciences

Feasibility Study on Release Rate of Phosphorous and Trace Elements from Basaltic Glass by Using Batch Reaction Experiments

Abdul Samad Khan

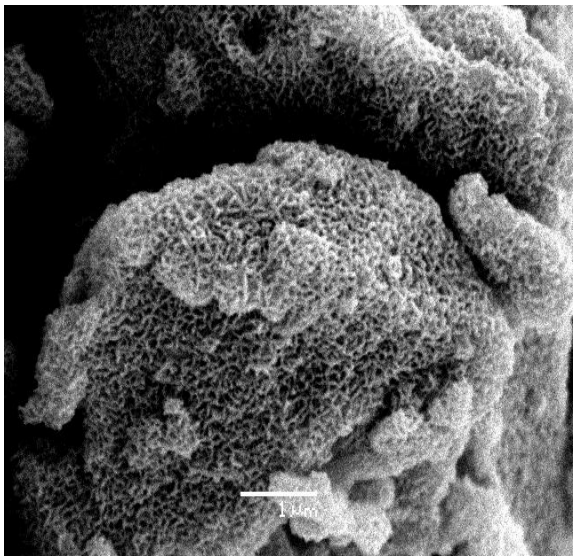

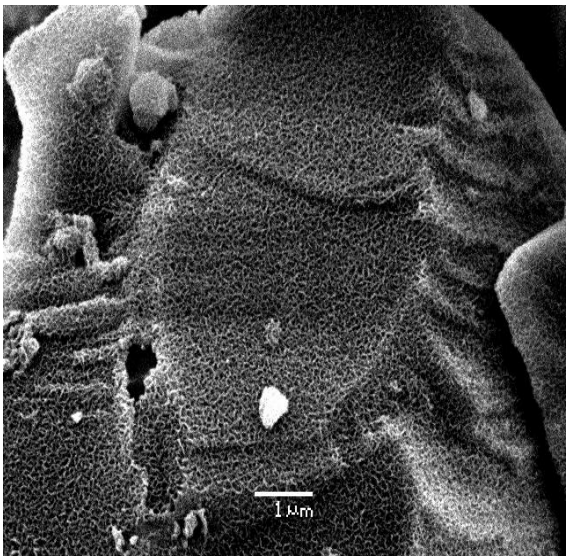

UNIVERSITY OF OSLO

FACULTY OF MATHEMATICS AND NATURAL SCIENCES

Feasibility Study on Release Rate of Phosphorous and Trace Elements from Basaltic Glass by Using Batch Reaction Experiments

Abdul Samad Khan

Master Thesis in Geosciences

Discipline: Environmental Geology and Geohazards

Department of Geosciences

Faculty of Mathematics and Natural Sciences

University of Oslo

June 03, 2013

Dedication

This work is dedicated to my beloved parents.

Acknowledgements

I would like to thank all who has helped me throughout this study. I am forever grateful! First of all would like to thank my advisors Dr. Helge Hellevang for giving me opportunity and for his support, fruitful advice and contributions. Thank you to my senior Beyene Gilma Haile in Oslo for his help and the countless discussion on both academic and non-academic subjects. I would also like to thanks the following persons: the technical staff at the department of Geosciences, University of Oslo; Mufak Naoroz, a person who did a great job in the lab analysis; Berit L. Berg for assisting with the SEM analysis and Maatern Aerts for the XRD analysis. And I especially thankful to my numerous friends who did helped me along this whole study. I am everlastingly grateful to my parents and brother for their support throughout my studies.

Abstract

The production of world phosphate rock might reach to its peak before mid-century due to the potential demand for phosphate fertilizer consumption especially in developing countries, and as a result this could eventually lead to depletion of well-known easily exploitable reserves worldwide during the following decades. The slow natural-mineral fertilizer may be one possible strategy to meet the future possible lack of cheap and high-P sources. For this I investigated to what extant basaltic glass has enough capability to provide sufficient amount of nutrients, especially phosphate, for the food production in future. This was done by performing batch reaction rate experiments and MATLAB simulations. In this study the effect of grain size and temperature on basaltic glass dissolution has been studied using batch reaction (closed system) at 50^{o}C and 90^{o}C. The result shows that dissolution rate of basalt glass increases with the decreasing grains size and also by increase of temperature. The effective size of gains for dissolution rate were identified by using an ideal condition reaction (i.e. Matlab simulations), where found that very fine particles fraction (i.e. <1.5 µm diameter) are dissolving efficiently at 10^{o}C throughout year and can last for several years. The high-temperature experiments showed that phosphate was effectively removed from the solution, probably by sorption to secondary clays, oxides, and/or hydroxides formed during the experiment. A clay phase, probably smectite, is forming on the grains surface at 90 ^{o}C. The release rates of nutrients at 10 ^{o}C, suggest that the amount of phosphate required as a fertilizer is more than 400-500 Kg/ha/year, whereas if basalt is also used as a nitrate source, the amount of basalt required for these elements are 930 and 1852 Kg/ha/year respectively. Continuous supply of phosphate and nitrate can be ensured by taking some necessary actions like proper use of grain size fraction (e.g., finer grains) and pretreatment of basalt etc., to reduce sorption in the soils.

Table of Contents

List of Figures

List of Tables

1.0 Introduction

Fertilizers are as an important agriculture input next only to water, which contributes to increasing agricultural yield (Isherwood, 1998). Fertilizers are food for plants which replace the nutrients that crops remove from the soil. Without the addition of adequate fertilizers, crop yields may significantly be reduced. For the growth and development, plants need a supply of carbon, hydrogen and oxygen which they get from the air and water, and thirteen essential element elements (nutrients) also, which they normally acquire from the soils. Generally the plants take up nutrients in the form of ions, except boron, which is taken up from soil mainly in the boric acid (H_3BO_3) form rather than as a charged ion. Nitrogen is normally taken up as nitrate (NO_3^-) and ammonium (NH_4^+) and, potassium as potassium ions (K^+) and phosphorus mainly as phosphates (such as $H_2PO_4^-$ and HPO_4^{2-}) (Yara, 2009). According to Isherwood (1998), the crop takes up the main fertilizer nutrients in following proportion, nitrogen 50-70%, phosphate 15% and potassium 50-60% during the season of application.

Phosphorous is among the three macronutrients (i.e. phosphate, nitrate and potassium) that crops require in large quantity in order to grow and produce well. Phosphorous fertilizer and its products can either be used as raw or processed and are the key input for agriculture around the worldwide to improve agricultural yield to ensure food security. The phosphate rock is considered as the key source for phosphorus, and the main raw material from which phosphorus fertilizer products are obtained. Therefore, it is necessary to distinguish between phosphate rock and phosphorus as: the phosphate rock is a non-renewable resource and it has taken millions of years for the rock to be formed through different geological cycles and events. The phosphorus, conversely, is a renewable resource that can be reused within economically and technical limits (IFA, 2009).

Phosphorus can be available in the form of different phosphate elements naturally; so phosphorus is commonly referred to as phosphate. Phosphorus has a significant role in the major photosynthetic and metabolic processes and it is a vital nutrient for all the Earth's living organisms. Due to rapid population growth in the world, the demand for crop production and animal derived food has increased in the last decades (Ma et al, 2010). Modern agriculture practice depends greatly on phosphate addition to animal feed and the use of phosphate fertilizers for agricultural production, considers phosphorus an important component of the global food

market. However, the production of biofuels also heavily depends on phosphate fertilizer application and this currently leads to an additional in increasing trend for global demand in phosphate (Enk et al., 2011).

The basic purpose of the agriculture practice is to feed the world and it has been tried to estimate that approximately half of the world population (about 48%) is currently fed by artificial nitrogen fertilizer (Trenkel, 1997). In some parts of the world where food is in abundance but still millions of people are suffering from poor nutrition. However, in few parts of the world, the poor people also have insufficient access to energy from food to meet their basic energy requirements. Generally, in these localities, the shortage of food is often related to seasonal phenomenon and micronutrients are also generally lacking in the diet (Hawkes, & Ruel, 2007). According to current projected population growth and improving incomes, it is estimated that the demand for agriculture by 2050 will range from 50% to 80% more than today's level of production. The reduction in agricultural production intensity at any location can be compensated by additional production somewhere else; however, it is very important to optimize the current agricultural yield per unit of land to meet the future demand. It has been observed that good agricultural practices are not only helpful in increasing productivity but also moderating agricultural greenhouse gases (GHG) emissions, also having further sustainable development benefits like the greater food security, poverty alleviation, moisture retention in soils and soil conservation (Isherwood, 1998).

The element fertilizers are materials which are either naturally present or manufactured, having nutrients essential for the growth and development of plants. Some of these plant nutrients which are used directly for human food and others to feed animals, supply natural fibers or produce timber. There are basically three main plant nutrients such as phosphorus; nitrogen and potassium, which have to be applied in large quantities. The other nutrients like sulphur, calcium and magnesium are also required in substantial amounts. All these nutrients are important and are constituents of many plant components like proteins, nucleic acids and chlorophyll, and are also necessary for particular processes like energy transfer, maintenance of internal pressure and enzyme action. There are also seven other trace elements which are required in small or trace amounts, that are referred as "micronutrients" or "trace elements". However, these elements have number of essential functions in plant metabolism. The deficiency of any one nutrient can affect the development process of the plant (Isherwood, 1998).

Large number of studies on the effect of fertilizers on soils has been conducted during the last century. Basically, the research has focused on exchangeable cations and also soluble phosphorus. Therefore, there are only limited studies that have concentrated at the total storage in the soil and release of cations through weathering or the transfer between different pools of phosphorus. However, potassium and phosphorus has remained as a greatest interest in research area because of their high fertilizer demand in agricultural production (Guðmundsson, et al., 2005). Phosphorus is occurs in sedimentary rocks, generally in three main forms such as calcium phosphate elements (including carbonate fluorapatite), organic matter, and bound to iron elements. Therefore, after digenesis, much of the phosphorus is changed to carbonate fuorapatite. Phosphorus is also incorporated in igneous rocks especially in fuorapatite. The weathering of sedimentary and igneous calcium phosphates (i.e. apatites) is the largest phosphorus source and its release rate is dominantly influenced by plant activities, temperature and acidity. The phosphates rocks are alkaline and dissolve more readily in acidic environments and waterlogged soils (Lenton, 2001).

Phosphates are a naturally occurring resource deposited around the world with limited amounts. Phosphates which are among the primary nutrients for plants, thus the source of the element phosphorus are an essential nutrient for crop growth. However, phosphate rock reserves are rapidly dwindling and hence, the conversion of phosphate rock to water-soluble phosphorus fertilizer is considered as an expensive and inefficient process (Isherwood, 1998). The property of volcanic soil to retain the phosphorous is very high; it is because of presence of high content of Al and Fe compounds. Thus it makes them highly preferable for the agriculture practices as it reduces the need for further addition of fertilizer. This ultimately leads to better yields with dramatically lower cost of production of agricultural products as well. Volcanic soils have pHs range from 5 to 7, so this has a significant implication with respect to the ability to fix elements. Therefore, fluorine sorption is maximum at pH 6. Thus, volcanic soils show high concentration of fluorine sometime, which is toxic to animals and humans (Lebon, 2009). Phosphorus can be extracted from continental rocks and converted to biologically available forms, so plants stimulate terrestrial and marine productivity and thus, organic carbon burial. It is suggested that without plants, the weathering of phosphorus would be incomplete and the flux of biologically available phosphorus to the land and ocean would be suppressed (Lenton, 2001).

Environmental impacts such as eutrophication of aquatic ecosystems and acidify cation which are mostly connected to poorly managed fertilizer use can be prevented or reduced by adopting good agricultural practices. According to the Fourth Assessment Report of the Intergovernmental Panel on Climate Change (IPCC), it is estimated that direct agricultural emissions comprises 10-12% of total anthropogenic GHG emissions in 2005 (i.e. 5.1-6.2 Pg CO_2-eq). GHG emissions associated with tropical countries deforestation, supplied an additional 5.9 Pg CO_2-eq per year (having an uncertainty range of ±2.9 Pg CO_2-eq), which are equal or exceeding emissions compare to all other combined agricultural sources. However, to avoid further deforestation, improved agriculture yields are particularly very important and thus fertilizers practices can play a vital to increase production on current agricultural land. The current level of agricultural GHG emissions will continue to get higher for the foreseeable future as the agricultural production practice expands to keep pace with growing food, feed, fiber and bio-energy requirement (Trenkel, 1997).

1.1 Aim of the Study

This study aims to investigate to what extent basaltic glass has sufficient capability to provide sufficient amount of elements, especially phosphate, for the food production in future. This is done by performing batch reaction laboratory experiments. Also to see the necessary conditions required for release rate of elements. An introduction to and a discussion on factors controlling the bioavailability of the released phosphate, and on challenges of eutrophication with surplus phosphate releases to lakes and oceans, is not included here as this was outside the scope of the thesis. The main objective of the thesis:

1. To determine, what are dissolution rates of phosphate and other trace nutrients are released into the aqueous solution from the basalt glass necessary for plant growth and fluoride which is considered as poisonous?
2. To determine, can basalt glass combat with future problem by supplying sufficient amount of natural phosphate and trace nutrients for agricultural production than chemical fertilizers?
3. To determine, what secondary phases are formed from dissolution of basaltic glass?
4. To identity, which factors can affect the release rate of elements (nutrients) from basaltic glass in natural environment?

1.2 Theoretical Framework

1.2.1 Phosphate Fertilizer

Those soils having sufficient phosphate (P) and potassium (K) reserves frequently give larger production than the soils without these reserves. The access amounts can pose serious environmental impacts, and from that soil, can be lost by numerous ways like by wind or water erosion to streams, rivers and lakes takes its nutrient load with it (Johnston, 1997). Further in-depth study is required to define critical levels in soil under different conditions. Phosphate has considerably both direct and indirect effects, as the enlarged availability of phosphate has a positive effect in the form of yield and quality of agricultural outputs. So from indirect effects, phosphate increases the response of agricultural production to the other inputs like nitrogen and potassium has positive effects on biological nitrogen fixation, soil organic matter maintenance, water-holding capacity, soil erosion control and other soil physical and chemical properties. Combination of all of these positive effects result in improved agricultural output, land conservation and sustained productivity (Isherwood, 1998).

Phosphorus has fundamental impacts on the plants in the form of root development, the ripening process, to establish early in the season and predominantly in the manufacture and use of sugars and complex carbohydrates etc. A substantial amount of phosphorus supply is important in the early stages of a plant's life and for early maturity. Phosphorus is very scarcely soluble in the soil water. This means that very limited amount dissolved in the soil water at any one time and small amount can be available to the plant. Due to low solubility, very little amount of phosphorus is leached from the soil and hence movement is restricted. Those phosphorus residues left in the soils which are gradually converted into unavailable forms by combination with other elements. However, a little of this stored phosphorus will be available to plants in future. Very limited amount of available phosphorus in soil is usually identified by dull, bluish green leaves with purple or bronze tinting, but may also be pointed out by reduced growth. The development of root system is greatly affected; maturity and ripening could also be delayed. Deficiency of phosphorous is usually more distinct in highly acidic soils like peat or sands or alkaline soils such as chalk (Yara, 2009).

So, phosphate is important for good agricultural production which plays a key role in the global food security and bio-fuels production. Therefore, there are no alternatives for phosphate in

agricultural production. The considerable fraction of annual phosphate consumption is dispersed into the environment where it is largely lost to agriculture. Phosphate is an irreplaceable and to an extent non-renewable resource that is being exploited at an ever increasing rate.

1.2.2 Phosphorus Flow Cycle

Fig. 1.1 represented the global phosphorus flow cycle analysis through the food production and consumption system. It has been estimated that about 80% of the phosphorus is produced from phosphate rock which is particularly used for food production and never actually reaches the food on our forks because it is vanished at all key stages as from mine to field to fork. Therefore, there is a missing data and also considerable uncertainty present on some figures of the flows paths, however, such analysis is important because it nevertheless shows that phosphorus scarcity is due to mismanagement of phosphorus (Cordell et al., 2010). Currently mining five times the quantity of phosphorous than actually the humans are consuming in their food. It can be deduced from the analysis that to continuously address the phosphate scarcity and water pollution issue due to phosphorous leakage (Cordell et al., 2009). Therefore, an integrated approach must be adopted as:

- To reduce phosphorous leakages from the farm land and the estimated losses are around 8 MT P.
- To minimize the leakage from food commodity chains and the estimated losses are around 2 MT P.
- To adopt the alternative renewable phosphorous fertilizers sources such as manure (around 15 MT P), human excreta (3 MT P) and also food residues (1.2 MT P).
- To consider also the other valuable routes to minimize phosphorous overall demand like to optimize soil carbon to improve phosphate availability.

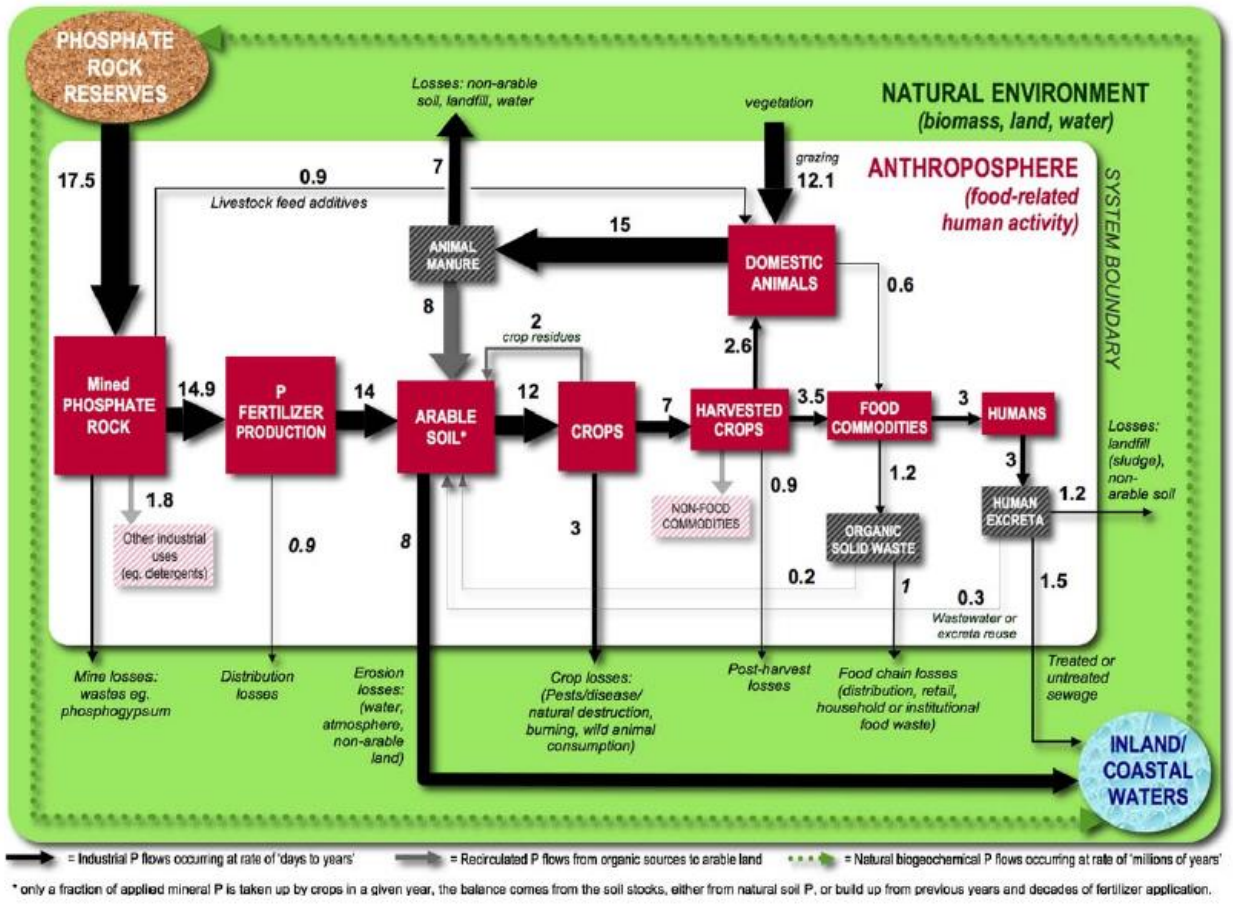

Figure 1.1: Key phosphorus flows through the global food production and consumption system, indicating phosphorus usage, losses and recovery at each key stage of the process. Units are in million tonnes phosphorous per year (Only significant flows are shown here, relevant to modern food production and consumption systems.). So the phosphorous in the natural system cycles at rates of 'millions of year' and flows in human food system cycle orders of magnitude faster at 'days to years'. (Source: Cordell, 2009 & 2010).

1.2.3 Availability of Phosphorous to Plants

Deficiency of phosphorus in plants can rigorously reduce crop development and its yield. However, phosphorus is greatly abundant in environment; alternatively it is one of the least biologically available nutrients for the plants. It is converted to such types of forms where it exists enough in the biosphere but often not available for plants. Therefore, plants can only uptake the soluble inorganic form of phosphorus such as orthophosphates, dissolved in soil solution (Fig. 1.2). Bacteria also play an important role in such a way that it decomposes and

elementizes dead plant matter in the soil, converts to available form of inorganic phosphorus. When phosphorus reacts and adsorbs to other compounds present in the soil environment like aluminum, iron or calcium compounds and organic matter, becomes imobilize (Johnston, 2000). So the strength of adsorbed bonds of phosphorus is highly dependent on the soil acidity and particle size. Hence, the natural bio-availability of phosphorus to plants is highly dependent on geo-chemistry (FAO, 2008).

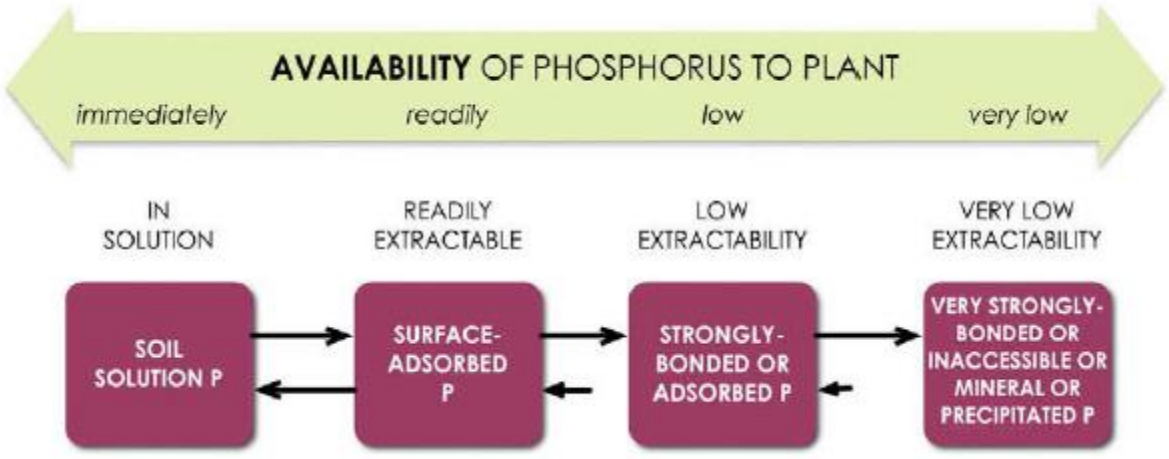

Figure 1.2: Availability of phosphorous to plants can be in different four phases like immediately available to plants for uptake when it is in soil solution, on the other end of spectrum; availability is quite low when phosphorous is very firmly bonded, inaccessible, element or precipitated in the soil. (Source: FAO, 2008).

1.2.4 Rocks for Phosphate Production

Almost all types of phosphate currently consumed are extracted from geological formations (Fig. 1.3) which contain higher concentration of phosphorus. To become a reasonable phosphate ore, the formations should contain minimum concentration of phosphorus that ensures its mining is economically feasible to extract. If we see historical record, this concentration was in range from 25 to 35 wt% of P_2O_5, however, the actual exploitation of the ore depends on following factors like ease of mining practices, extractability of the phosphate component and also the location of the ore deposits. Therefore, commercial product from phosphate mines is referred to a phosphate rock (Enk et al, 2011). In the past, phosphorus was reused to agricultural soils through the application of animal manure and human excreta. Afterward, this local organic matter was replaced by phosphate mined in distant places during the mid-nineteenth century, especially in

the form of guano, bird droppings deposited over thousands of years, but given much more importance to mined rock rich in phosphate (Cordell, 2010).

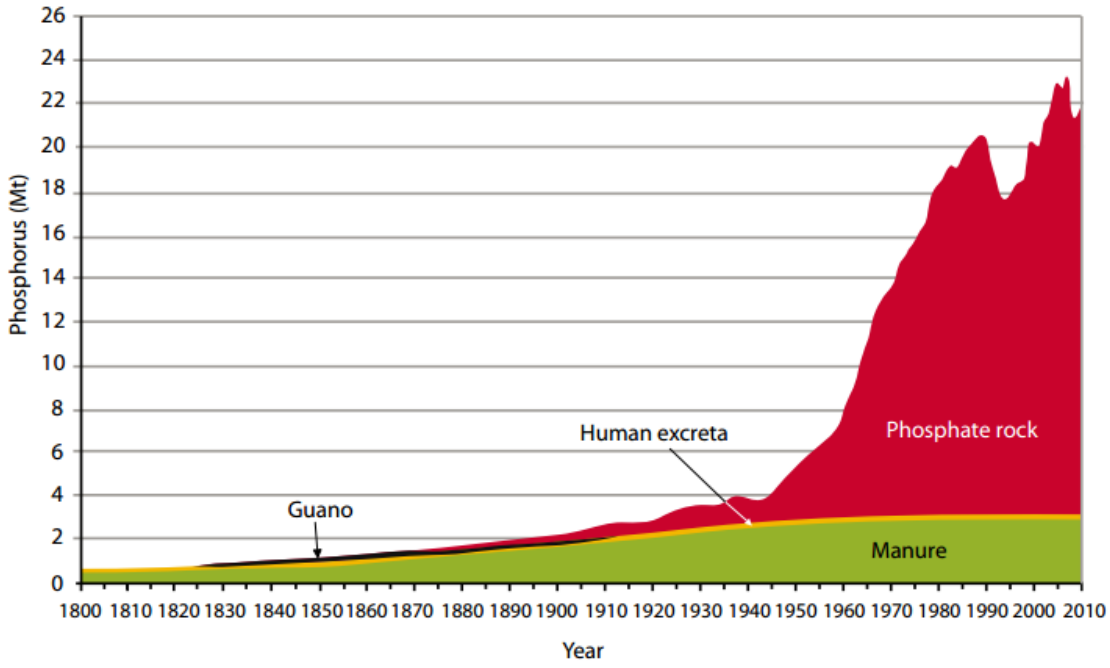

Figure 1.3: Historical global sources of phosphorous fertilizers (1800-2000) are including manure, human excreta, guano and phosphate rock. Since the mid of 1940 population growth accompanied by greater food demand lead to rapidly increase in the use of mined phosphate rock as compared to other sources of phosphorous (Source: Cordell, 2009).

1.2.5 Classification and Composition of Phosphate Ore

According to Enk et al, (2011), on the basis of genetic origin, the phosphate deposits are generally grouped in the following three categories as: sedimentary, magmatic and guano type deposits. The sedimentary and magmatic type deposits are widely spread throughout the worldwide, guano-type deposits are occurring mainly in the Pacific region.

1.2.5.1 Sedimentary Phosphates

Sedimentary phosphate type deposits are generally formed as part of marine sedimentary environments. These are mainly found in ages from the Eocene and Cretaceous; the precipitation process of phosphate elements from cold phosphorus enriched water takes place by flowing across warm and shallow shelf environments or also by mixing with warm ocean currents. The

precipitation of inorganic phosphate elements includes the deposition of the skeletal remains on the ocean floor of the aquatic organisms that are considered as the phosphate rich areas and also the inorganic fragments from the continent such as quartz and clay particles. A special category of sedimentary type of phosphate deposits also includes the weathering of phosphate sedimentary limestone. However, mostly these sedimentary phosphate deposits are present in the US, China and in a belt south and east of the Mediterranean as from Morocco to Jordan (Enk et al, 2011).

1.2.5.2 Igneous Phosphates

The origin of igneous phosphates is from magmatic activity. They are mostly present as apatite enriched deposits and also alkaline intrusive complexes forms. The alkaline deposits are relatively small in amount. The major phosphate containing alkaline complexes can be located in Russia, South Africa and Brazil. Some of the magmatic phosphates are coupled with magnetite iron ore. Those phosphate enriched iron ore deposits located in Kiruna, and Sweden are not directly the result of magmatic activity but they were perhaps originated from the extrusion of hot iron and phosphorus rich fluids on the seabed. However, the igneous phosphate rock is much harder relative to sedimentary deposits and, as a result this factor can make it more expensive to extract in terms of mining and processing. Hence, the resulting product will be of more valuable because of higher quality, as the apatite elements occurs in purer form and makes it easier to separate (Enk et al, 2011).

1.2.5.3 Guano Phosphates

These are those deposits were formed by the accumulation of droppings of the sea bird. From the current composition of guano deposits, mostly calcium phosphate vary considerably it is may be mainly due to leaching by surface water runoff. The major guano deposits occur in Oceania. However, recently guano reserves are decreasing rapidly and do not have ability to play a considerable role in the phosphate market. So, as a result, such type of deposit will not be given further consideration (Enk et al, 2011).

1.2.6 Current Phosphate Reserves

Worldwide reserves of phosphate rock were estimated at 15000 Mt in 2008 and 16000 Mt in 2010 (Fig. 1.4). Around 80% of the phosphate rock reserves consist of sedimentary phosphates and the remaining consists igneous phosphates reserves. The reserves like guano type deposits

are of in negligible amount. Just five countries around the world control about 90% of the world's remaining reserves. Countries like China, Morocco and the US are by far the leading producers of phosphate rock. China and USA consume all or almost all of their own domestic production of phosphate, and Morocco is the only the chief exporter of phosphate rock and its products throughout the world. Morocco currently occupies the Western Sahara and controls its vast phosphate rock reserves. However, Russia, South Africa, Canada, Brazil and Finland are the mainly producers of phosphates and its products from igneous masses (USGS, 2009). According to Kauwenburgh (2010), the world phosphate rock reserves in percent distribution are as follows; 85% in morocco, 6% in China, 3%in US, 2% in Jordan, 1% in Brazil and also 1% in Russia (Fig. 1.5).

The fluctuation took place in the range between 125 and 145 Mt til 2006, afterward the mine production jumped to 167 Mt in 2008. Therefore, over this period of time, phosphate rock reserves also increased from 11000 Mt to 18000 Mt in 2006 and currently decreasing trend seen to 15000 Mt. Recently an increase in phosphate prices observed, it is only because these reserves depend on long term price developments but not mostly on spot prices (USGS, 2009).

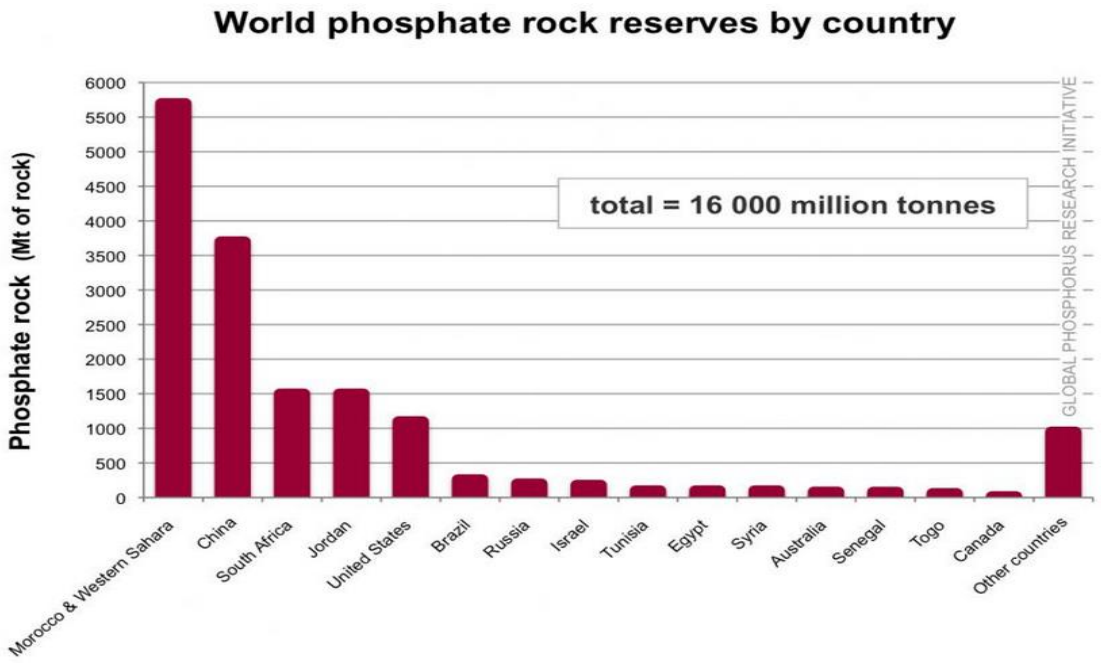

Figure 1.4: Globally occurrence of phosphorous reserves as reported in 2008 & 2010. Reserves are mostly geographically centered only in hands of few countries. (Note: units are in phosphate rock, not in P). (Source: Jasinski, 2009).

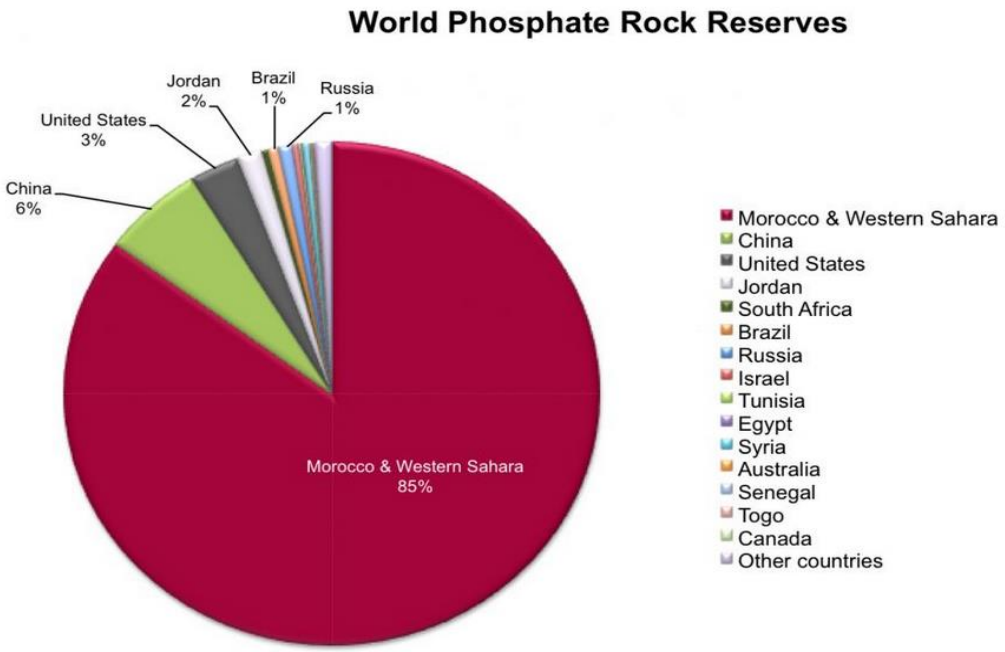

Figure 1.5: World phosphate rock reserves distribution presented in percent. (Source: Kauwenburgh, 2010).

1.2.7 Global Phosphate Consumption

Currently the world population growth rate is around 1.5% per year. The United Nations estimated that the world population will reach about 9 billion in 2050, which is a 50% increase on the current 6 billion (United Nations, 2005). It is expected that the population growth rate will drop around 2050 and then it will remain almost stable or slight increase. It is assuming that food consumption is proportional to the agricultural production which will keep at same pace with population growth; and it is also expected that a similar growth rate trend for global phosphate production and its consumption. According to Heffer, (2008) prediction that, the consumption will grow by 2.7% per year, which shows almost higher growth compared to the world population growth trend. As IFA predicted that the world population will grow at the rate of 1.4%, but the production of phosphate rock will rise at the rate of 4.4% per year. This is all probably due to improved living standards and change in consumption pattern especially in the western communities. So a meat based diet production normally requires three times more phosphate compared to the production of a vegetarian diet (Cordell et al., 2009), and it is also predicted that the phosphate consumption will continue to increase at a substantially higher rate than the population growth if India, China and Brazil continue to develop to American or European food consumption standards in the future.

There is huge difference in per capita phosphate consumption pattern between the developed world (like, US, Australia, Canada and New Zealand) that is > 20 kg P2O5/ capita and the developing countries like Africa that is < 1 kg P2O5/capita. During last 100 years the consumption of phosphate rock has increased by around 3.4%, but, the phosphate prices have remained almost stable. Currently phosphate prices started to increase very rapidly from ~30 US$/ton in 2005 to 113 US$/ton in 2008. It is assuming that in near future these high spot prices will go down (Enk et el., 2011). Currently Inorganic phosphate is used in different kinds of products, and it has been estimated that around 18.9 mln tons of phosphorus (P) entered the world economy in 2004 (Villalba et al., 2008). However, the phosphate rock is used for the production of fertilizers (74%), industrial phosphates e.g. feed additives and detergents (7%), and other uses encompass around 10%. The remainder 9% is lost during the transportation and handling activates (Cordell et al., 2009; Villalba et al., 2008).

1.2.8 Future Trends of Phosphate Consumption and Sufficiency of Resources

By using the various scenarios for global phosphate consumption and also considering the additional effect of increasing bio-fuel production, the sufficiency of the current phosphate reserves is estimated for the future. Therefore, particularly interlink between bio-fuel production and phosphate reserve is difficult to assess here, it is estimated that that the current phosphate reserves will exhaust near future somewhere between 2040 and 2070. The size of the reserve and reserve are based on rock phosphate prices of 20 to 40 US$/ton. At prices of 50 to 100 US$/ton the future reserve base would roughly double and phosphate sufficiency will last well into the next few centuries (Enk et al., 2011).

1.2.9 Concept of Peak Phosphate Theory

Few years back, based on numerous conducted studies, there has been theory that production of world phosphate rock might reach to its peak before mid-century due to the potential demand for phosphate fertilizer consumption especially in developing countries, and as a result this could eventually lead to depletion of well-known reserves worldwide during the following decades (IFA, 2009).

Currently there is much awareness among the people about with the reality of ‘peak oil’, but on the other hand there is less knowledge about rock phosphate which is also a non-renewable

resource and its supply is expected to 'peak' in near future (Fig. 1.6). This peak theory first given by Hubbert (1956) in relation to peak oil, it is not related to when a resource is entirely vanished and problems will soon arise, but when the high quality and highly major accessible reserves have been exhausted. At this point where production reaches to its maximum (its peak) level and after that the quality of the remaining reserves remained lower, thus they are harder to access, which lead to an ever more uneconomical to mine. Ultimately the price will rapidly increase due to decline in supply. According to Cordell et al., (2009) the peak in global phosphorus production could occur by 2033 and afterward the peak supply is expected to decrease over time, as of constrained by economic and energy costs, despite rising demand. And estimated that phosphate rock could approximately 50–100 years remain as of according to current known reserves. The analysis of peak phosphorus theory is based on estimated P in current world phosphate rock reserves which is approximately 2358 MT P based on US Geological Survey data.

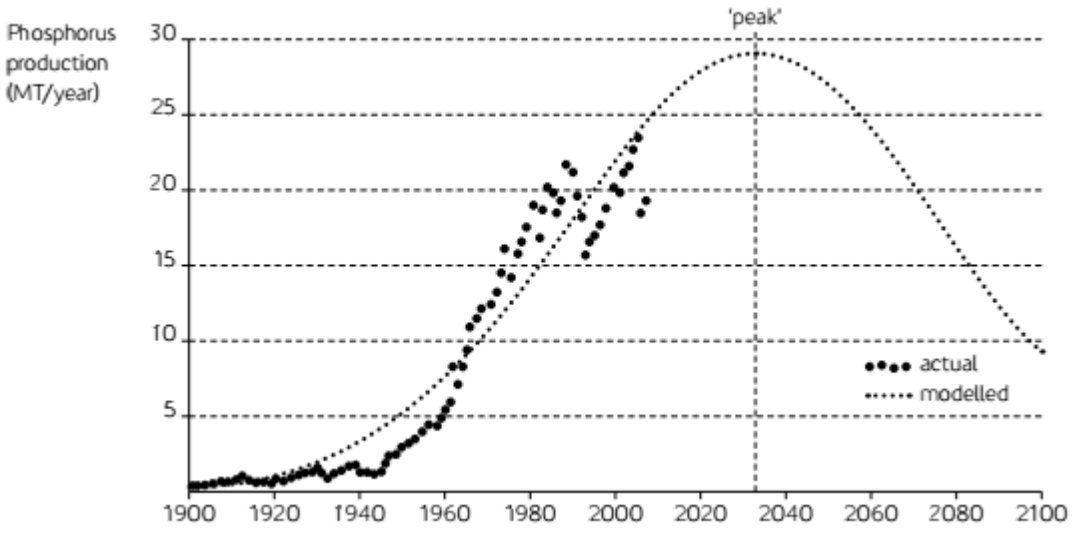

Figure 1.6: Peak phosphorus curve based on industry data, illustrating that, in a similar way to oil, indicating a global phosphorous production are likely to be peak in 2033 after which production will be significantly decreased. (Source: Cordell et al., 2009).

On the other hand many experts do not agree with the "peak phosphate" theory. They think that phosphate rock reserves are dynamic and the level of these reserves is gradually rising upward as with discoveries of more new deposits. However, the modeling of future phosphate rock consumption trend has not been enough to ascertain how quickly these reserves could be

exhausted. So the predictions of "peak phosphorus" theory also ignore important issues like practicality and economic feasibility of phosphorus recycling and its reuse.

International Fertilizer Development Center (IFDC) in 2010 conducted a study and concluded that current global phosphate rock resources appropriate for phosphate based products production as including phosphate fertilizers, however, were far more extensive than earlier predicted. By assuming the current extraction rates, these resources would be accessible for several centuries. Therefore, United States Geological Survey (USGS) in 2011 updated the figure of worldwide phosphate rock reserves from 16 billion tonnes (estimated in 2010) to 65 billion tonnes. Hence, this predicted estimate correlated with the IFDC study about worldwide phosphate rock reserves and it is around 60 billion tones (IFA, 2009).

1.2.10 Controlled Fertilizer

The concept of slow and controlled release fertilizers can be described as, these are those fertilizers which are containing a plant nutrient in a form which are either available by little delay for the plants uptake and use it after application, or these nutrient available for plant appreciably longer than a reference, refers to 'rapidly available nutrient fertilizer' like ammonium nitrate (urea), ammonium phosphate or potassium chloride. *Slow release* fertilizer is a chemical substance release rate in the form of a plant available nutrient, which is certainly lower than normal requirement, however, in general can be described as the release rate from the application of fertilizer to a plant available nutrient. Therefore, the *controlled or slow nutrient release* or availability can be attained by physical and chemical characteristics. The principal procedure for controlled release of fertilizers is one whereby soluble fertilizer materials are generally given a special protective coating (encapsulation) which is water insoluble, semi permeable or impermeable with pores, which controls water penetration and the rate of dissolution, and nutrient release is synchronized to the plants' needs (Trenkel, 1997).

1.2.11 Phosphate Release Rate

Massive quantity, rapid physical and chemical weathering made volcanic glass valuable for the cycling of numerous nutrients and chemical species at the Earth's surface. The soil fertility and the formation of new clay elements can be attained trough chemical weathering of volcanic glasses in soils governs (Wolff-Boenisch et al., 2004). Due to high volcanic activity along

different islands and mountains ranges across the Pacific 'Ring of Fire' which produces enormous glassy material such as ash, pumice, and scoria. Therefore, weathering of this glassy material produces andisols, which is more fertile and supports a dense vegetation cover, including Hawaii, Chile, Indonesia, and South Japan. The rate of weathering is strongly affected by different environmental conditions which include temperature, rainfall and vegetation etc. (Moulton et al., 2000 and Chadwick et al., 2003). It has been estimated that due to rapid cooling of magma on the Earth surface, around one billion cubic meters (1 km^3) of glass per year is produced, which is mainly beside the 70000 km oceanic ridge system (Morgan and Spera, 2001). The basalt composition can vary from 100% glass to 100% crystalline element (Oelkers and Schott, 1995; Schott et al., 2009). Major composition of this glass is of basaltic in nature. However, exposed continental crust surface is made up of about with 12% volcanic glass, being surpassed in abundance only by plagioclase (35%) and quartz (20%) (Nesbitt and Young, 1984).

Form different conducted studies, it has been concluded that the dissolution rates of elements and glasses are to be proportional to their interfacial surface area (e.g. Pačes, 1983; Helgeson et al., 1984; Lasaga, 1984; Siegel and Pfannkuch, 1984; Schott and Oelkers, 1995; Oelkers, 2001; Schott et al., 2009). However, different factors influence solubility for elements and glasses such as their composition, pH, and grain size. In modern agriculture practices, it has become very difficult to effectively formulate the fertilizers, especially in heavily leached laterite soils of the tropics. These types of soils have not enough ability to fix soluble phosphates and also frequently seen the lackness of large number of major and minor nutrients (Kronberg, 1977).

Therefore, it is given consideration currently to the chemically complex glasses for slow release of fertilizers to meet phosphate and also other major and minor nutrients requirements which are often found at their low levels in soils. Phosphate is normally used to soils system either in soluble *(like,* superphosphate) or less soluble *(like,* rock phosphate, basic slag) forms. The factors like soil type, crop type, and climate, etc determine the effectiveness of the applied phosphate material at any location. But it has been studied that, where the considerable concentrations of aluminum and iron oxides are found, there enormous quantities of soluble phosphate fertilizer (of the order of 1 ton ha^{-1}) may be required to satisfy the soil's phosphate fixing capacity (Fyfe et al., 1978).

Natural solutions in soils often contain complex forming ligands, which influence dissolution rates at acid conditions (Ullman and Welch, 2002). The dissolution rate of glass may also be affected by numerous variables including, 1) the aqueous transport of chemical species away from its surface (Murphy et al., 1989); 2) the effect of reverse reaction at near to equilibrium conditions (Grambow, 1985 and Oelkers et al., 1994); and 3) the far-from equilibrium dissolution rate. There have been a large number of researchers intended to characterize the natural glass dissolution rates, but no simple relationship has been found to depict the variation of far from equilibrium natural glass dissolution rates as a function of glass composition at low temperatures, typical of Earth surface environmental conditions (Wolff-Boenisch and Gislason et al., 2004).

It is seen that natural glasses are relatively less stable compared to igneous elements at the Earth's surface. It is only because of glass retains more energy from its parent magma than the elements (Gı´slason and Arno´rsson, 1990). Basalt composes the major part of the oceanic crust. So at neutral to alkaline pH environments, the basaltic glass dissolves significantly faster compared to basaltic elements (Daux and Guy et al., 1997). At regional scales, weathering of basaltic glass supplies dissolved nutrients which are made available to vegetation cover or also it can neutralize catchment areas which were affected by acid rain. However, at global scales, weathering has strong influence on the chemistry of the oceans and also on the regulation of CO_2 concentrations in the atmospheric. (cf. Navarre-Sitchler and Brantley, 2007).

Dissolution rates are generally considered to be proportional to the reactive surface area of grains (cf. Hochella and Banfield, 1995). The dissolution rates are commonly normalized to either the experimentally measured BET specific surface area (A_{BET}) or the theoretically derived geometric specific surface area (A_{geo}). Therefore, A_{BET} specific surface area is significantly greater than the A_{geo}, it is because of the former includes contributions of surface roughness; whereas, the latter is calculated by assuming all grains have smooth geometric shapes. Therefore, those dissolution rates which are normalized to A_{BET} are therefore substantially slower than those normalized to A_{geo} (cf. Wolff-Boenisch and Gislason, et al., 2006).

Generally, the dissolution rates of silicate elements and glasses are estimated from Si release rates. Because Si metal holds altogether the element or glass framework, it provides a good proxy for determining dissolution rates (Oelkers, 2001). Silicon release rates from crystalline

basalt are comparable to release rates from basaltic glass of the same chemical composition at low pH and at temperatures greater or equal to 25^{o} C but slower at alkaline pH environments and temperatures greater or equal to 50^{o} C. However, reverse situation seen for Mg and Fe release rates, as these decrease continuously with increasing pH at all temperature ranges. The basalt glass dissolution can also be improved by an increase in surface area or its better access to under saturated aqueous solutions (Gislason and Hans, 1987). Chemical weathering on land and the ocean floor takes place at temperatures from 0° to 30°C and pH 2 to 11 (Gislason et al., 1992; Chester, 2000). One challenge in quantifying glass or element dissolution rates is that there are two different distinct surface reactions that can tend to lead to rate variation with solution composition such as: 1) the inverse reaction, or the tendency to re-precipitate a solid as equilibrium is approached, and 2) the reaction forming the rate controlling activated or precursor complex. The first of these effects is often quantified in terms of the chemical affinity of the dissolving phase (Aagaard and Helgeson, 1982; Lasaga, 1981; Helgeson et al., 1984; Helgeson and Murphy, 1987; Oelkers, 2001).

1.2.12 Environmental Problems

The basic aim, to use of fertilizers is to properly supply naturally occurring nutrients to plants to a certain levels to attain crop yields economically. Therefore, try to avoid addition of chemicals by fertilizers to the soil that which are not already present in it. Sustainable use of fertilizers has very little or no undesirable effect on environment. Proper supply of nutrients according to requirement of crops, leftover very minute quantity of nutrient unused has later on been lost to the environment by different routes like soil erosion or surface water runoff etc. However, fertilizer related environmental problems can occur by following ways such as; by leaching of nitrate into aquifers or surface waters, the loss of phosphorus enriched soil particles to surface waters that help to develop eutrophication (Hawkes, 2007), which is considered as one of the tremendously negative effects because of intensive use of phosphorus fertilizer (Savci, 2012).

Shortage of agricultural production intensity at any location in the world would need to be compensated by supplementary production somewhere else, for this it is very necessary to maintain agricultural yield per unit of land to easily meet future demand. However, this should be done by using efficient methods that helpful to greatly reduce the environmental impacts such as greenhouse gas (GHG) emissions, eutrophication and acidification processes. Thus, the

efficient and accountable agricultural production, distribution and also use of fertilizers are the key to easily attain these goals (FIA, 2009).

Currently, due to high consumption of fertilizer increased exponentially serious environmental impacts worldwide. As it is already mentioned that the increased concentration of phosphate in drinking water and rivers as a result of the transport of phosphorous fertilizer with surface water runoff. During eutrophication condition in the bottom layer which causes much reduction of free oxygen and water becomes unsuitable for drinking purpose, the reduction in the number of living species in the aquatic environment fish kills, propagates the growth of unwanted species, odor problem and also becomes awful for recreation activities. According recent studies, the effects of chemical fertilizers on the soil are not immediately obvious. It has been noticed that soils have strong buffering power due to components present in it. After period of time, these emerged from the pollution and causing the deterioration of soil fertility, soil degradation reactions processes occurs in the soil which lead to deterioration of the balance of the current element. On the other hand, those toxic substances accumulate within the food chain and causing harmful effects in humans and animals as well are fed (Savci, 2012).

1.2.13 Beneficial Impacts on Environment

Sustainable use of fertilizers not only improves food quality and quantity but also protect the environment in several ways as (Yara, 2009):

- Improved productivity from cropped land avoids the need to destroy further areas of natural forest and grassland.
- Sustained green crop growth essential for maintenance of the atmosphere.
- Reduced losses of soil due to wind or water erosion. Many of eroded soil particles end up in watercourses potentially causing pollution of surface waters. Erosion is reduced by the maintenance of green crop cover with active healthy root system. Improved crop rooting systems which can make better use of both the soils nutrient supply and applied fertilizers. This reduces the risk of nutrients entering ground water.
- Land reclamation and safe disposal of degradable wastes is improved by fertilizers encouraging active crop growth. Increased soil organic matter through incorporation of greater amounts of stubble, straw and stalk residue associated with higher crop yields.

2.0 Analytical Methods

The Scanning Electron Microscopy (SEM), Particle Size Analyzer (PSA) and X-Ray Diffraction Analyzer (XRD) were analytical methods used to characterize solid samples (basalt glass) like, size, shape and composition of particles etc. The brief description of each method and how we analyze samples is presented below.

2.1 Characterization of Solids

2.1.1 Preparation of Samples for Analyses in SEM

The scanning electron microscope (SEM) was used to analyze the crushed basaltic glass powder. The two different basaltic glass crushed powders were separately mounted on black carbons which were attached with cylindrical stubs. Before examination of these two different basalt samples in SEM, the stub with samples were first coated with gold in Quorum (Q150R S – sputter coater) instrument to hold the samples in place on the cylindrical stubs. Afterward, these cylinder stubs were fixed in the sample holder and then attached with the sample stage of the SEM chamber. From stage, these basaltic glass crushed samples were analyzes separately by using secondary electrons.

2.1.1.1 Scanning Electron Microscopy (SEM)

The Scanning Electron Microscopy (SEM) (Fig. 2.1) is a microscope that uses electrons instead of light that generate different types of signals at the surface of solid specimens and as a result forms an image of material. Due to electron-sample interactions, signals derive information regarding the sample which includes: texture (external morphology), chemical composition, and crystalline structure and orientation of materials form the sample, allows examining a much different variety of samples (Swapp, 2012). Due to its wider application, the SEM allows more of a sample to be in focus at one time. Because of its much higher resolution capacity, closely spaced specimens can be greatly magnified. So the SEM only uses electromagnets instead of lenses, so more control in the degree of magnification can be achieved (Schweitzer, 2010).

The higher amount of kinetic energy is carried out by the accelerated electrons in SEM as a result an electron-sample interactions and this energy is dispelled into range of signals. However, these variety of signals consists of number of energy forms such as: secondary electrons that

produce images (which shows morphology and topography on samples), backscattered electrons (BSE) that are most important for illustrating contrasts in composition in multiphase samples, diffracted backscattered electrons (EBSD) that are helpful to determine crystal structures and orientations of elements, photons which are the characteristic X-rays which are applicable for elemental analysis and continuum X-rays, visible light, and also heat (Swapp, 2012).

Therefore, the main principle of the equipment is the X-ray produced by inelastic collisions between the incident electrons and electrons in discrete orbitals of atoms in the sample. As when the excited electrons return to its lower energy levels, they produce X-rays that are of a fixed wavelength. Hence, the certain characteristic X-rays are generated for individual element in a element that is "excited" by the beam of electrons (Swapp, 2012).

Figure 2.1: A typical representation of SEM instrument, showing the electron column, sample chamber, EDS detector, electronics console, and visual display monitors (adopted from Swapp, 2012).

The sputter coating is used (Fig. 2.2) in the SEM which provides an eclectically conductive thin coated layer/film representative of the surface topography of the sample to be analyzed

efficiently. Such thin film having characterized feature like inhibit charging, reduces thermal damage and also enhances secondary electron emission. Q150R S employs a magnetic sputter target assembly which make the process efficient by using low voltages and giving fine grain size such as in ~ nm grain size (QUORUM, 2013).

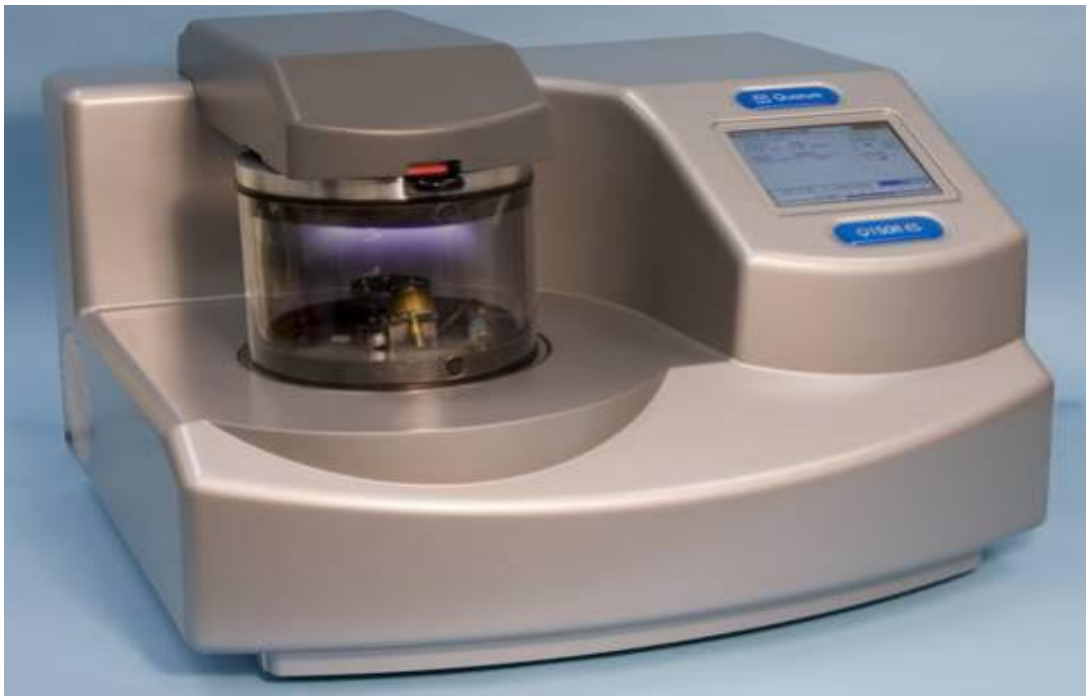

Figure 2.2: View of Quorum Sputter Coater (Q150R S/E/ES) a Sample Preparation Instrument (adopted from QUORUM, 2013).

2.1.2 Preparation of Initial Material

The 100g of basaltic glass was crushed into fine grain powder mechanically with the help of micronizer and done by manually through mortar and agate as well. When basalt glass was crushed with mortar agate, the equipment was placed in the fume hood to avoid the exposure of acetone vapors, which was used to keep the small hard grains of basalt glass inside the mortar during crushing process. While crushing the basaltic glass in micronizer, we added ethanol (about 7ml). The hard rounded rubber pellets were arranged in a small container with the help of special frame then fixed it in the micronizer and finally micronizer was run for 10 mints to fine crush the basaltic glass. At the end both crushed samples were kept in the oven for drying at

60^{o}C. The dried basaltic glass powder was separately collected in small plastic containers for further analysis.

2.1.3 Preparation of Sample for Particle Size Analyses (PSA)

We added a very small amount of sample (around 0.6g) and a chemical such as sodium metaphosphate $(NaO_3P)_n$, also known as calgon in beaker and stir few minutes on the ultrasonic bath to properly mix the sample. The main aim of the sodium metaphosphate is to separate each grain of the sample to make ease for the instrument to count each particle size distribution. Before running the sample in the Beckman Coulter, instrument was adjusted according to the background; because micro bubbles can be present in the water-sample running tube can generate wrong results. After adjusting the background, sample reading started from zero on the grain size distribution plot. On the each run of sample x-rays hits the particles and some of the rays reflected and some were diffracted which were counted in the form of grains size distribution by the detectors installed in the chamber. The principle is that, instruments consider that all grains are in spherical shape to make it easy to measure the average size distribution of grains in the sample. By running different samples, instrument flushed each time with water to remove any kind of material present in the sample carrying tube and also from the chamber.

2.1.3.1 Particle Size Analyses (PSA)

Operation of the Beckman Coulter **(**LS 13 320) is a Laser Diffraction Particle Size Analyzer. This instrument, if efficiently used for the analysis of natural sediment samples. Where the aqueous liquid module (ALM) used in the instrument has capability of suspending samples in the size range of 0.04 µm to 2000 µm. however, the Polarization Intensity Differential Scattering (PIDS) provides the prime size information for grains size in the range of 0.04 µm to 0.4 µm. The PIDS assembly also has capacity to enhance the resolution of the particle size distributions till 0.8 µm. So such kind of additional measurement is very important as it becomes very difficult to distinguish particles of different sizes by diffraction patterns alone when especially the particles are smaller than 0.4 µm in diameter (OEWRI, 2008).

Therefore, before analysis, samples are treated with hydrogen peroxide and acetic acid to remove organic matter. The addition of sodium-hexametaphosphate improves separation of grains and

dispersion of aggregates before sonification process. After pretreatment of samples are then loaded into the Auto-Prep Station (APS) (OEWRI, 2008).

Hence, APS sonicates each sample and then adds the sample to the ALM bath by flushing the sample tube with water. Therefore, ALM contains filtered tap water which suspends the sample where ALM sonicates the sample and uses a circulating pump to disperse it in the tap water. Circulating water in this analysis is pumped from a holding tank that contains heaters which keep the water at a constant temperature. The sample is recirculated in a closed-loop system while it is delivered to the sample cell in the optical bench (OEWRI, 2008).

A typically optical system comprises of a source of illumination, where a sample in sample chamber interacts with the illuminating beam where a Fourier lens system targets the scattered light, and an array of 126 photo-detectors that records the scattered light intensity patterns. The diffraction scattering patterns size ranges from 0.4 µm to 2000 µm, are measured by 119 out of 126 photo-detectors. The remaining seven detectors are associated with the PIDS assembly and measure particle size range from 0.4 µm to 0.4 µm (OEWRI, 2008).

2.1.4 Preparation of Sample for X-Ray Diffraction (XRD) Analyses

The Bruker D8 Advance XRD instrument was used for the identification of unknown phases of elements within short period of time from the basaltic glass sample powder. The basaltic glass was crushed to quite fine powder with micronizer. Specimen was prepared from the sample powder by loading into sample holder. Afterward the match analysis was performed using the Bruker Diffrac evaluation 2.0 software.

2.1.4.1 X-Ray Diffraction (XRD)

X-ray powder diffraction (XRD) is a rapid analytical technique primarily used for unknown crystalline material (such as elements, inorganic compounds) for phase identification and it has capacity to show information on unit cell dimensions. The crystalline substances behave like three-dimensional diffraction gratings for acting X-ray wavelengths similar to the spacing of planes in a crystal lattice. Currently X-ray diffraction is seemed an important technique for the study of atomic spacing and crystal structures (Dutrow & Clark, 2012).

The X-ray diffraction is dependent on a crystalline sample and constructive interference of monochromatic X-rays. The cathode ray tube is used for the production of these X-rays which are filtered to generate monochromatic radiation and with the help of collimated to concentrate, which afterwards focuses on the sample. These specific wavelengths are representative of the target material (such as Cu, Fe, Mo, and Cr). To produce monochromatic X-rays which are needed for diffraction, so these rays are filtered by foils or crystal monochrometers is required. When incident rays interact with the sample which produces constructive interference and a diffracted ray when meets with requirements of Bragg's Law (i.e. $n\lambda=2d \sin \theta$). This law depends on the wavelength of electromagnetic radiation to the diffraction angle and also on the lattice spacing in a crystalline sample. At latter, the diffracted X-rays are then detected on detector, process this x-ray signal and counted. By using range of 2θ angles for the scanning of sample, all possible diffraction directions of the lattice are attained due to the random orientation of the sample powdered material. After conversion of the diffraction peaks to d-spacing which allows identifying the element because each element has it's a set of distinctive d-spacing. However, this is typically done by comparison of d-spacing with standard reference patterns (Dutrow & Clark, 2012).

2.2 Characterization of Reacted Aqueous Solutions

2.2.1 pH Measurement

A Metrohm 702 Titrino pH apparatus was used to measure the pH of the samples, including the blank sample as well. The pH measurement of the working solution was done after the collection of samples. The measurement of pH was done through special designed glass electrode connected to a data processor having a specific software program name Metrom Tiamo 1.2. Therefore, prior to measuring the pH, the pH electrode was calibrated with buffer solutions with pH at 4.0, 7.0 and 9.0 at 25°C temperature. The measurement of pH was done with an accuracy of ±0.02 at room temperature (25°C) and with an accuracy of about 95.7% (Thermo Fisher Scientific Inc., 2013).

2.2.2 Ion Chromatography System (ICS)

The Dionex ICS-1000 Ion Chromatography System (ICS-1000) was used for the analysis of samples which performs ion analyses using suppressed or non-suppressed conductivity detection.

This ion chromatography system typically consists of following six components as: a liquid eluent, a high-pressure pump, a sample injector, a guard and separator column, a chemical suppressor, a conductivity cell, and a data collection system. However, before running a sample, the ion chromatography system is calibrated using a standard solution. Therefore, by comparing the results obtained from a sample to that obtained from the known standard solution, then sample ions can be identified and quantified. The data generally collected through a computer running chromatography software, which produces a chromatogram (i.e. a plot of the detector output vs. time). Then chromatography software converts each peak in the chromatogram to a concentration of sample and in response produces results (Dionex Cor., 2005).

2.2.3 Colorimeter (the Autoanalyzer)

Colorimetr was used to measure the Si concentration of samples collected from the reservoirs where basalt glass was dissolved over time.

The autoanalyzer is consisting of modules connected in sequence to perform an automatic chemical analysis. This operation of the instrument gives a concept of continuous flow which allows for flexibility and versatility in chemical analyses. It can be used to analyze air, water, waste effluent, soil, metal, and samples of pharmaceutical, agricultural and biological materials. However, auto-analyzer is generally used for determining levels of nutrients in plant, soil, and water samples. The colorimetric determination is based on the Beer Lambert's Law. According to this law, the absorbance (optical density) of a substance is directly proportional to the concentration of that substance. This means that a change in concentration of a sample will cause a change in color intensity, changing the optical density of that substance. So this law gives a graph of absorbance versus concentration is used to calculate the values of concentration for samples under analysis (Gallentine, 2013).

3.0 Experimental Methods and Materials

Basaltic glass from Iceland previously characterized as normal Mid-Ocean Ridge basalt (N-MORB) ($Na_{0.08}Ca_{0.263}Mg_{0.281}Fe_{0.188}Al_{0.358}SiO_{3.32}$; Gislason and Oelkers, 2003), was used for the laboratory dissolution rate experiments. Before starting the experiments the material was characterized by SEM, and the particle size distribution of crushed materials was analyzed.

3.1 Dissolution rate experiments and sampling

All basaltic glass dissolution experiments were performed in a batch reactor system. The solution within the reactor was covered with specially designed lids to avoid loss of water from the reservoirs. Two different types of crushed basaltic glass samples were used to see the dissolution rates at different temperature ranges by using of initial water with pH 5. Each experiment was performed under same conditions for the two basaltic glass powders. A specific mass of dry glass powder was placed in the reactors. When the reactors were filled with the starting water solution, closed and placed in JB Aqua 26 system (Fig. 3.1), the temperature was adjusted to desired settings. The temperature of dissolution rates of basaltic glass experiment one and two runs performed at 50^{o}C and 90^{o}C respectively. A total of 6 beakers/reactors were placed in the system, and each reactor was initially filled with 350 ml pH 5 solutions. Two reactors were filled with blank/reference solutions and from the remaining four reactors, two of them were separately added 20 mg of hand crushed sample and in the remaining other two added 10 mg of micronizer crushed samples. So the one blank, one hand crushed and one micronizer crushed were kept in JB Aqua apparatus at 50 ^{o}C and the remaining three were place in other JB Aqua apparatus at 90 ^{o}C.

Each sample was collected from the batch reactor with the help of a syringe by mounting on it a specially designed filter (of 0.45 mic) named Minisart, which is hydrophilic. So each time, collected 10 ml of sample volume from the reservoirs and stored in plastic bottles, which is afterward used for the measurement of pH and also for the measurement of element phases with the help of Ion Chromatography. The batch reaction reservoirs were refilled each time with 100 ml of pH 5 aqueous solution when reservoir's initial water level of 350 ml were lowered to 200 ml due to continuous collection of samples.

Figure 3.1: Showing JB Aqua 26 Plus Bath.
(Source: LabSource, 2013)

Why diluted the experiments at given some times?

1. The main reason is that this is batch experiments, and because of the sampling a replenishment of solution is needed. The secondary reasons are that:
2. Concentrations are prevented from reaching unreasonable high values; and,
3. Replenishment will be similar to a natural setting, where rainwater periodically will dilute the soil.

3.2 Characterization of Initial Material

3.2.1 Analysis of Samples in SEM

The SEM was used at different resolutions and at different scales (in μm) to take the pictures of 3the initially crushed basaltic glass samples. It can be clearly seen from Figure 3.2 and 2.3 that both (hand and micronizer) crushed basaltic glass sample contains mixture of fine and coarse basaltic glass grains. The micronized crushed sample as compared to hand crushed having relatively more number of finer and fewer coarse grains. To precisely determine the particle size distribution and surface roughness in the crushed basalt glass samples, the Beckman Coulter-particle size analyzer was used and plotted the particle diameter distribution against differential volume percent and differential surface area percent which can be seen from Figures 3.6 to 3.11.

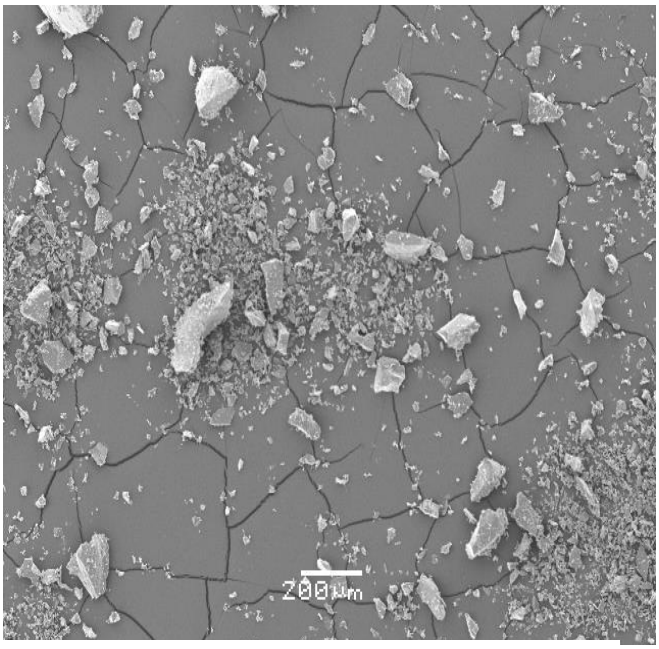

(A)

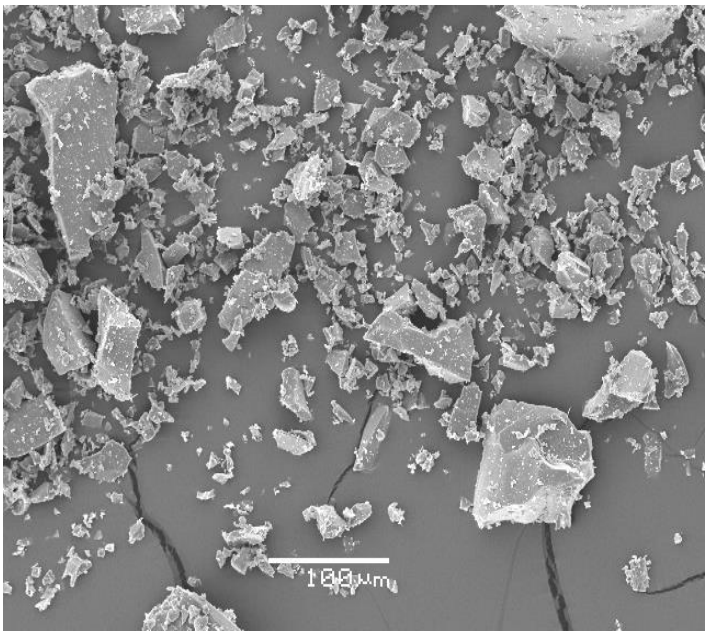

(B)

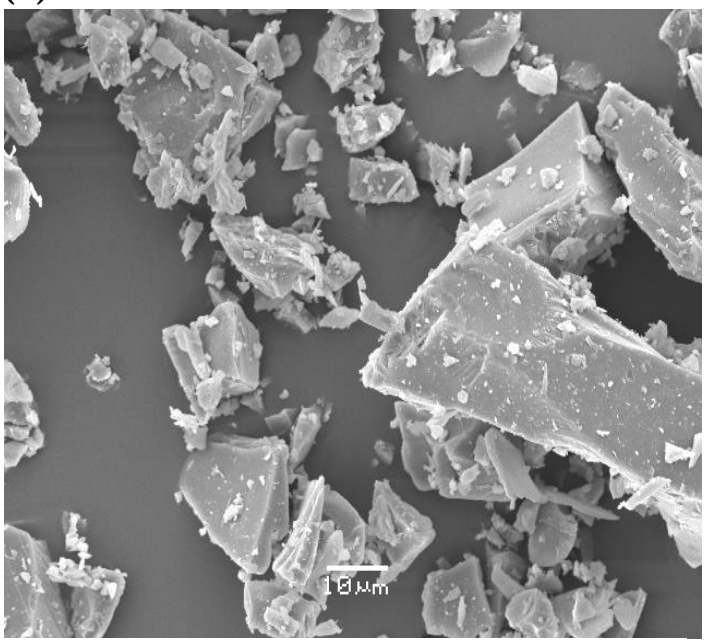

(C)

Figure 3.2: Scanning electron images of basaltic glass powder, crushed with mortar agate used in this study. The images A, B and C are of the basaltic glass before experiment. Image B and C are the magnification of image A (X60) to X220 and X1100 respectively which are showing the surface roughness and the grain sizes distribution in sample.

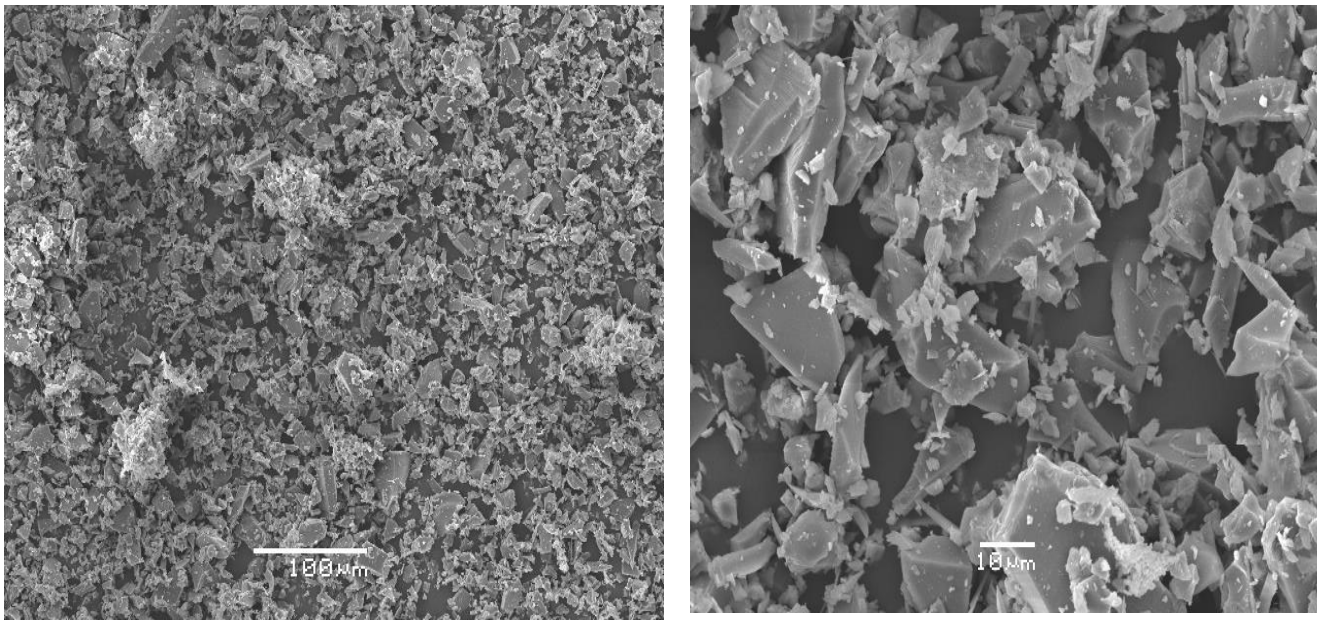

(A) **(B)**

Figure 3.3: Scanning electron images of basaltic glass powder, crushed with micronizer used in this study. The images (A) and (B) are of the basaltic glass before experiment. Image (B) is the magnification of image (A) (X220) to X1100, which is showing the surface roughness and the grain sizes distribution in sample.

Randomly selected the grains of basaltic glass crushed in micronizer in Fig. 3.4 for identification of element composition. So for, from the selected basaltic glass grains the element composition spectrum was identified with the help of SEM is shown in Fig. 3.5. The basaltic glass is mostly consisting of Ca, Au, Si, Mg and Fe elements with their descending order of concentration in the element.

Figure 3.4: Scanning electron image of basaltic glass powder crushed in micronizer is showing selected grains of basaltic glass for the identification of elemental composition.

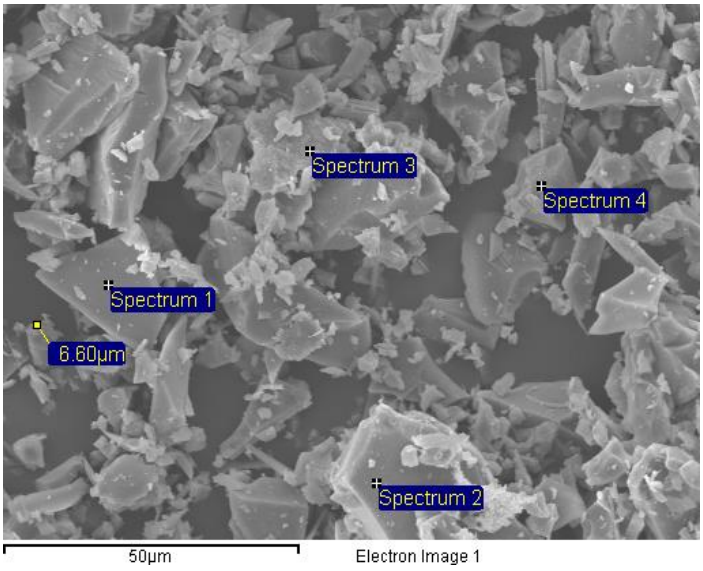

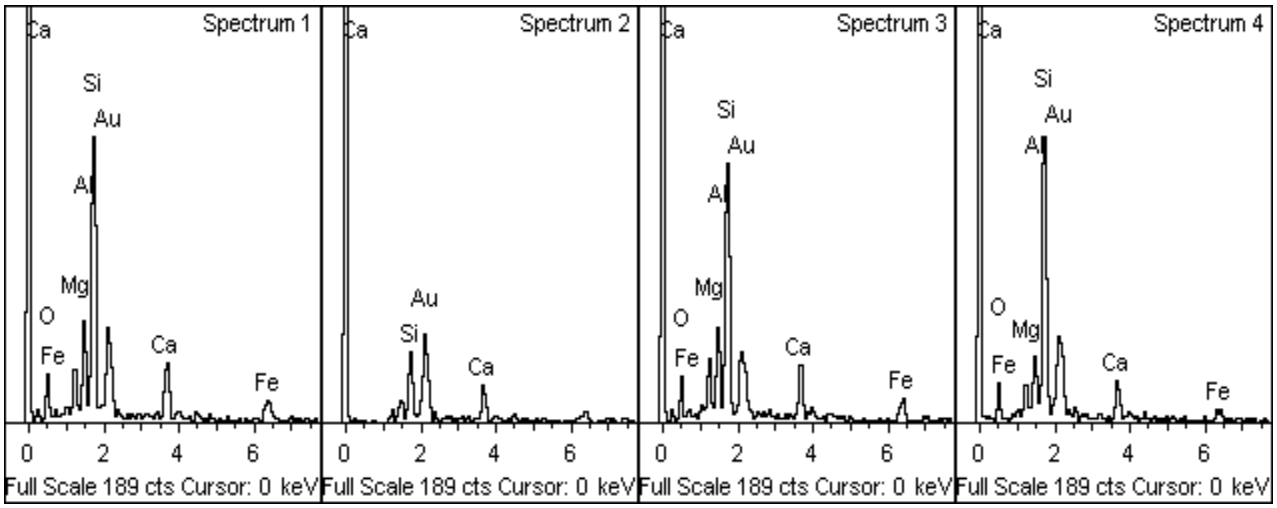

Figure 3.5: Scanning electron graphs of basaltic glass powder crushed with micronizer showing spectrum of elemental composition of sample.

3.2.2 Analysis of Grain Size Distribution in PSA

A. For Hand Crushed Sample

The distribution of grain size was determined for both hand crushed and micronized crushed basaltic glass samples by using the Beckman Coulter (LS 13 320) instrument. From Figure 3.6, it can be seen that there are three different types of grain size distribution present for hand crushed sample. Firstly, the very fine grain size diameter range starts from 0.4µm to 10µm, comprises differential volume of about 0.9%; secondly, medium coarse grain size diameter range is from 10µm to 250µm with differential volume is around 0.9% to 3.9% and finally, the coarse grain diameter size from 400µm to 800µm with very little differential volume of around 0.4% maximum.

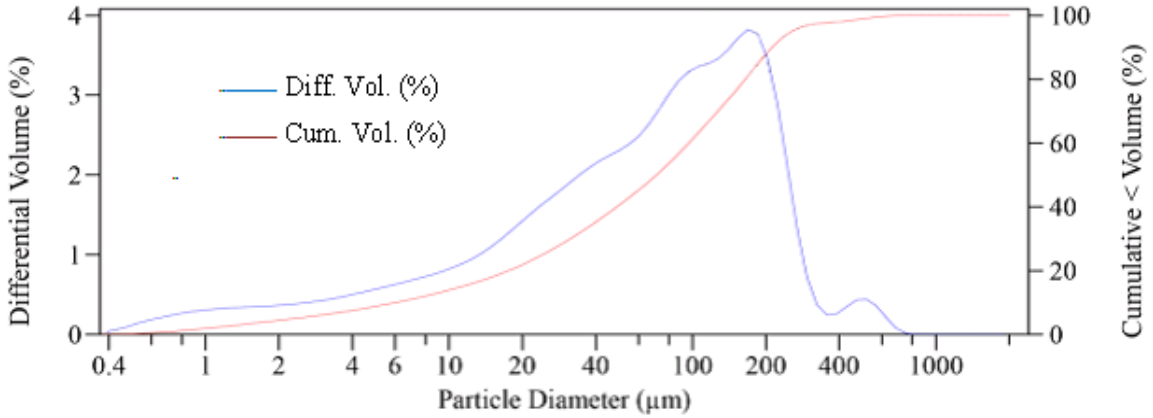

Figure 3.6: Showing grain size distribution versus differential volume percent and cumulative volume percent for hand crushed basaltic glass sample which is obtained from Beckman Coulter LS apparatus.

The Fig. 3.7 depicts that hand crushed basaltic glass sample consists of high distribution of small diameter particles, which are providing major part of differential surface area percent in overall compare to medium and coarse grains. So, 0.4µm particles are contributing about 1.1% differential surface area relatively less in number than the 0.8µm particles are highly distributed which are contributing to around 3.9% in differential surface area. The medium coarse grains (from 2µm to 10µm) and coarse grains (>10µm) are gradually less distributed and show their decreasing trend in their differential surface area percent with increase in their size.

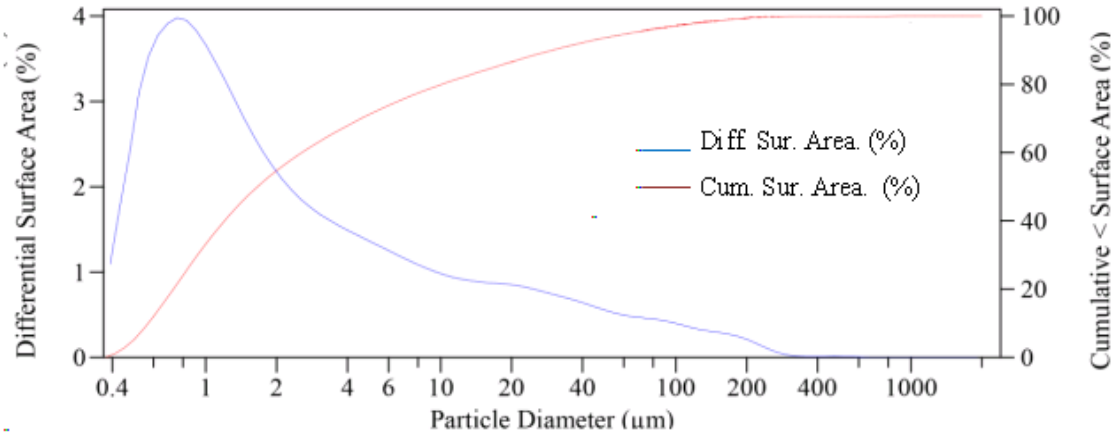

Figure 3.7: Showing grain size distribution versus differential surface area percent and cumulative surface area percent for hand crushed basaltic glass sample which is obtained from Beckman Coulter (LS 13 320) apparatus.

By using the Beckman Coulter apparatus, grain diameter in μm was found and their relative differential surface area in percent and differential volume percent presented in Table 3.1, which is used and helpful while calculating the specific surface area of the hand crushed particles through particle size distribution method. I refer to 0.474 μm each of these grain diameters as a particle size group, and during the later Matlab simulations, these groups are used as the initial grain size and changing during the dissolution (the grain size of each group changes during the dissolution).

Table 3.1: Presentation of the distribution of particles sizes, differential surface area and differential volume percent of hand crushed basalt glass (density 2.9 g/cm^3) sample.

Grain Diameter (μm)	Diff.Surface area (%)	Diff.Vol. (%)
0.474	11.9	0.5
0.755	19.5	1.24
1.204	16.2	1.63
1.919	11.3	1.81
3.06	8.44	2.16
4.878	6.87	2.8
7.776	5.53	3.59
12.4	4.6	4.78
19.76	4.24	7.03
31.51	3.62	9.54
50.23	2.78	11.6
80.07	2.23	15
127.7	1.65	17.5
203.5	0.98	16
324.4	0.12	2.92
517.2	0.043	1.79
824.5	0.0017	0.1

As we know that fine particles have relatively larger specific surface area than the coarse grains. So then finer grains contribution becomes higher to the dissolution rate of basaltic glass as compared to the coarse grains, it is only because more reaction takes place at the surface of particles and dissolves rapidly.

It is estimated that hand crushed basaltic glass sample having a cumulative specific surface area about 0.175m^2/g, calculation procedure can be seen in the Appendix 3.1. In our sample the

distribution of grain size of $4.47x10^{-7}m$ are providing distributed specific surface area of about $0.022m^2/g$ and while the grains size of $7.55x10^{-7}m$ are relatively highly distributed and contributing with the highest distributed specific surface area of around 0.034 m^2/g in overall sample, Fig. 3.8. So as gradually coarse grains are distributed and contributing less to specific surface area in overall of the sample.

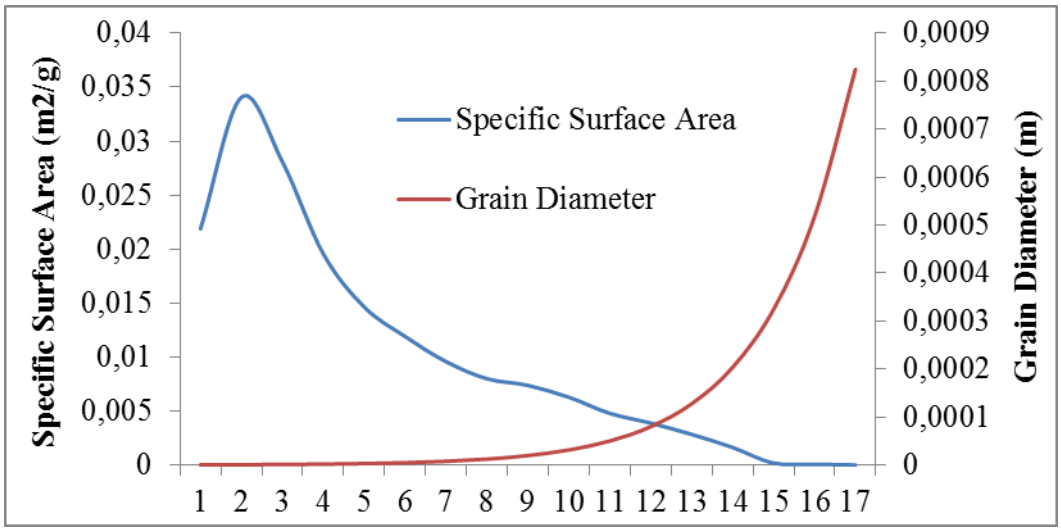

Figure 3.8: Comparison of grain size distribution versus specific surface area of hand crushed glass sample.

B. For Micronizer Crushed Sample

There are also three types of grain size distribution seen for micronizer crushed basaltic glass sample, which is almost similar in pattern as we see in hand crushed sample but here relatively more differential volume for fine grains portion is percent.

The grain size distribution for micronizer crushed basaltic glass sample is shown in Fig. 3.9. Firstly, the fine grains size range starts from 0.4 µm to 10 µm having differential volume of about 3.3%; secondly, the medium coarse grains diameter is in range from 10µm to 19µm with differential volume is around 3.3% to 4.1% and finally, the coarse grains size is in range from 80 µm to 130 µm, showing very small differential volume which is <0.2%.

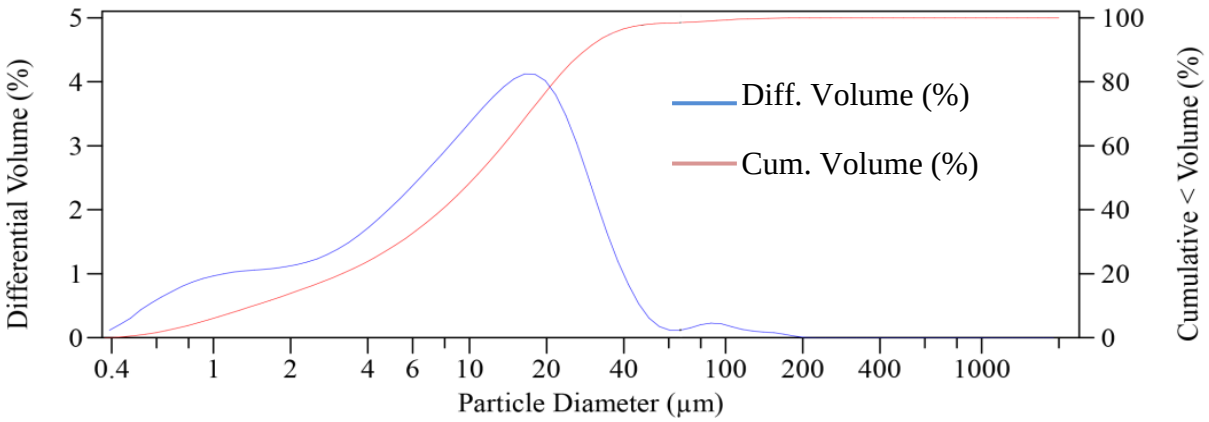

Fi

Figure 3.9: Showing grain size distribution versus differential volume percent and cumulative volume percent for micronized crushed basaltic glass sample and graph is which is obtained from Beckman Coulter analysis.

The Fig. 3.10 shows that micronizer crushed basaltic glass sample having very high distribution for smaller diameter particles, which are more contributing to the differential surface area in percent. However, in this case as compared to hand crushed basaltic glass sample there are finer and homogeneous particles are found. Generally, 0.4µm size particles are contributing to around 1.1% differential surface area, the 0.8µm size particles are very highly distributed and having around 4.3% differential surface area. So the medium coarse grains (i.e. from 2µm to 10µm) and coarse grains (>10µm) are gradually less distributed and showing their decreasing trend in differential surface area percent as with increase in particles diameter size.

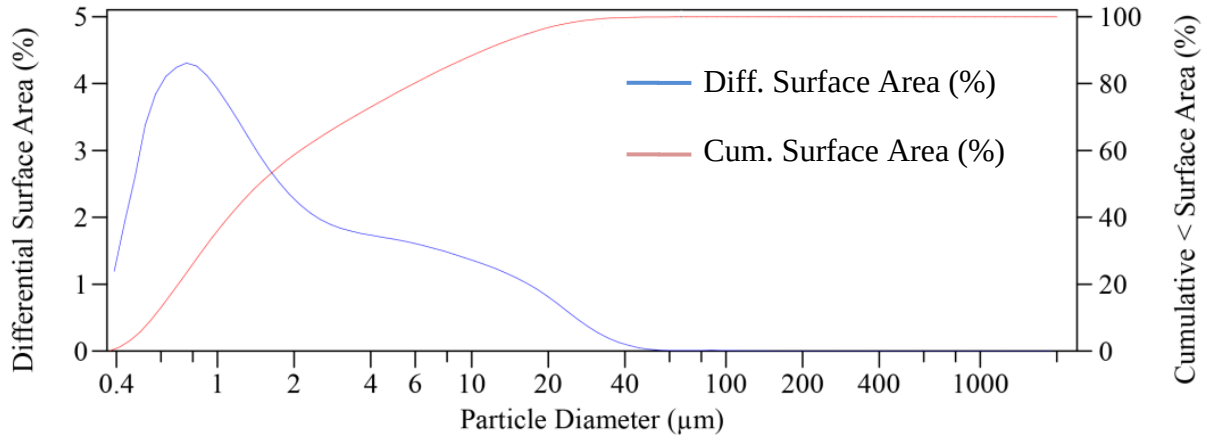

Figure 3.10: Showing grain size distribution versus differential surface area percent and cumulative surface area percent for the micronizer crushed basaltic glass sample and graph is obtained from Beckman Coulter LS analysis.

The grains diameter, relative differential surface area percent and differential volume percent found by using Beckman Coulter instrument is presented in Table 3.2 for the micronizer crushed sample. This information is helpful while calculating the specific surface area for the crushed grains by using the BET method.

Table 3.2: Showing the particles sizes distribution, differential surface area percent and differential volume percent of micronizer basalt glass crushed (density 2.9 g/cm^3) sample.

Grain Diameter (μm)	Diff.Surface Area (%)	Diff.Volume (%)
0.474	12.9	1.6
0.755	21	3.95
1.204	17.2	5.09
1.919	11.8	5.58
3.06	9.25	7
4.878	8.38	10.1
7.776	7.45	14.3
12.4	6.14	18.7
19.76	4.07	19.5
31.51	1.42	10.5
50.23	0.17	1.96
80.07	0.046	0.92
127.7	0.019	0.57
203.5	0.002	0.085

The more numbers of fine grains are present in micronizer crushed basalt glass sample than the hand crushed basaltic glass sample. It is calculated that micronizer crushed basaltic glass sample having a cumulative specific surface of about 0.515 m^2/g (see calculations in Appendix 3.1). It can be clearly seen in Fig. 3.11, the distribution of particles size of 4.47x10^{-7} m are providing much higher distributed specific surface area i.e. 0.07 m^2/g than the hand crushed at same particles (i.e. 0.022m^2/g). The grains diameter of 7.55x10^{-7}m are highly distributed and contributing with the highest distributed specific surface area of around >0.1m^2/g in overall sample which is again much higher than the hand crushed sample (i.e. 0.034 m^2/g). Thus, coarse grains are less distributed and similarly providing the less distributed specific surface area.

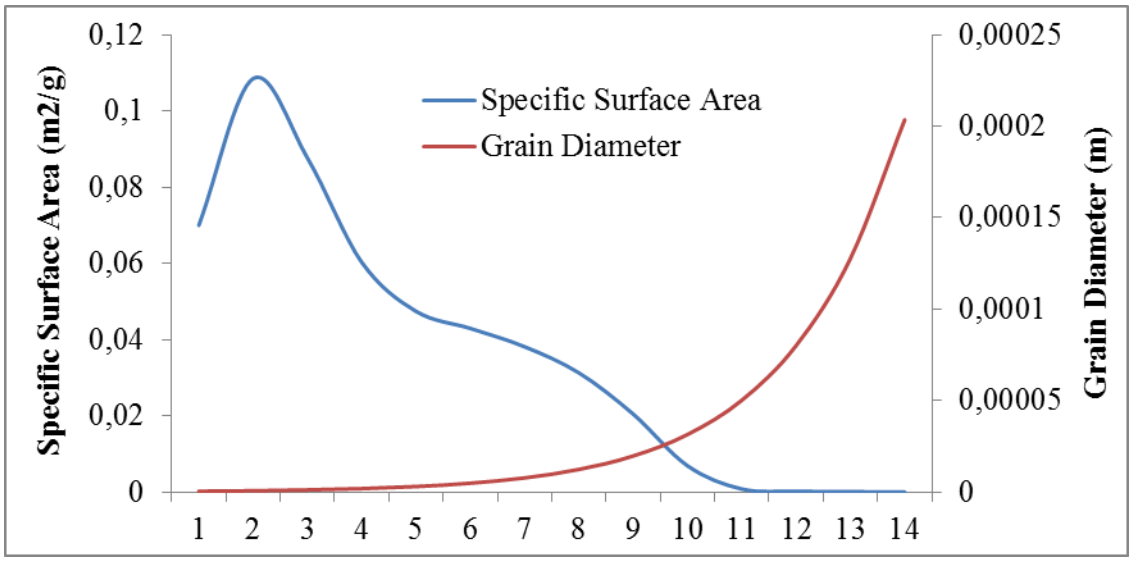

Figure 3.11: Comparison of distribution of grains diameter versus specific surface area of micronizer crushed basalt glass sample.

3.2.2.1 Procedure for the Calculation of Specific Surface Area

The specific surface area of the basaltic glass grains is determined in m^2/g with the help of derived equation 3.1.

$$A = \sum_i A_i \qquad \text{Eq. 3.1}$$

Where, A is the cumulative specific surface area in m^2/g of the basaltic glass grains and Ai represents the specific surface area of individual basalt grains. The specific surface area of the individual grain is calculated by using equation 3.2.

$$A_i = a_i n_i \qquad \text{Eq. 3.2}$$

Where, a_i is the calculated surface area in m^2 of the grains and ni is the number of particles per gram of basaltic glass. The ai and ni can be calculated by using equations 3.3 and 3.4 respectively.

$$a_i = 4\pi r^2 \qquad \text{Eq. 3.3}$$

$$n_i = \frac{V_i}{V_p} \qquad \text{Eq. 3.4}$$

So, r is the radius of particles and Vi represents the fractional volume of basaltic glass grains in cm^3 and it is calculated by using equation 3.5.

$$V_i = V_{dif} V \qquad \text{Eq. 3.5}$$

Where, V_{dif} represents the differential volume of basaltic grains which was determined throuugh Beckman Coulter LS -Particle Size Analyzer and V is the total basaltic glass volume (cm^3) per gram i.e. $V = \frac{1g}{2.9g/cm^3}$, which is equals to 0.3448 cm^3. So V_p is the volume of basalt grains in cm^3, which is calculated by using equation 3.6.

$$V_p = \frac{4}{3}\pi r^3 \qquad \text{Eq.3.6}$$

3.2.2.2 Dissolution Rate of Basalt Glass

The dissolution rates of basaltic glass have been calculated at 25°C, 50°C and 75°C temperatures and at pH 8.5 (where Ea is 3257 J/mol), presented in Figure 3.12. This dissolution rate is estimated by using the dissolution rates of crystalline basalt given in Fig. 2 from Gudbrandsson and Wolff-Boenisch, et al. (2008). The dissolution is higher at 75°C and lowest at 25°C. It means that the dissolution of basaltic glass increases with the increases of temperature.

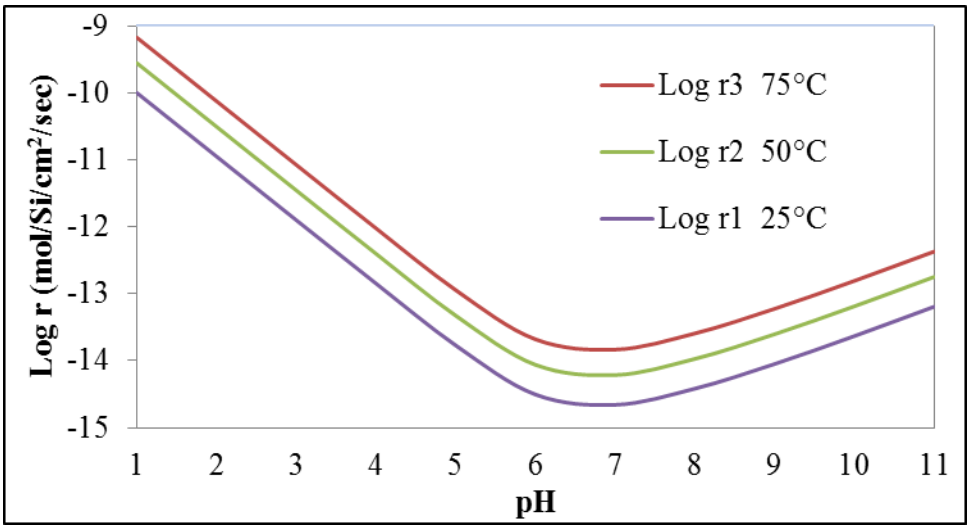

Figure 3.12: Dissolution rates of basaltic glass samples from Ice Land.

However, this dissolution is calculated by using an equation 3.7 as;

$$r = A\sum_i k_i a_{H^+}^{n_i} \qquad \text{Eq. 3.7}$$

Where r is the basaltic glass dissolution rate in molSi/cm^2/sec, far from-equilibrium state, k^t is mol of Si/cm^2/s variable and temperature dependent, A is the specific surface area in m^2/g and ai represents the activity of the hydrogen ion species.

The rate constant $k^{(T)}$ can be estimated at any temperature from Eq. 3.8 as;

$$k(T) = k(T^0)_e^{(\frac{-Ea}{R}(\frac{1}{T} - \frac{1}{T^o}))} \qquad \text{Eq. 3.8}$$

Where, $k^{(To)}$ is constant, E_a designates a pH independent activation energy which is equal to 26 kJ/mol (Gudbrandsson et al. 2008), R stands for the gas constant which is 8.314 J/Kmol, T is temperature in K. The detail procedure for the calculation of basaltic glass dissolution rate at various temperatures and at different pH is given in Appendix 3.2.The dissolution rates for our hand crushed and micronized crushed samples are presented in Table 3.3 and 3.4 respectively, where the dissolution rates at different temperatures are added with specific surface areas of samples respectively as well. The dissolution of basaltic glass is higher in acidic environment and becomes lover in neutral pH and then again slightly increases in basic environment.

Table 3.3: Dissolution rates of hand crushed basalt glass sample for given specific surface area (0.175 m^2/g) at different temperatures.

pH	**Log Dissolution** 25°C (mol/Si/g/sec)	**Log Dissolution** 50°C (mol/Si/g/sec)	**Log Dissolution** 75°C (mol/Si/g/sec)
0	-6.757596	-6.313239	-5.932819
1	-7.707561	-7.263204	-6.882785
2	-8.65725	-8.212893	-7.832473
3	-9.6044	-9.160043	-8.779624
4	-10.52779	-10.08344	-9.703025
5	-11.26163	-10.81728	-10.43695
6	-11.41527	-10.97094	-10.59091
7	-11.17318	-10.72887	-10.34908
8	-10.80598	-10.36168	-9.982026
9	-10.38862	-9.944321	-9.564725
10	-9.950771	-9.506477	-9.126905

Table 3.4: Dissolution rates of micronized crushed basalt glass sample for a given specific surface area (0.515 m^2/g) at different temperatures.

pH	Log Dissolution 25°C (mol/Si/g/sec)	Log Rate Dissolution 50°C (mol/Si/g/sec)	Log Dissolution 75°C (mol/Si/g/sec)
0	-6.29	-5.85	-5.47
1	-7.24	-6.80	-6.42
2	-8.19	-7.75	-7.36
3	-9.14	-8.69	-8.31
4	-10.06	-9.62	-9.24
5	-10.79	-10.35	-9.97
6	-10.95	-10.50	-10.12
7	-10.71	-10.26	-9.88
8	-10.34	-9.89	-9.51
9	-9.92	-9.48	-9.10
10	-9.48	-9.04	-8.66

3.2.2.3 Calculation of Sampling Time

We decided to keep the concentration below a maximum of 200 ppm of Si for analytical reasons. We therefore calculated the time required to reach 200 ppm at the different temperatures. For example, in our study, it is tried to estimate that how much time is required for basaltic glass to release the silicate in water to reach a 200 ppm.

In this study it is tried to estimate the sampling timing at 5 pH and at 50°C, where log(r) value is around 10^{-13} mol basalt/cm^2/sec (Fig 3.12). It is calculated that, to get 200ppm of silicate concentration in water requires 14 days (or 339 hours), so the detail calculation can be seen in Appendix 3.3.

It is estimated by using an Equation 3.9 as;

$$t_{req.} = \frac{C_{S_i(req.)}}{R_{Basalt}} \qquad \text{Eq.3.9}$$

Where $t_{req.}$ is the time required to reach a certain concentration of an element in water, R_{Basalt} is the silica release concentration from basaltic glass, the unit is in (mol/s/L). Where, $C_{S_i(req.)}$ is the silicate concentration in per mol of basalt glass.

3.2.3 Analysis of Initial Material in XRD

The XRD analyses showed a background signal indicating that the majority of the material was amorphous (glass). Some reflections (peaks) on the background indicated that basaltic glass is the mixture of other elements and we identified that these are forsterite and quartz crystals. However, it was estimated that the sample is consisting of 85% amorphous and only 15% crystalline material.

3.3 Preparation of Aqueous Solutions

For this study requires the ultrapure water to get efficient results and was used in all activities of the experimental work. Therefore, these consists of, preparation of solutions, washing of instruments etc. The tap water is purified in a first step through exclusive Jet pore ion exchange resin, synthetic activated carbon and a UV lamp emitting at 185 nm and 254 nm to reach a resistivity of 18.2 MΩ.cm at 25°C and a total oxidizable carbon (TOC) value below 5 ppb; both values are monitored by advanced analytical techniques. This water is sent through a small recirculation loop to the Application Pak, where a final purification step, critical for specific experiments, removes contaminants just before water leaves the system (LabSource, 2013).

All the experiments were conducted in aqueous solutions. The initial solution of pH 5 was prepared from 0.01 molar solution of HCl. For the total 2 liter volume of water to make it a 5 pH solution, we added 2 ml of 0.01 molar HCl, the calculating procedure is as follows;

0.01mol of HCl/L * X = 0.00001 mol/L * 2L

X = ((0.00001 mol/L) / 0.01 mol of HCl)) * 2L

X = 0.002L or 2ml of HCl

3.4 Preparation of Reacted Solids and Liquids for Analyses

At the end of the experiment the reacted solid basaltic glass materials was separated from aqueous solution. Firstly, the reservoir solution was poured out, and then we added deionized water in the basalt glass to remove the extra salts. The reacted basalt was separated from the aqueous solution on filter paper by using of suction pumps. Afterward, the reacted basaltic glass was dried in oven over night at 60^{o}C that was used for the identification of secondary phases and also elemental composition analysis in SEM.

Before measuring the element phases in the aqueous samples solutions with the help of Ion Chromatography System (ICS), the samples were diluted in following ways as: two times dilution of first four samples, 5 times dilution of the 5th and 6th samples and 10 times dilution from 7th to onward at the end sample. Less dilution of those samples which were ecpected to have less concentration initially were having less concentration of dissolved elements from basalt glass and vice versa.

3.5 Calculation Procedure for Glass Rate at 10^{o}C from Experimental Rates

At given temperature rate of nutrients k_i is recalculated by using Eq. 3.10.

$$k_i = \frac{R_{Basalt}}{X_{Nutrient}} \qquad \text{Eq. 3.10}$$

The dissolution rate constant of nutrients (e.g. at 90^{o}C) was calculated from the experimental rate of nutrient at certain temperature by using Eq. 3.11.

$$X_{Nutrient} = \frac{R_{Basalt}}{R_T^{Nutrient}} \qquad \text{Eq. 3.11}$$

R_{Basalt} is the rate of basalt calculated from by using stoichiometric number (N_{Na}) of element like Na (0.08) from basalt glass formula and nutrients rates from experiment at certain temperature (e.g. in our case 90^{o}C), as Eq. 3.12;

$$R_{Basalt} = \frac{R_{Na}}{N_{Na}} \qquad \text{Eq. 3.12}$$

3.6 Calculation Procedure for Experimental Rate

After measuring the concentration of elements with the help of ICS, the dissolution of elements founds by change in concentration over change in change in time. For this purpose, rate of each diluted series calculated along with from experimental series. The Eq. 3.13 was used to calculate this rate as;

$$R = \frac{C_2 - C_1}{t_2 - t_1} \qquad \text{Eq. 3.13}$$

Experimental rate (R) was calculated in mols/sec. Where, C_2 and C_1 are the final and initial concentration of elements for each series, and t_2 and t_1 are the final and initial times.

4.0 Experimental Results

4.1 Variation of pH over Time

The variation of pH for the experiment run at 50^{o} C is shown in Fig. 4.1, a very fast increase in pH was observed within 5 days, going from the starting pH at 5 up to approximately 8. Afterward, very sharp decrease in pH occurred within 10 days that is reaching to minimum value of pH about 7.6. The pH increases after each dilution, and then drops when added the fresh solution. It continues to increase after each dilution (from 7.7 or 7.8). This is almost the same observation for both hand and micronizer crushed basalt glass samples.

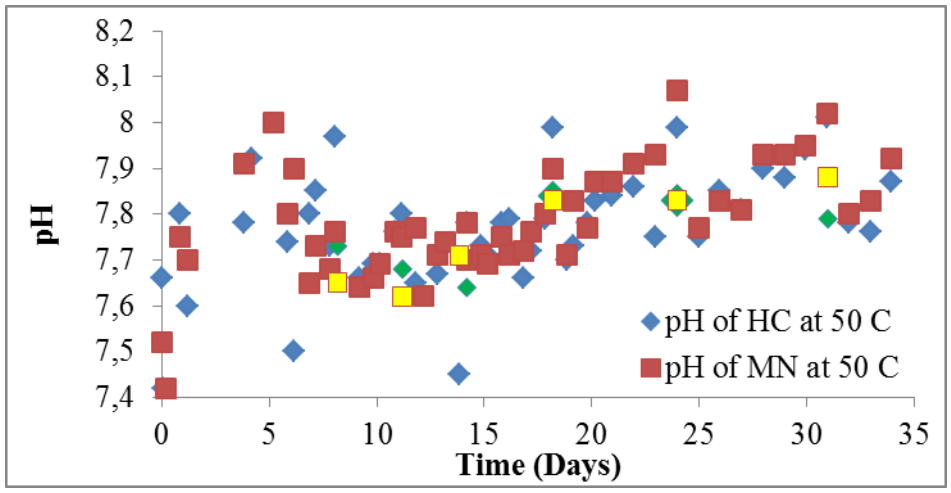

Figure 4.1: Change in pH over time for hand and micronizer crushed samples at 50^{o}C.

If we see the variation of pH trends at 90^{o}C conducted experiment, fast increase from 5pH to around pH 7.8 has been observed within 3 days. And after 5 days, pH of aqueous solutions for both reacted hand and micronizer crushed samples in reservoirs gradually started to increase has been noticed. At the end of experiment (after 34 days), the maximum pH for micronizer reached to around 8.1and for hand crushed pH stabilized around 7.9 (Fig. 4.2).

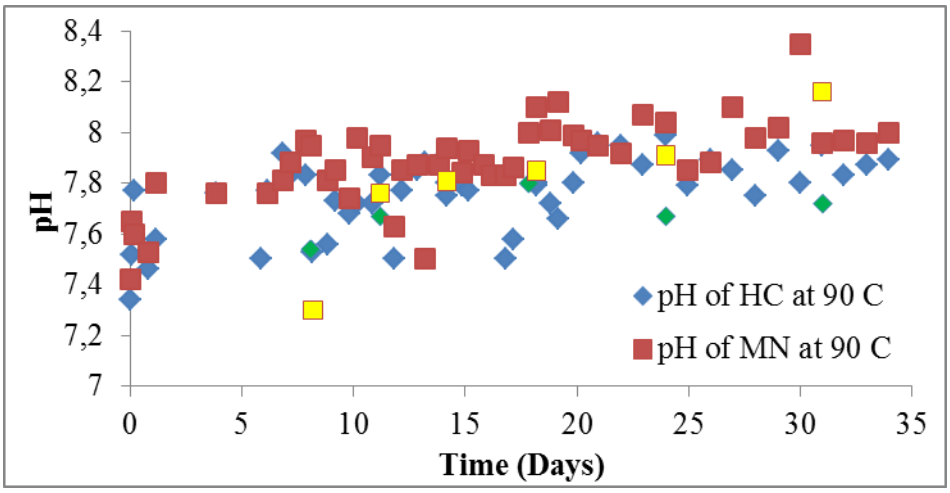

Figure 4.2: Change in pH over time for hand crushed and micronizer crushed samples at 90^{o}C.

4.2 Variation of Cl^- and Na^+ Rates with Time

To estimate the changes in rates with time due to changes in the particle size distribution or to other factors such as surface coatings, the Cl^- release was chosen to be monitored, since it was assume to be the conservative and not incorporating into secondary phases or sorbed (Fig.4.3). Na^+ was analyzed as well to see if it acted conservatively (Fig. 4.4), i.e. it follows Cl^-. The experimental data shows that Na follows Cl and that these two elements therefore both are not being consumed into secondary phases (Figs. 4.3 and 4.4). The concentration decreases after each dilution and again started to increase. The dissolution rates of Cl^- and Na^+ elements from hand and micronizer crushed basaltic glass samples were seen to slow down over time, when they were reacted at 50^{o}C and 90^{o}C. If we look at Cl^- dissolution rates; there was higher dropping in rate observed at 50^{o}C (about more than 1.5 orders) compared to 90^{o}C (about 1 or less than 1 order) for both samples (Fig. 4.5). There was almost similar dropping trends in rates found for Na^+ element at 50^{o}C and 90^{o}C temperatures from both samples as well. In all cases, the drop in dissolution rates started to stabilize around after 15 days.

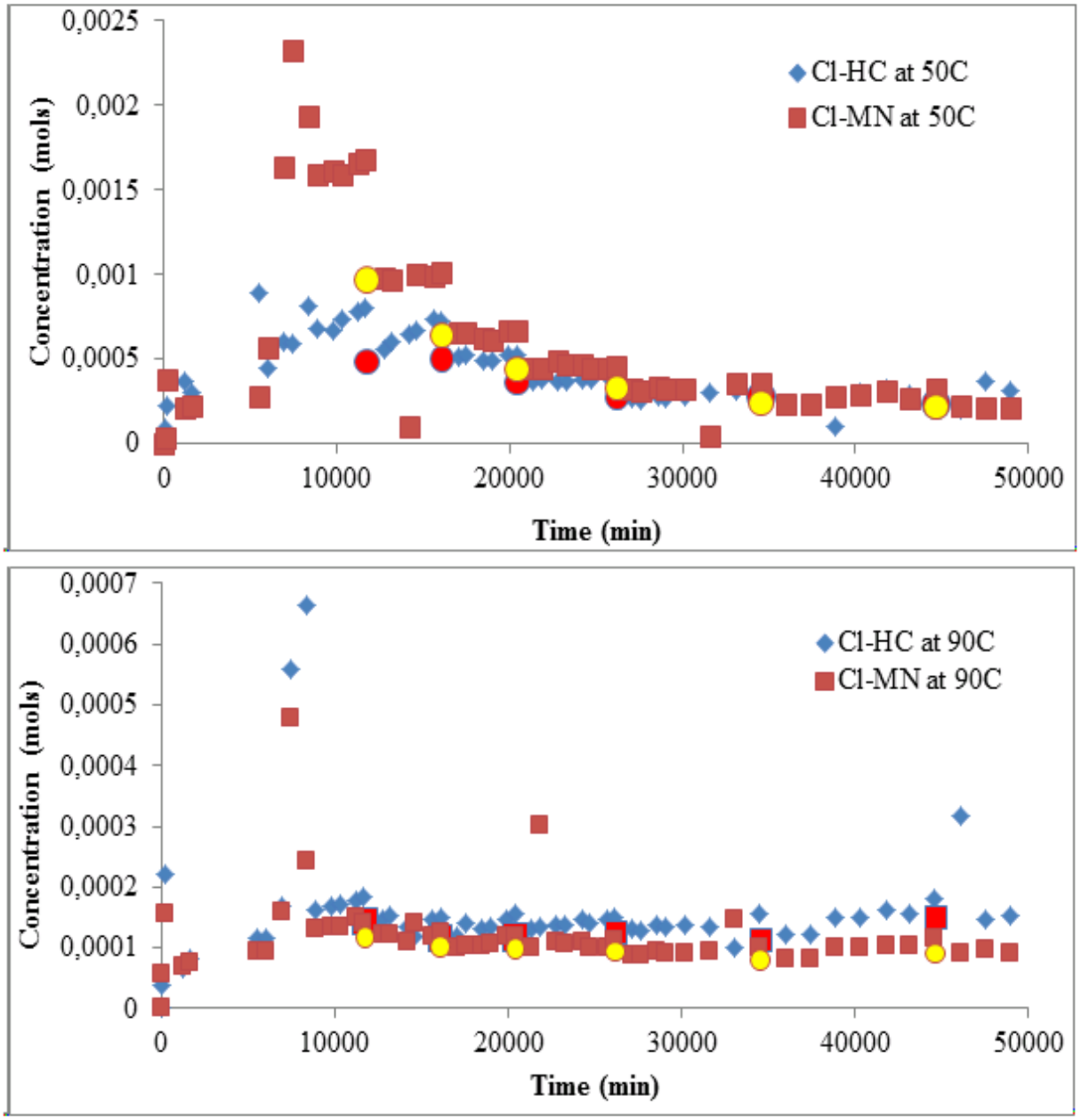

Figure 4.3: Aquesous concentration (mols/L) of Cl^- from dissolution of glass at 50°C and 90°C.

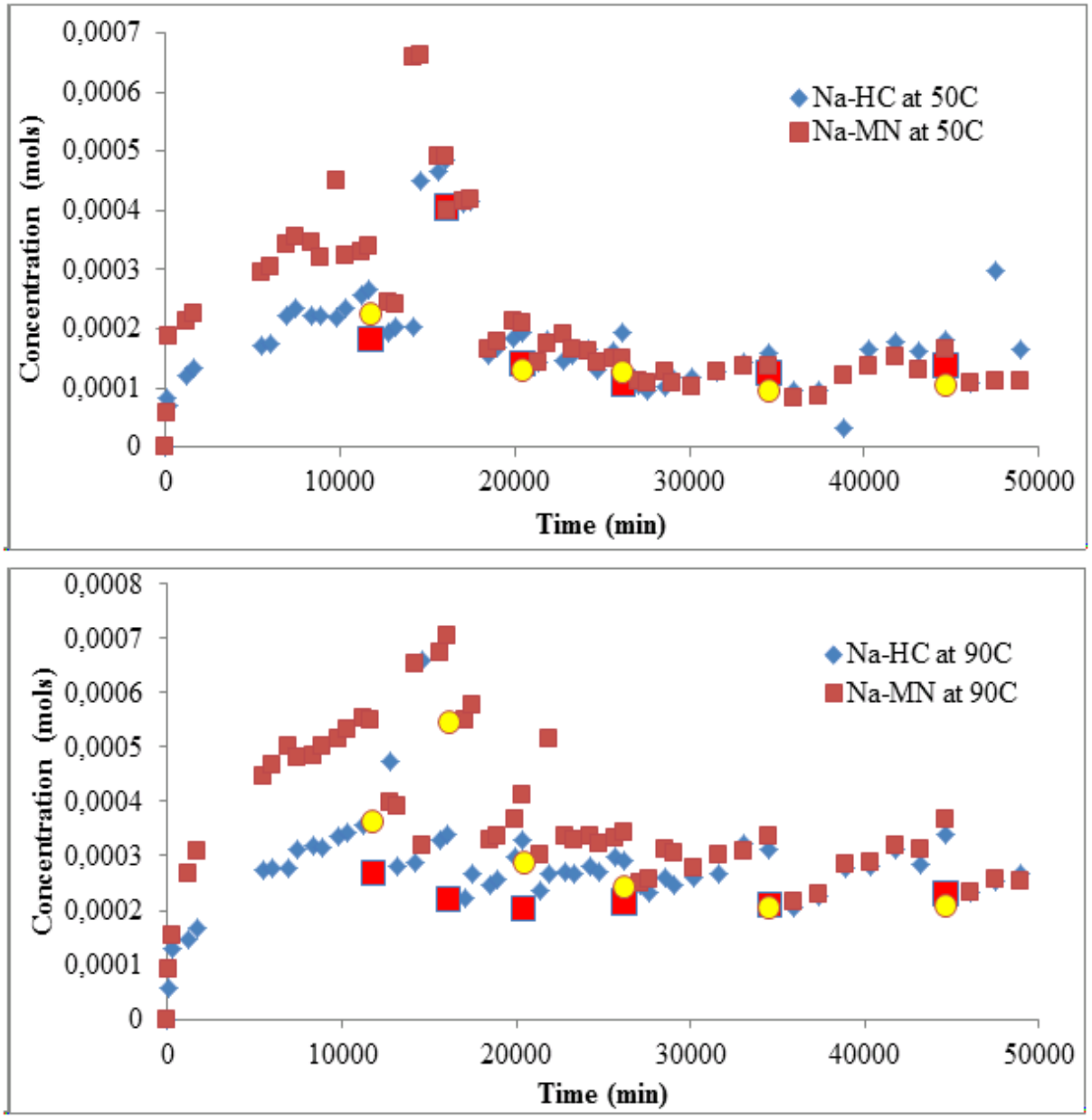

Figure 4.4: Aquesous concentration (mols/L) of Na^+ from dissolution of glass at 50°C and 90°C.

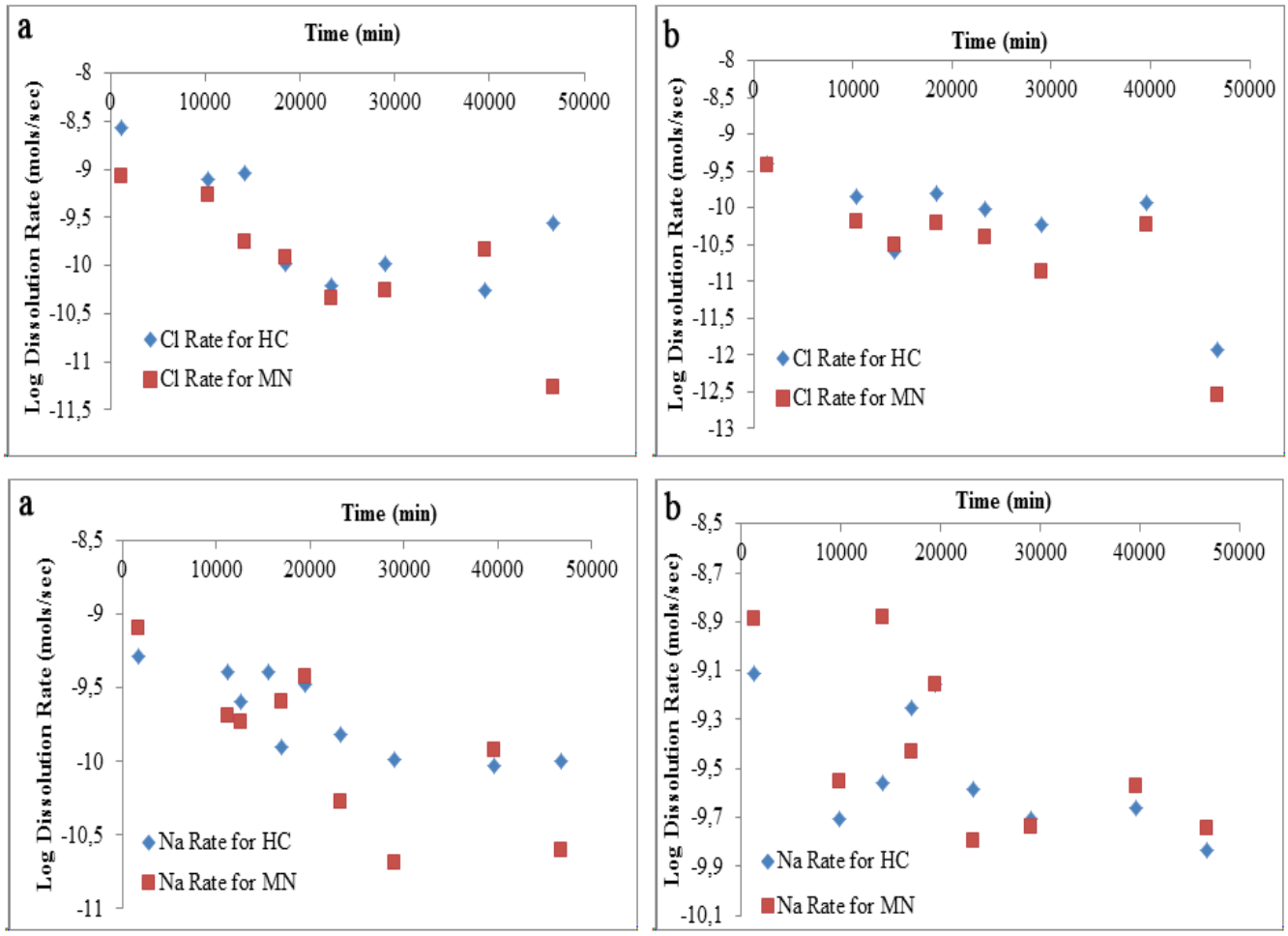

Figure 4.5: Dissolution rates of Cl and Na^+ elements from hand and micronizer crushed basalt glass samples at 50°C (a) and at 90°C (b) temperatures, calculated with equation 3.13.

4.3 Variation of PO_4^{3-} and NO_3^- and K^+ Concentrations with Time

Initially, the aqueous concentration of phosphate (PO_4^{3-}) (Fig. 4.6), (NO_3^-) (Fig. 4.7) and potassium (K^+) (Fig.4.8) nutrients increased until 13, 13 and 7 days respectively(fig..) and after that started to decrease when basalt glass samples were reacted at 50°C and 90°C. After 27days and 21days phosphate (Fig. 4.6) and nitrate (Fig. 4.7) started to behave in different ways as compared potassium (Fig. 4.8). The aqueous concentrations of phosphate and nitrate were continuously dropping to zero and slightly increasing over some times, which is almost in a similar fashion for both samples and at two different temperatures. However, when hand crushed (b from Fig.4.6 & 4.7) basalt glass samples were reacted at 90°C, the phosphate and

nitrate were not dropping to their zero concentrations compared to the micronizer crushed sample after 27 and 21 days respectively.

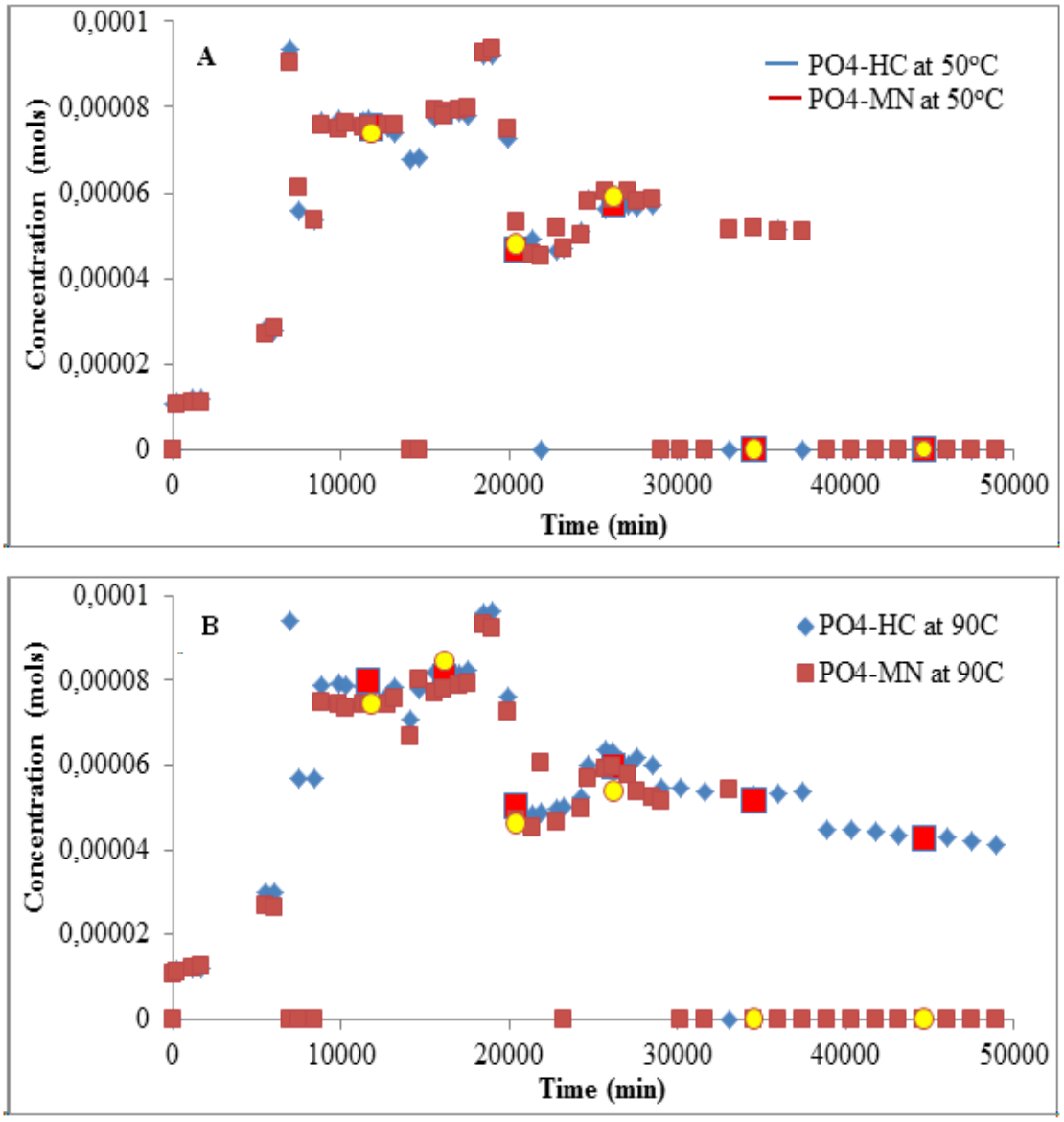

Figure 4.6: Dropping in aqueous concentrations (mols/L) of phosphate with time from dissolution of hand and micronizer crushed basalt glass samples at 50°C and 90°C temperatures.

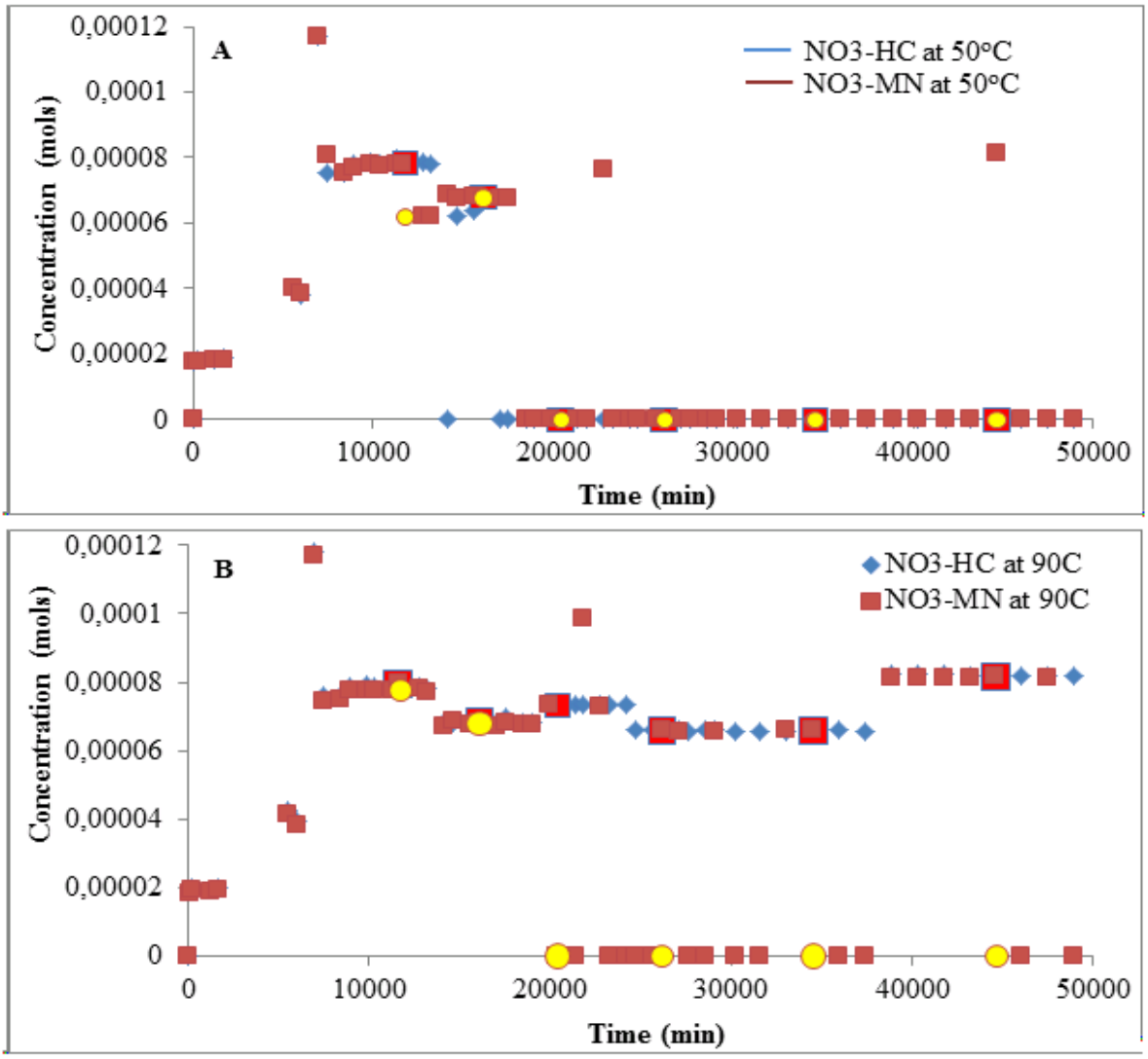

Figure 4.7: Change in aqueous concentrations (mols/L) of nitrate with time from dissolution of hand and micronizer crushed basalt glass samples at 50^{o}C and 90^{o}C temperatures.

The aqueous concentration of K^{+} nutrient increased up to 7 days (Fig. 4.8) and then started to drop in similar way to the conservative elements (Fig 4.5). Throughout time series, there has been no drop in concentration of K^{+} observed. Higher concentration of K^{+} is found at lower temperature (50^{o}C) than higher temperature (90^{o}C). Initially, there was sudden higher increase in concentrations noticed for all nutrients noticed within 7 days.

The yellow and bright red points on the concentration series are showing the dilution steps.

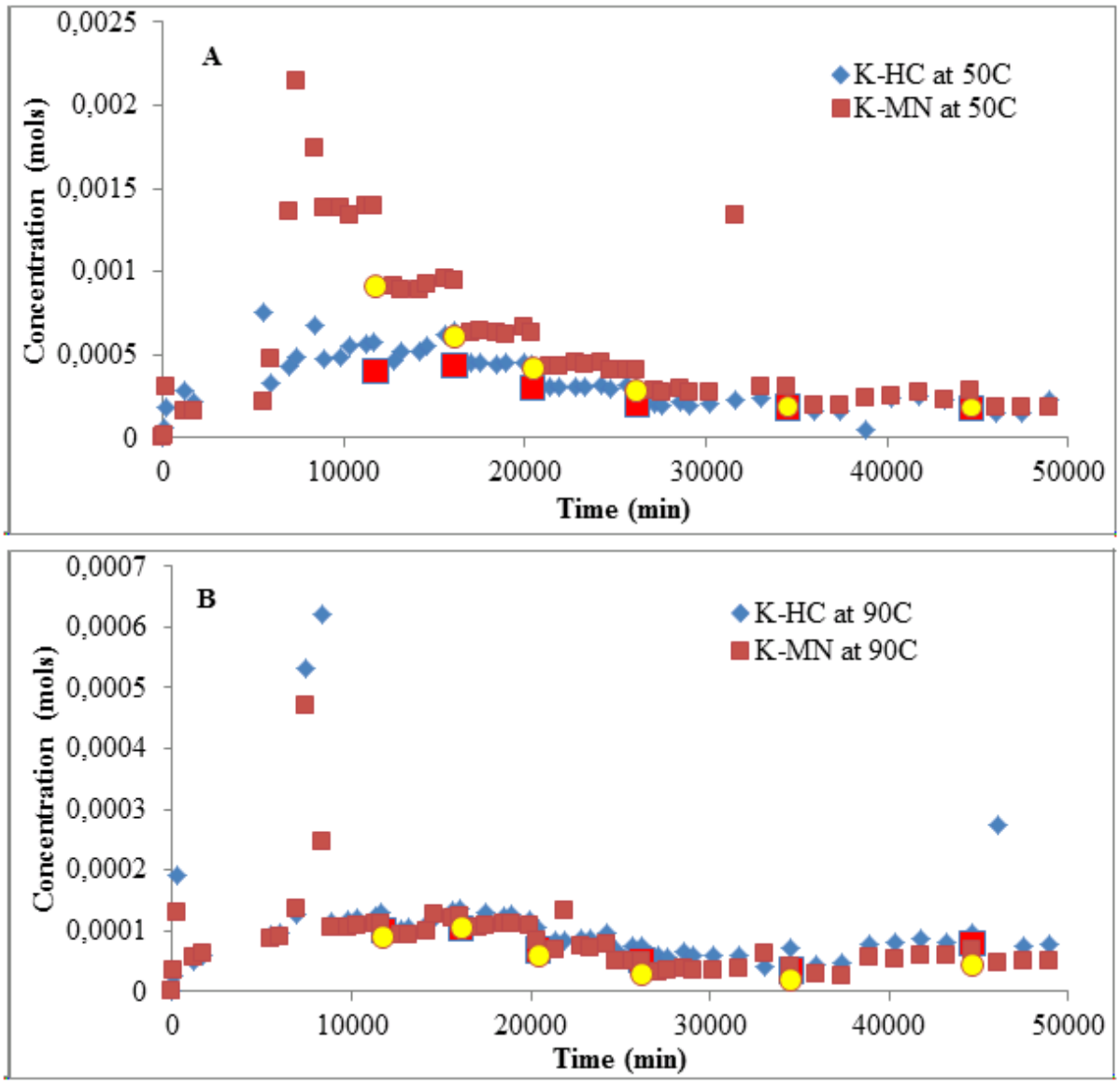

Figure 4.8: Decrease in aqueous concentrations (mols/L) of potassium with time from dissolution of hand and micronizer crushed basalt glass samples reacted at 50^{o}C and 90^{o}C temperatures.

4.4 Dissolution Rates of Nutrients from Basaltic Glass

The nutrients like phosphate (PO_4^{3-}), nitrate (NO_3^-) and potassium (K^+) are considered as the most important for efficient food production from agriculture practices. It is already mentioned that, deficiency of any of these nutrients is having serious impacts on plants growth, development and also on its food production. The dissolution rate in Table 4.2 is calculated from experimental rate (Table 4.1). It has been noticed from this study (i.e. batch reaction) that,

dissolution rates of different elements into aqueous solution increases with the increase of temperature (Table 4.1 & 4.2). So, at 90^{o}C elements are releasing relatively at a higher rate compared to 50^{o}C temperature. The rate is proportional to temperature and grain size distribution of the basaltic glass material. If we compare hand crush to hand crush and micronizer crush to micronizer crush basalt glass materials for PO_4^{3-} release rate which is almost two fold at 90^{o}C than at 50^{o}C. Similar dissolution rates have also been observed for other nutrients as well.

The dissolution rates of phosphate and nitrate (Table 4.1) were mostly given by fast dissolution of fine grain fractions (see Figs. 4.16 to 4.18). Phosphate is available for longer period (27days) at 50^{o} C temperature compared to 90^{o} C (for 21 days) (Fig. 4.6). The phosphate is released faster at 90^{o}C, but sorbents are forming faster, so more is sorbed. However, the availability of nitrate is for shorter time (13 days) at 50^{o} C compared to 90^{o} C (for about 27 days) (Fig. 4.7). This can be due to sorption properties of nitrate compared to phosphate. The dissolution rate of fluorine (F) element is higher relative to other tabulated nutrients and is considered as a poisonous for living organisms.

Table 4.1: Dissolution rates of nutrients from HC and MN basalt glass at 50^{o}C and 90^{o}C.

Nutrients form Basalt Glass	**Rate of Dissolution Experiment at 50^{o}C**		**Rate of Dissolution Experiment at 90^{o}C**	
	HC (mol/sec)	**MN** (mol/sec)	**HC** (mol/sec)	**MN** (mol/sec)
PO4	2.53E-11	1.81E-11	4.73E-11	3.47E-11
NO3	1.00E-11	2.00E-11	3.98E-11	3.98E-11
K	1.10E-10	8.73E-11	8.97E-11	5.53E-11
F	3.16E-11	8.32E-12	9.97E-11	7.94E-11

Table 4.2: Dissolution rates of nutrients from basalt glass at 10^{o}C.

Nutrients From Basalt Glass	**Dissolution Rate from Basalt Glass** (mol/sec)
PO_4^{3-}	1.32E-11
NO_3^{-}	1.514E-11
K^{+}	2.104E-11

4.5 SEM Analysis of Reacted Basalt Glass Material

4.5.1 EDS Analysis-Calculation of Elements to Si Ratios

Arbitrarily grains were selected from un-reacted basaltic glass sample (Fig 4.9) to get elemental spectrum through EDS analysis (Table 4.3). Afterward each element was converted to Si ratios to compare and see which elements are consuming into secondary phases formation.

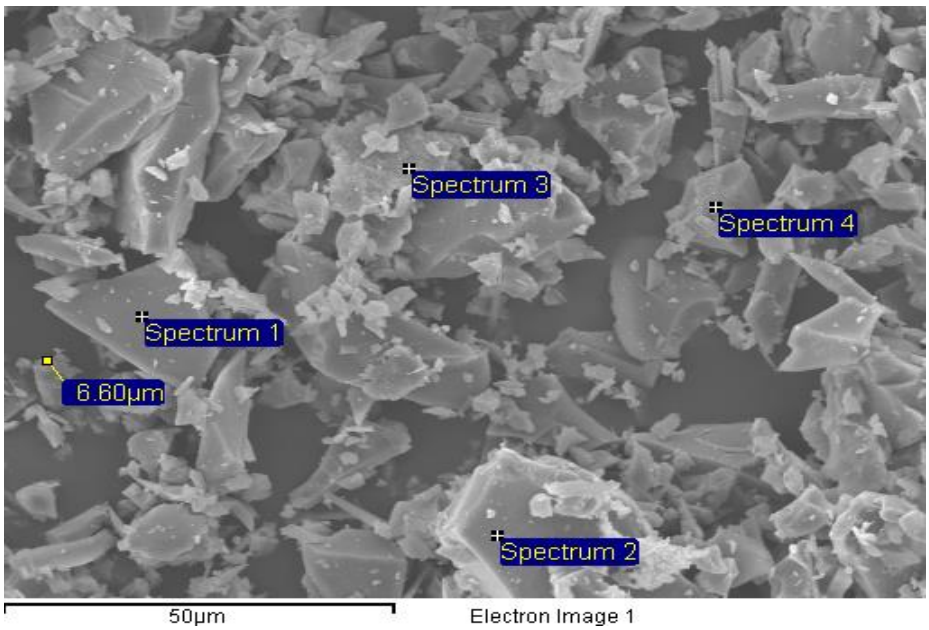

Figure 4.9: Image shows the selection of sites on the un-reacted basaltic glass for EDS analysis.

Table 4.3: Element to Si ratios for different EDS spectrums of un-reacted basaltic glass.

	Spectrum 1	**Spectrum 2**	**Spectrum 3**	**Spectrum 4**
Si	1.00	1.00	1.00	1.00
O	0.92	0.24	0.87	0.53
Mg	0.17	0.13	0.21	0.11
Al	0.29	0.24	0.30	0.16
Ca	0.39	1.04	0.45	0.29
Fe	0.39	0.83	0.45	0.24

Only reacted basaltic glass grains from both hand and micronizer crushed samples were selected at 90^{o}C experiment for EDS analysis (Appendix 4.2). Therefore, the reacted basalt glass samples at 50^{o}C were ignored for the EDS analysis due to not formation phases on the grains surfaces (Figures 4.10 and 4.11 in phase's identification section). After getting the elemental spectrum of reacted grains through EDS analysis, each element was then converted to Si ratio by dividing Si

values. It is done because to see either which element(s) are going to secondary phase's formation on grains surface. When the reacted and un-reacted elements to Si ratios were compared, there was no fruitful information perceived for the formation of secondary phases. Because, for the most of reacted glass samples elements to Si ratios were falling within the range of un-reacted elements to Si ratios except for few spectrums of calcium.

4.5.2 Analysis of Phases by Using SEM

The basaltic glass dissolution rate experiments were conducted for about 34 days. The two experiments were performed at two different temperatures i.e. 50^{o}C and 90^{o}C. Elements were released into aqueous solutions due to dissolution of basaltic glass. Some elements were capable to form secondary phases on the reacted basalt glass surfaces which were studied in SEM after the completion of experiments.

4.5.2.1 Hand Crushed Basaltic Glass Experiment at 50^{o}C

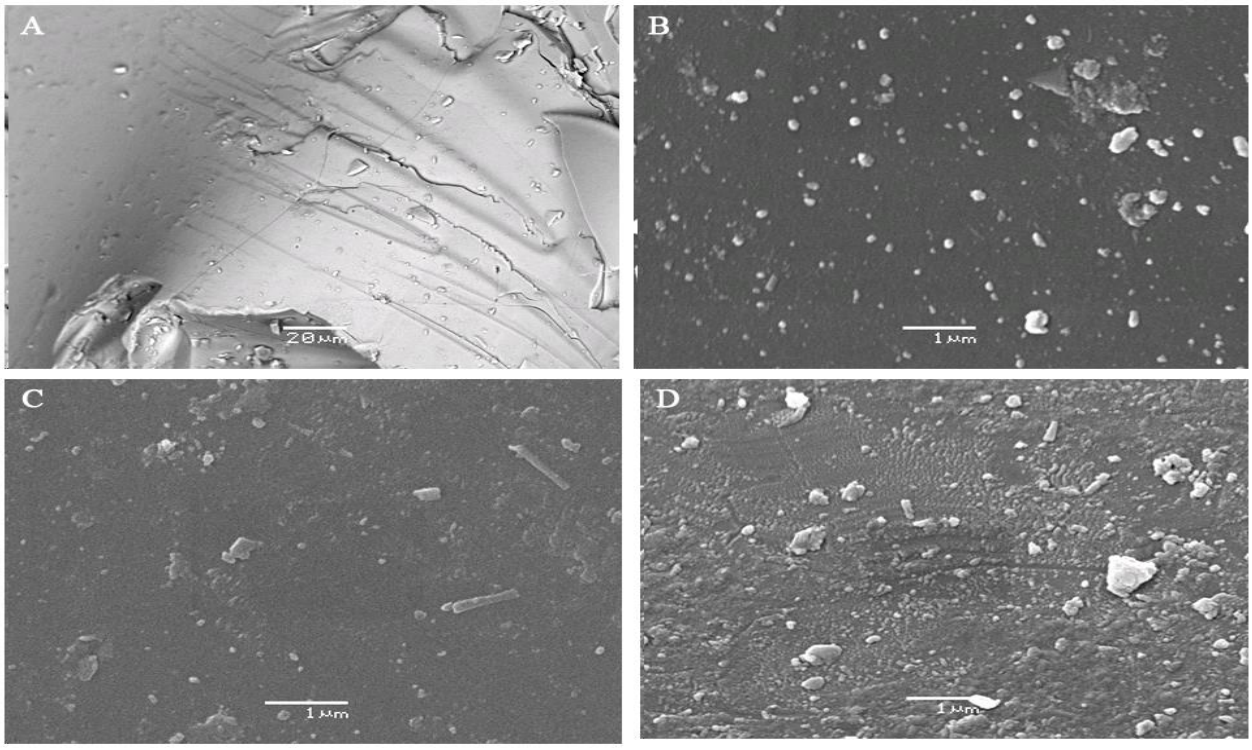

Figure 4.10: Scanning electron images for hand crushed basaltic glass. The basaltic glass before experiment (A). (B), (C) and (D) images are of the reacted glass at 50^{o}C which were magnified to X15000, X17000 and X15000 respectively.

Image (A) is showing the surface of un-reacted basaltic glass (Fig. 4.10). When the hand crushed glass was treated at 50^{o}C temperature for about 34 days then surface changes have been observed as compared to un-reacted glass under SEM analysis. It can be seen in image (B), (C) and (D) that due to dissolution of glass grains surfaces become smoother and also the sharp corners of the both smaller and bigger grains were converted to rounded edges. However, there has been not secondary phases seen especially in (B) and (C) but may be in case of (D) there has been just started the formation of secondary phases.

4.5.2.2 Micronizer Crushed Basaltic Glass Experiment at 50^{o}C

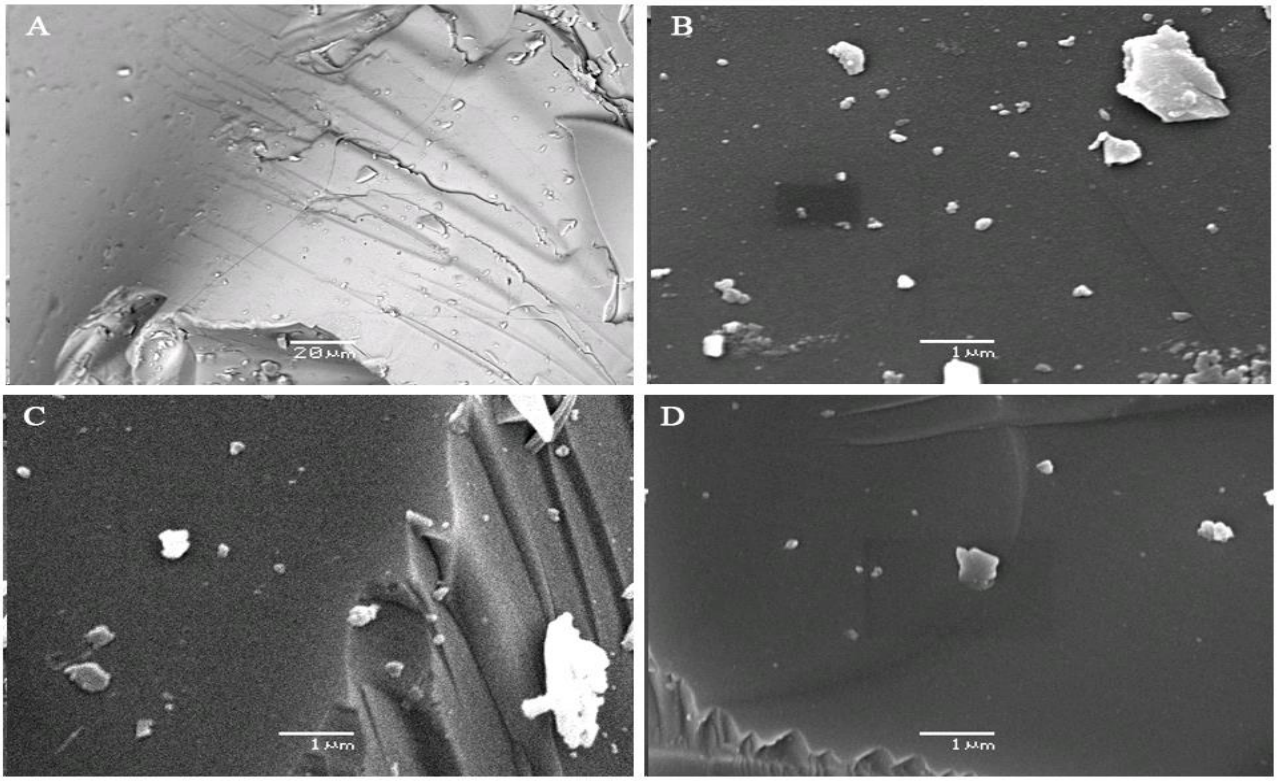

Figure 4.11 Scanning electron images for micronizer crushed basaltic glass. Image A is the basaltic glass before experiment. B, C and D images are of the reacted basalt glass at 50^{o}C which were magnified to X15000, X15000 and X15000 respectively.

When we compare the un-reacted basalt glass (A) with the reacted basalt glass (B, C and D) at 50^{o}C temperature (in Fig. 4.11), it is clearly seen that reacted glass surface is smoother even more than the hand crushed treated at the same temperature. Dissolution from the edges of grains

can also be observed. However, there is no secondary phase's formation seen on the grain surfaces in this case during SEM analysis.

4.5.2.3 Hand Crushed Basaltic Glass Experiment at 90^{o}C

When same hand crushed basaltic glass (A) was treated at increased temperature i.e. 90^{o}C, there has been formation of secondary phases seen on the grains surface (as from image B, to D) (Fig.4.12). The magnification was increased from image (B) to (D) to clearly identify which phases are forming on basalt grains. It was difficult to clearly scan the images of phases with the help of SEM due to very its very thin layer of its development. However, scan 4 was tried with high magnification and also by using micro meter scale, still did not manage to get clear image of phases to identify it. So, by comparing the un-reacted basalt glass (A) with the reacted basalt glass, the development of amorphous clay coating can be clearly seen on the grains surfaces.

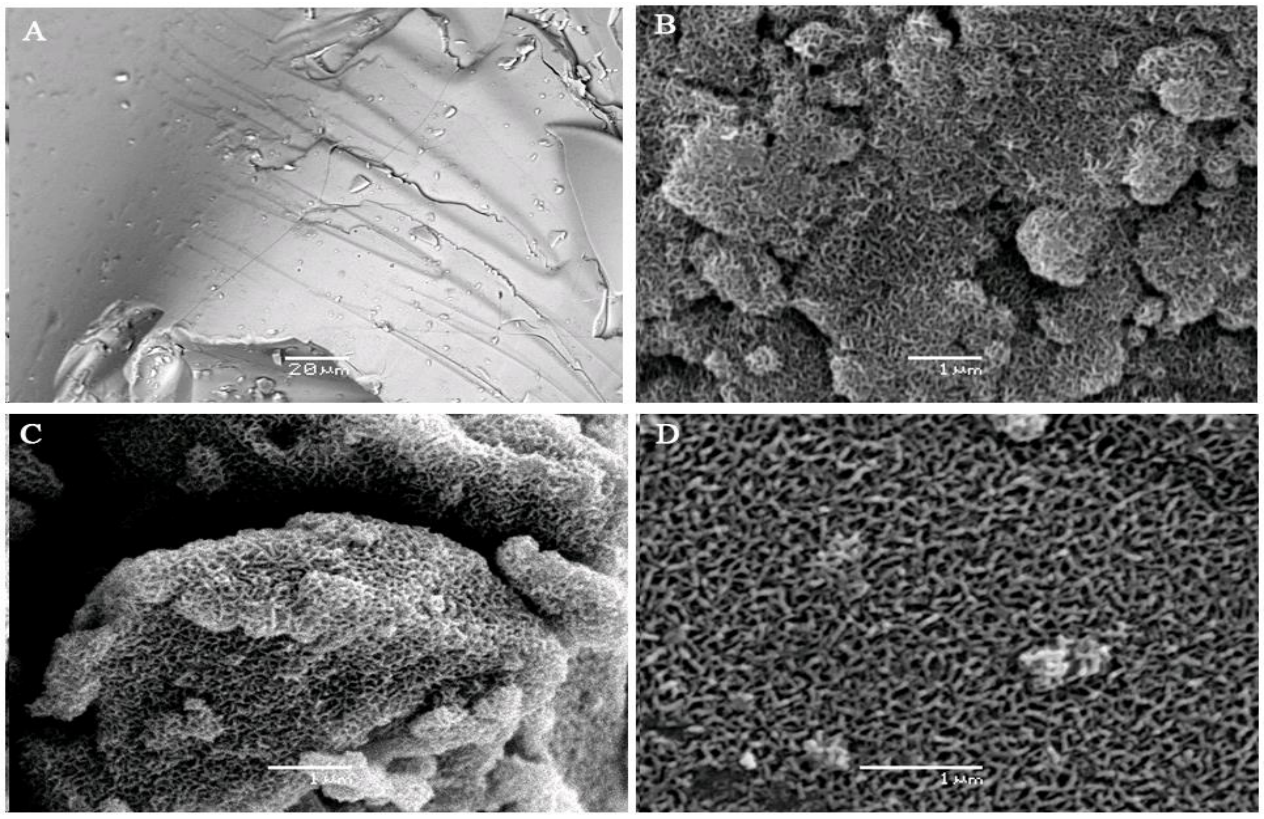

Figure 4.12: Scanning electron images for hand crushed basaltic glass. Image A is the basaltic glass before experiment. B, C and D images are of the reacted basaltic glass at 90^{o}C which were magnified to X15000, X17000 and X25000 respectively.

In Fig. 4.13, another randomly hand crushed reacted glass grain at 90^{o}C was chosen from the same sample (like in Fig. 4.12), where also found the (amorphous) clay phases development on grains (Fig. 4.13- from B to D). Therefore, image (A) is from un-reacted basaltic glass, which is acting as a reference for grains morphological changes when reacted at higher temperature.

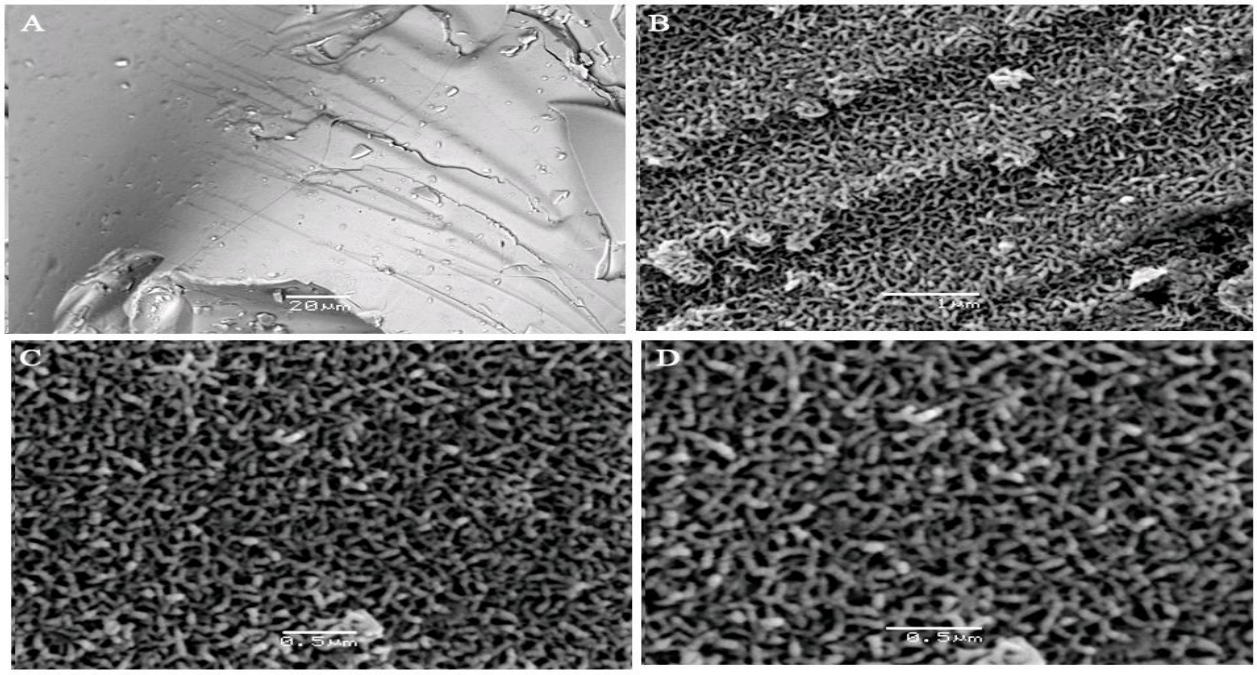

Figure 4.13 Another scanning electron images for hand crushed basaltic glass. Image A is the basaltic glass before experiment. B, C and D images are of the reacted basalt glass at 90^{o}C which were magnified to X20000, X30000 and X40000 respectively.

4.5.2.4 Micronizer Crushed Basaltic Glass Experiment at 90 ^{o}C

When micronizer crushed basaltic glass was treated at 90^{o}C for about 34 days, there also has been observed the secondary phase formation in SEM analysis (Figs. 4.14 & 4.15). However, in both these figures, image (A) is from un-reacted basaltic glass. It is just used for comparison with images from B to D, to see the surface morphological changes and also formation of secondary phases on grains surface.

The formation of flat and spherical amorphous phases is similar to the hand crushed sample (Fig. 4.12 & 4.13), which were treated at the same temperature. This reveals that the probably formation of clay phase on grains.

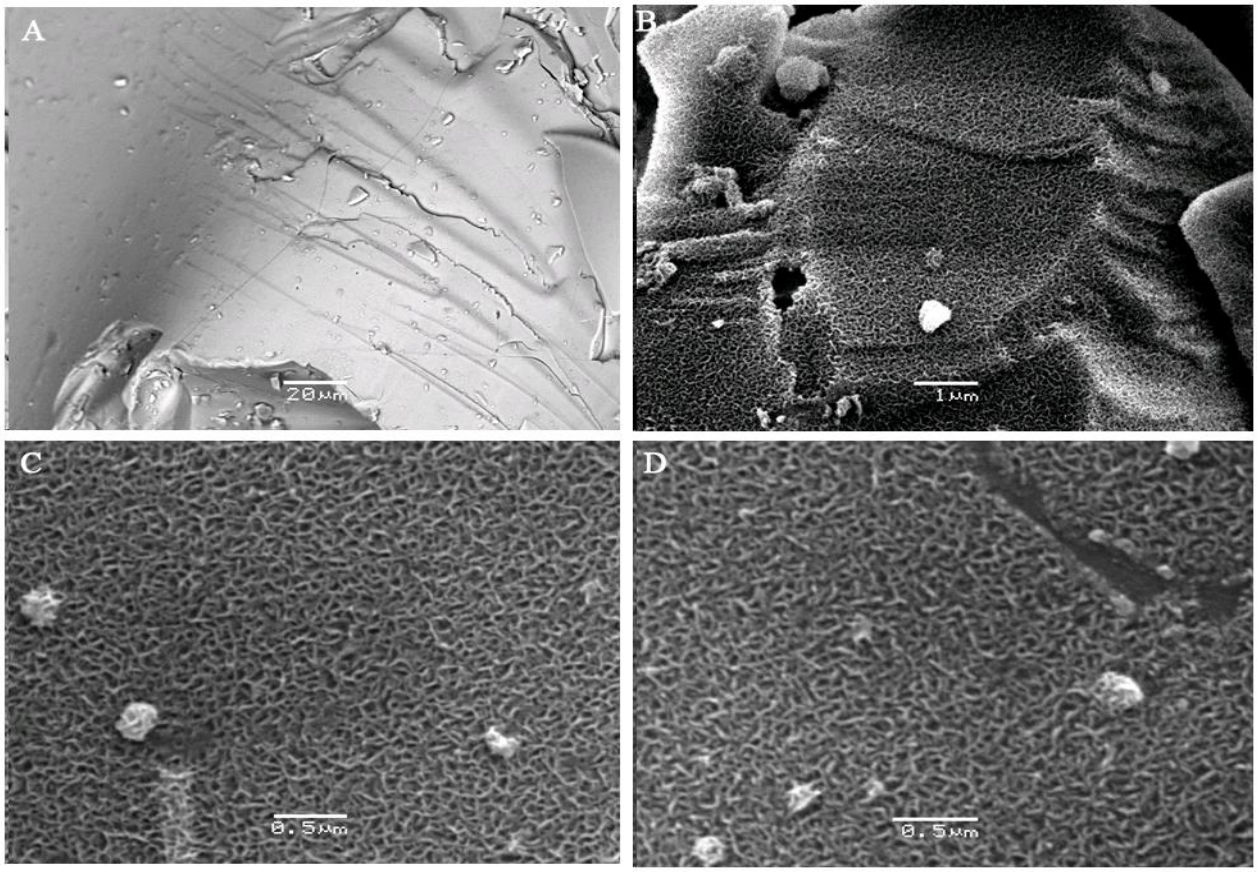

Figure 4.14: Scanning electron images for micronizer crushed basaltic glass. Image A is the basaltic glass before experiment. B, C and D images are of the reacted basalt glass at 90^{o}C which were magnified to X13000, X30000 and X35000 respectively.

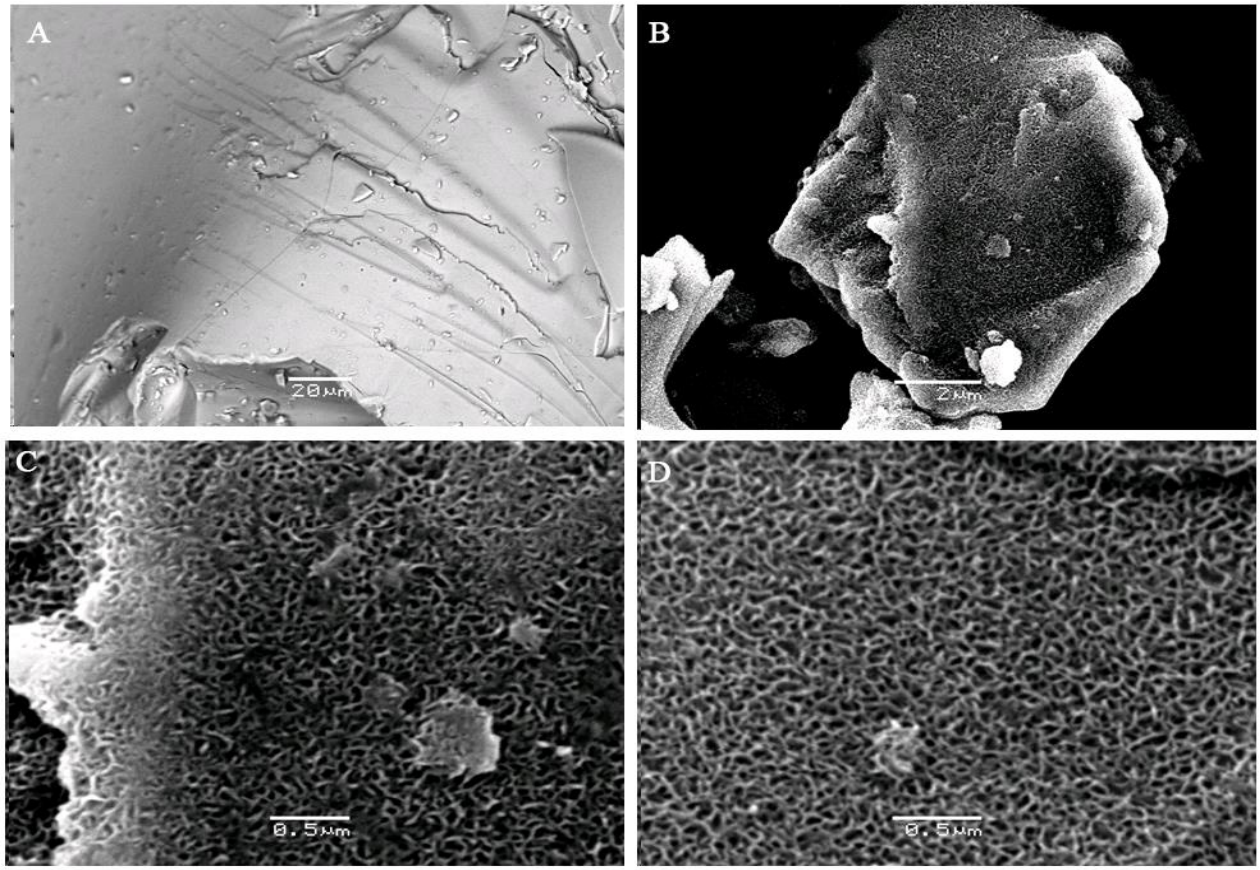

Figure 4.15: Another scanning electron images for micronizer crushed basaltic glass. Image A is the basaltic glass before experiment. B, C and D images are of the reacted basalt glass at 50^{o}C which were magnified to X9000, X33000 and X37000 respectively.

4.6 An Ideal Condition for glass Particles Dissolution-Matlab Analysis

4.6.1 Dissolution Properties of Initial Basaltic Glass Samples

The dissolution properties of initial hand crushed and micronizer crushed basaltic glass samples have been analyzed in MATLAB program at different temperature ranges and also in different time steps. The program for this analysis was made by Helge Hellevang; the obtained results are presented below.

4.6.1.1 Hand Crushed Basalt Glass Sample Dissolution at 10°C for 1 Year

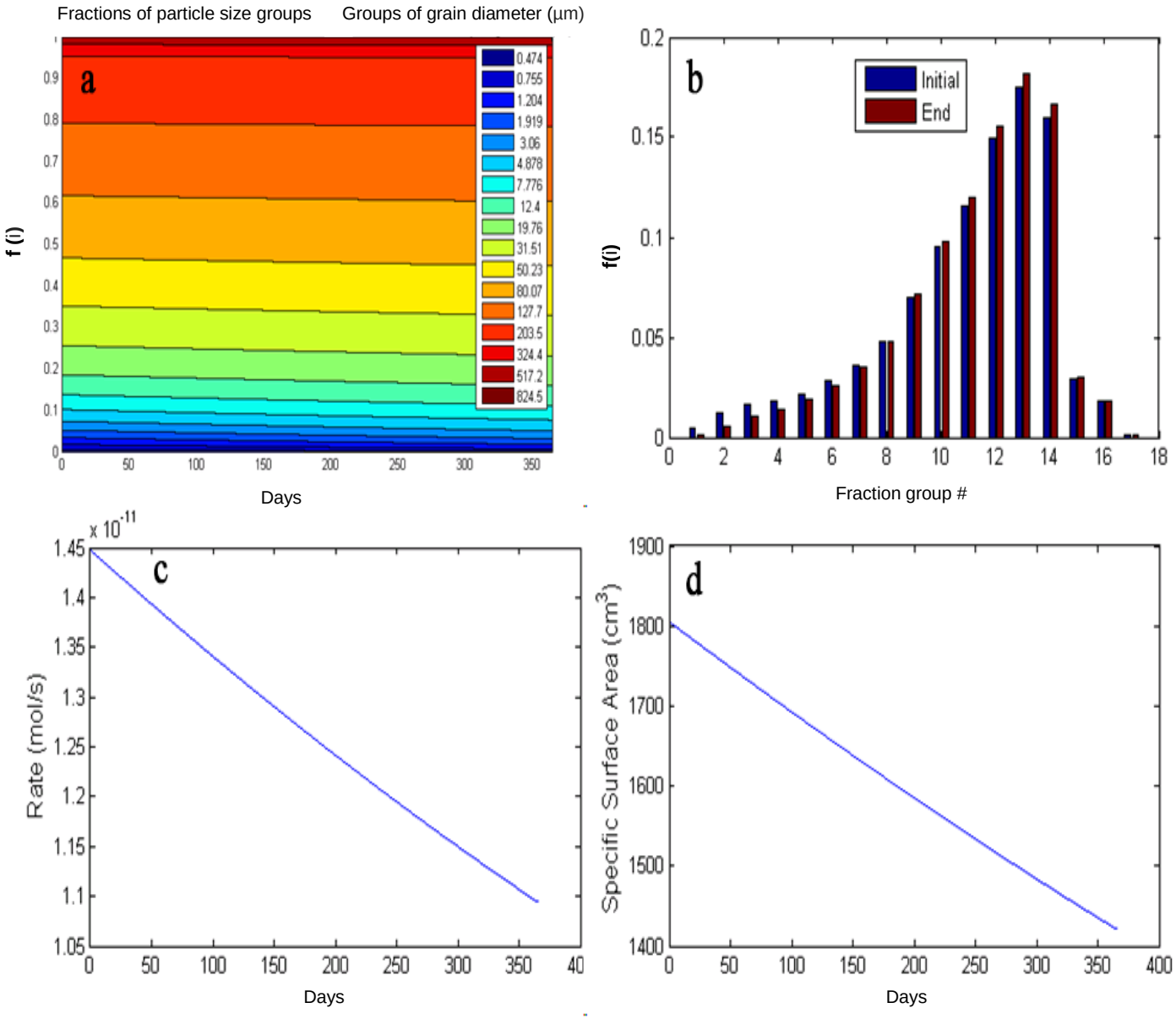

Figure 4.16: The images of initial hand crushed basaltic glass sample reaction at 10°C for 1 year, shows that; (a) the dissolution of different fraction of particle size groups throughout year, (b) the dissolution of individual fraction of particle size within different fraction group numbers, (c) the dissolution rate (mol/sec) of particles in one year and (d) change in specific surface area (cm^3) of particles in different time steps of a year.

Fig. 4.16 shows, when hand crushed basaltic glass was reacted at 10°C for one year time period, the fraction of very fine particle size groups (i.e. groups of grain diameters of 0.474µm, 0.755µm

and 1.204µm) were dissolving only within one year (a). Therefore, as the groups with an increasing grain diameter, dissolution was decreased and become quite minor in groups of highest grain diameters. The results of figure (b) are supporting figure (a), where the fractional groups with fine grains (from 1 to 6 groups) were disappeared more relatively to the coarser grains at the end of year. Whereas, those groups which were consisted with highly coarser grains (from 8 to onward) did not affected and their overall fractional volume increased in sample at the end of year. This revealed that coarser grains were remained unaffected in the sample at the end of experiment.

The dissolution rate was decreased by factor of $0.35x10^{-11}$mol/sec within one year (c), which is mostly given by dissolution of very fine fraction of grains. Therefore, no change has been observed in dissolution rate and it was continually started to decline at constant rate. Thus, figure (d) is supporting all the previous results. As, the overall initial specific surface area of the sample was 1800cm^3 which is reduced by factor of 380cm^3 and still seemed to decline at a constant rate after one year.

4.6.1.2 Micronizer Crushed Basalt Glass Sample Dissolution at 10°C for 1 Year

In Fig. 4.17 (a), it is showed that only very fine fractional particle size groups were dissolving fast compared to coarse grains and hand crushed sample as well. It due to presence of higher fraction of fine particles in sample than the hand crushed sample. The results in figure (b) are supportive to (a), where groups (i.e. from 1 to 5 groups) with finest grain fractions were dissolved much and left very little in their final fractions as compared to subsequent increasing grains size. Even, from medium to largest grain fractions became much prominent in the final sample.

The faster dissolution rate of micronizer sample (c) than the hand crushed sample which made confirm the higher specific surface area (in figure d) provided by more number of fine grains. The dissolution rate is decreased by factor of $1.5x10^{-11}$ mol/sec after a year as the specific surface area decreased (by 880 cm^3) over the same time but declination of rate was still at constant pace.

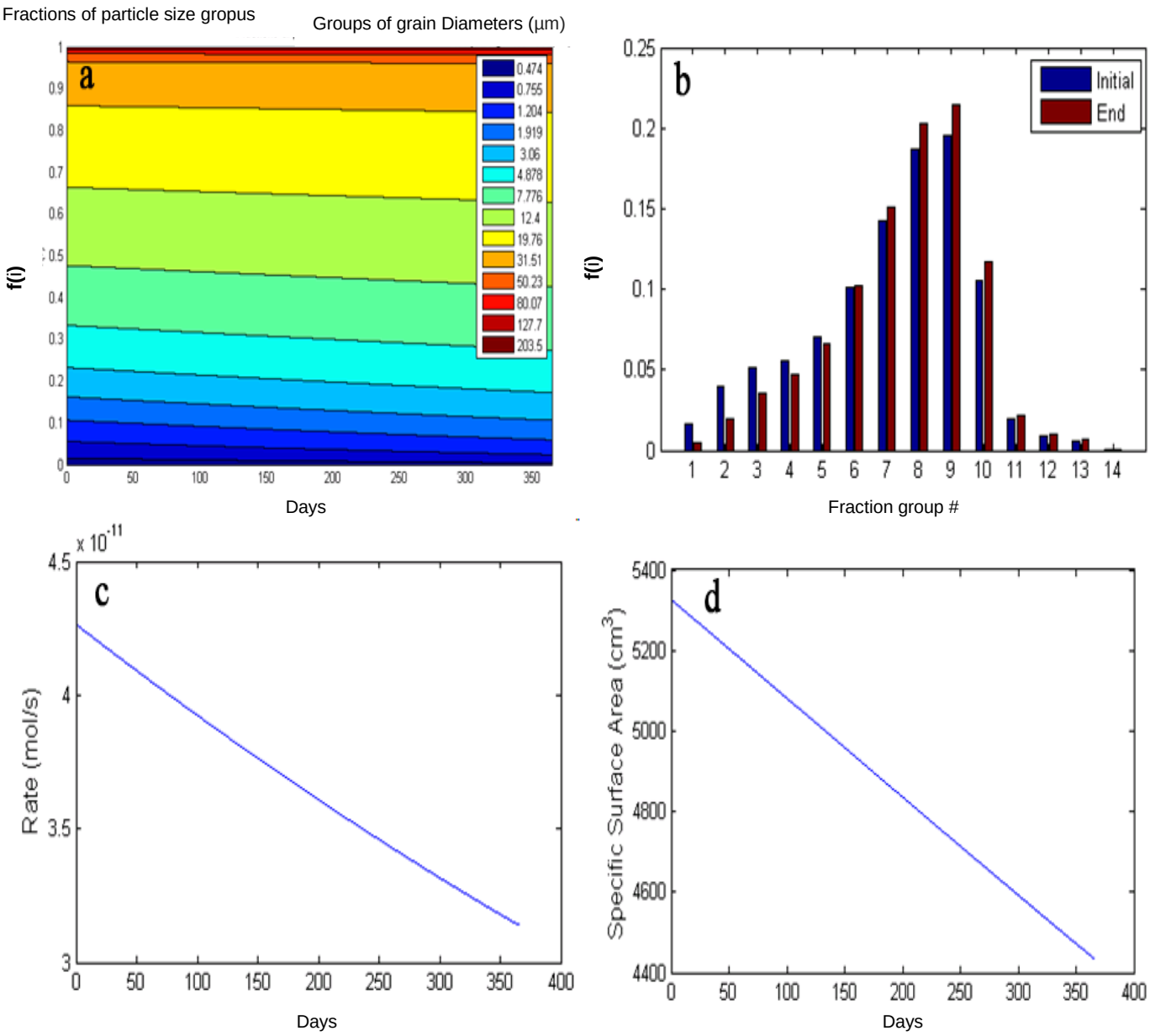

Figure 4.17: The images of initial micronizer crushed basaltic glass sample reaction at 10°C for 1 year, shows that; (a) the dissolution of different fraction of particle size groups throughout year, (b) the dissolution of individual fraction of particle size within different fraction group numbers, (c) the dissolution rate (mol/sec) of particles in one year and d) change in specific surface area (cm^3) of particles in different time steps of a year.

4.6.1.3 Synthetic Crushed Basalt Glass Sample Dissolution at 10°C for 1 Year

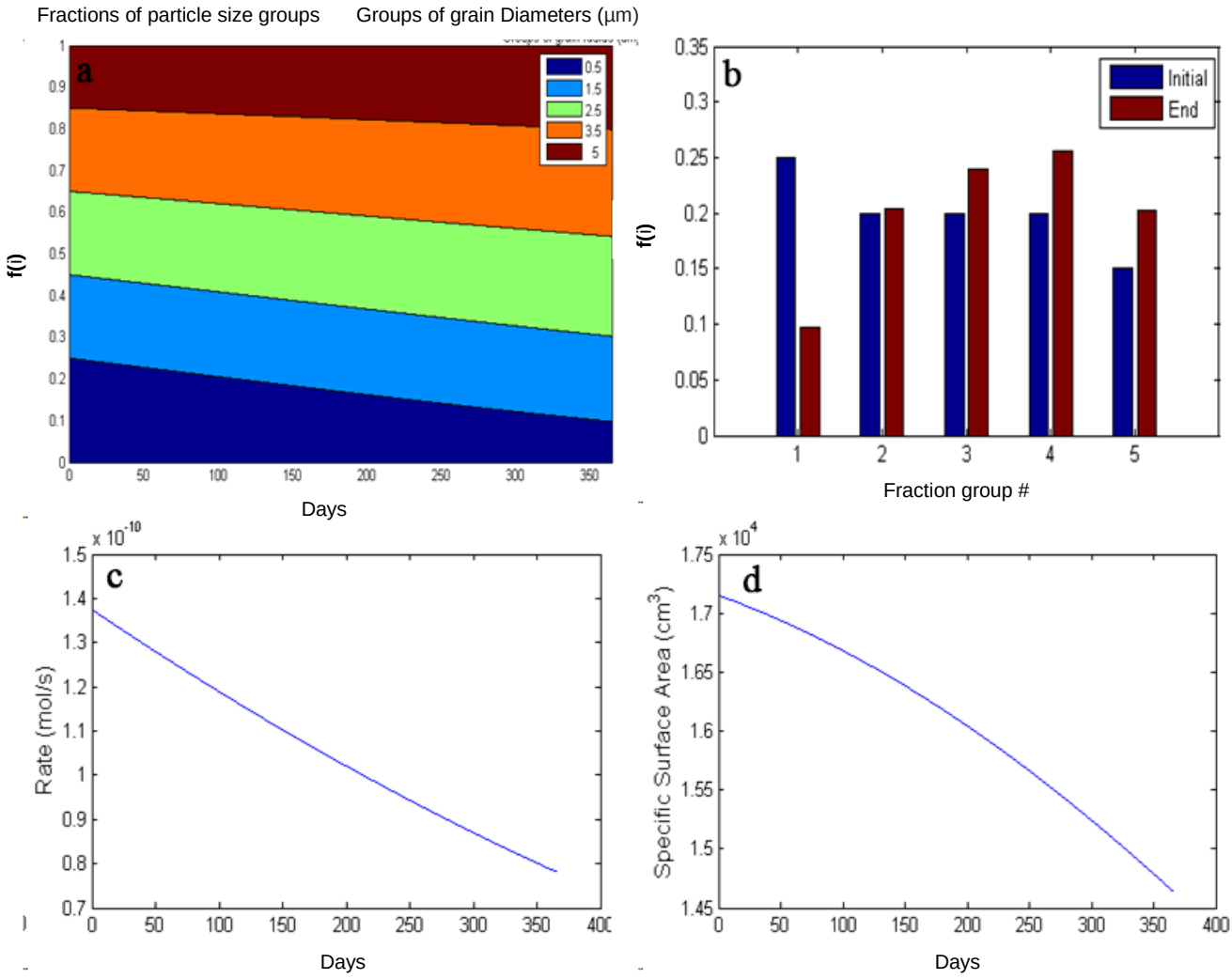

Figure 4.18: The images of synthetic crushed basaltic glass sample reaction at 10°C for 1 year, shows that; (a) the dissolution of different fraction of particle size groups throughout year, (b) the dissolution of individual fraction of particle size within different fraction group numbers, (c) the dissolution rate (mol/sec) of particles in one year and d) change in specific surface area (cm^3) of particles in different time steps of a year.

The dissolution was only observed for finest fraction of particle size belongs to group of smallest grain diameter (i.e. 0.5 µm) (Fig. 4.18). This group of grain diameters remained almost one third at the end of year. All groups are dissolving (fractions of each group), so if one group is reduced (the finest fractions), then the other will increase (passively increased because they dissolve less

than the finer grains). This result is much elaborated in figure (b), where it showed, smallest particles were depleted much which were belonging to first group. Therefore, fraction of larger grains increased in the final sample after one year.

Over period of one year the dissolution rate was dropped around $0.6x10^{-10}$ mol/sec factors. The fast drop in rate was only due to rapidly dissolution of finest fraction of grains. The corresponding specific surface area of sample was lowered about $0.25x10^{4}$ cm^{3} factors over same time period.

5.0 Discussion

5.1 Amount of Basalt Glass Required for the Agriculture Production

If the agricultural soil only needs PO_4^{3-} which will be the limiting phase in the future because of peak-phosphate, then amount of basalt glass can be used as an alternative to conventional phosphate sources. By using the experimental dissolution rates of nutrients from basaltic glass at 10°C (Table 4.2) and actual nutrients requirement (kg/ha/year) for crops production (Table 5.1), the quantity of basaltic glass that will be needed (in Kg/ha/year) found in Table 5.2. Wheat and rice crops are used as a reference for the calculation of current requirement of nutrients from basalt glass quantity have used. The amount of basalt required to supply sufficient nitrate and potassium, is two times and four times respectively that required for phosphate. Size of particles is playing major role in basalt quantity needed per hectare per year.

Table 5.1: Quantity of different nutrient's fertilizers required for crops production.

Nutrients From Fertilizers	Crops	Fertilizer Needed (kg/ha/year)	Source
PO_4^{3-}	Wheat	23-28	McKenzie (2013)
NO_3^-	Wheat	40-80	Sahota (2009)
K^+	Rice	166	Srinivasarao et al., (2011)

Table 5.2: Quantity of Basalt glass required for crops production at 10°C.

Nutrients From Basalt Glass	Country	Basalt Glass Needed (kg/ha/year)
PO_4^{3-}	Wheat	462
NO_3^-	Wheat	930
K^+	Rice	1852

The aqueous concentrations of PO_4^{3-} (Fig. 4.6), it is higher around 22 days and after that dropping very fast to almost zero concentrations. This can be probably be explained by one fast dissolution of fine grains and secondly the sorption of PO_4^{3-} is occurring in batch reactors. The sorption of these nutrients explained in many studies, a few studies (like; Haygarth and Jarvis (2002); Cahn et al., (1992)) has treated well the sorption of phosphate and nitrate in soils. The

supply of the phosphate in the soil depends upon the quantities of reactive iron, aluminum, and calcium in the soil and the moisture characteristics of the soil etc. (Huffman and Taylor, 1963). According to Haygarth and Jarvis (2002), numerous studies have been focused on clay elements, hydroxides and metal oxides and it is proposed that the important sites for anions adsorption are surface coatings of Fe^{3+}, Al oxides and oxyhydroxides. Hydroxyl groups (OH^-) are formed at the solid-water interface. The exchange process enables phosphate to adsorb with the surface hydroxyl groups. The strength of binding depends on the pH of solution, number of exchangeable hydroxyl groups per unit area of grain and specific surface area of the grain.

According to Cahn et al., (1992), he reported from different studies that, the of sorption of NO_3^- is to be due to attraction positively charged sites on kaolinitic and allophanic materials, and protonated hydroxyl groups of aluminum and iron oxides. And the sorption of NO_3^- increases with decreasing pH and with increasing electrolyte concentration. Sorption can cause bio-unavailability of nutrients from soil system. The calculated dissolution rates in Table 4.1, for these nutrients were mostly given by initially fast dissolution of very fine fractions of particle (Fig. 4.16 to 4.18). After period of time formation of clay phases (probably smectite) on grains faces (Fig. 4.12 to 4.15) started to sorb the aqueous concentration of phosphate and nitrates (Fig. 4.6 & 4.7). Even though phosphate is seen to be sorbed by secondary phases forming from the basaltic glass, the rate appears sufficient, and basaltic glass can therefore be used for nutrient supply, especially for phosphate and nitrate but need to adopt some remedial measures to avoid from sorption in the soil system.

5.1.1 Can Basalt Glass be used as a Fertilizer?

The amount basalt glass is looking feasible for phosphate compared to nitrate and potassium to add to the soil, because it is almost two fold and four fold less required respectively. If we compare basalt glass mass to normal fertilizers for phosphate, nitrate and potassium, basalt glass needed 18, 16 and 11 times respectively than the current application rate. Relatively less hundred kg of basalt glass required compared to nitrates and phosphate, as 462 kg/ha/year for phosphate, 930 kg/ha/year for nitrate and 1852 kg/ha/year for potassium. This needed quantity of basalt glass is higher for phosphate, especially for nitrate and potassium respectively. Crushing of basalt glass to very finer grains is one of the major options that can enhance the dissolution rate of nutrients and finally less quantity of basalt glass will be needed, especially for phosphate.

Crushing of basalt glass to finer grains is possible for phosphate, but more material is required for K^+ or NO_3^-, or it has to be crushed to an even finer material to support K^+ and NO_3^-. Crushing of basalt glass along with other treatment for phosphate will add more energy and cost, this question can be addressed by continuing this research in future.

5.2 Formation of Secondary Phases from Dissolution of Basaltic Glass

The formation of secondary phases on hand and micronizer crushed grains surface were only observed at higher temperature (i.e. 90^oC) environment (Fig. 4.12 to 4.15). This may be due to high release of elements in aqueous solution that made it capable to convert into secondary phases. In our case, it is seen that clay phases are forming (Fig. 4.12 to 4.15), probably looks like smectite (Fig.5.1 & 5.2). Due to thin layer of phase development it was not possible get high resolution images to exactly identify them with the help of SEM. The decrease in dissolution rates of some elements (Fig. 4.5) shows that elements are probably changing into phases or just precipitating in the system.

Therefore, to make sure which kind of these phases are forming from basalt glass dissolution, few relevant studies have been investigated. Formation of phase (from Fig. 4.12 to 4.15) is quite similar to the Pelayo et al., (2011) study, where smectite phase is forming from volcanic glass fragments (Fig. 5.1).

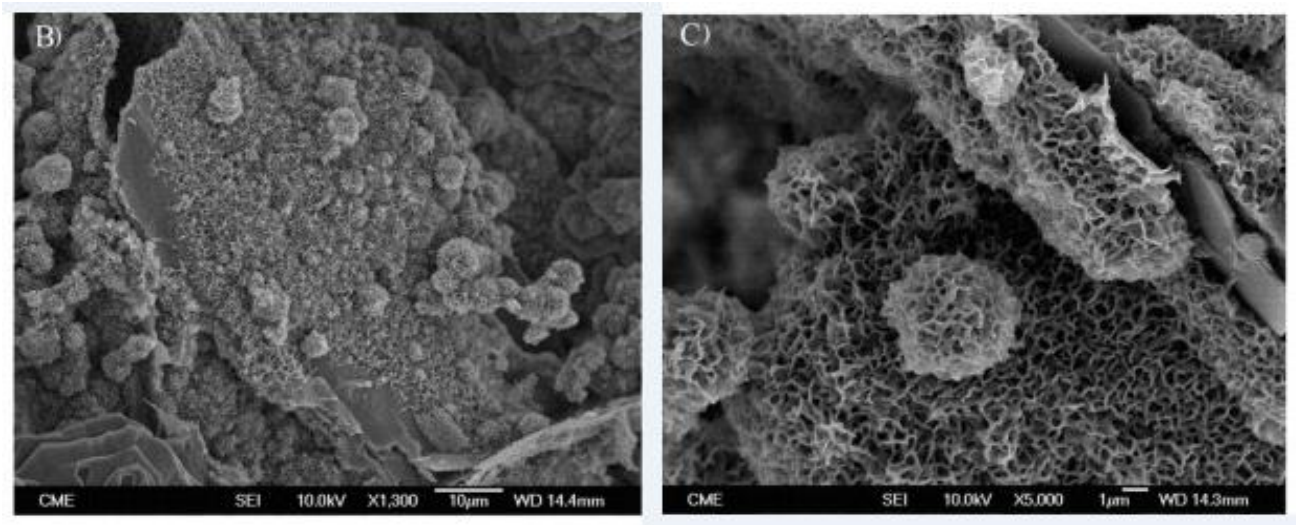

Figure 5.1: Images from SEM analysis of: (B) probably transformation of volcanic glass fragments into smectite; (C) a detail of image (B), where spherical aggregates of smectite with honeycomb morphology can be seen (Adopted from Pelayo et al., 2011).

The clay phase which is formed in this experimental work (from Fig. 4.12 to 4.15) is also quite similar to another study of Gong et al., (1998) (Fig. 5.2). Where it shows the morphological changes of the glass surface with passage of time and honeycomb like smectite layer has developed locally and afterward got matured and also shows development of other phases on its surface such as opal, analcime, gyrolite and a spherical calcium silicate.

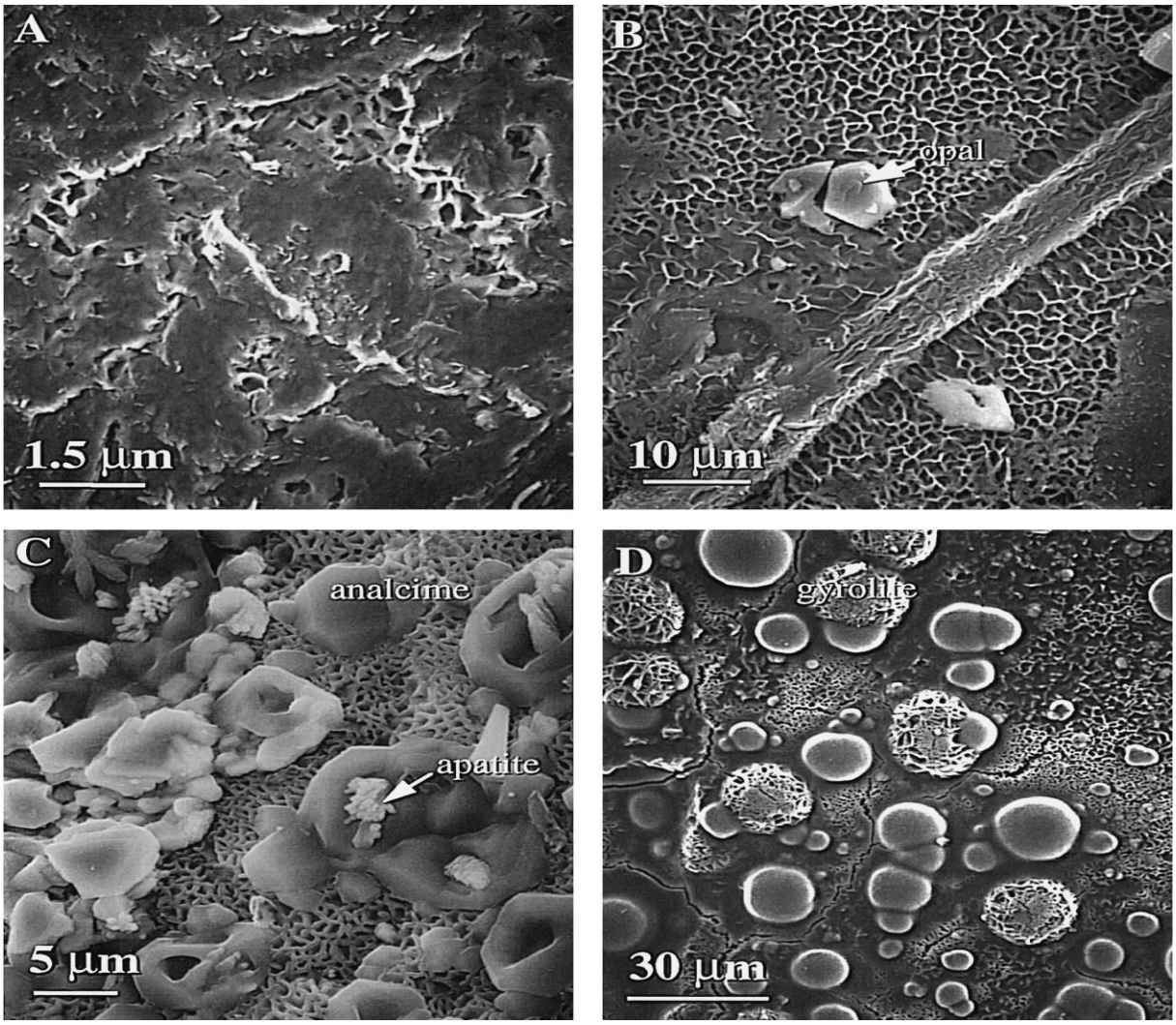

Figure 5.2: A sequence of micrographs from SEM analysis is showing the morphological changes of the glass surface with increasing alteration time. (A) Honeycomb like smectite layer has developed locally, without secondary phase was found on it. (B) Honeycomb like smectite layer is now well developed. Only opal precipitation occurs on the surface, as pointed by the arrow. (C) Honeycomb like smectite layer is very well developed with precipitates of like analcime and apatite on surface. (D) gyrolite and amorphous calcium silicate are the two major precipitates occurred on the 'honeycomb' of smectite crystals (Adopted from Gong et al., 1998).

5.3 Dissolution Rates of Basaltic Glass at 10^{o}C, 50^{o}C and 90^{o}C

Dissolution Rates at 10^{o}C

When comparing hand crushed (Fig. 4.16), micronizer crushed (Fig. 4.17) and synthetic crushed (Fig. 4.18) basalt glass sample's results, which were obtained in an ideal environment, showed that only very fine particle fractions (i.e. around 1µm grain diameters) are providing the effective dissolution rate throughout the year. Thus, particle diameters greater than 1.5µm were remained almost unaffected at 10^{o}C temperature after one year.

Dissolution Rates at 50^{o}C

The calculated dissolution rates (at 50^{o}C) of basalt glass from Matlab are dropping at constant rates (Fig. 5.3-a & b). Therefore, the experimental dissolution rate of basalt glass is slowing down after 10 days (Fig. 5.3-c). The Matlab analysis is showing an ideal condition for calculation of rates, whereas; the experimental setup is somehow looks like to natural conditions. In Matlab analysis, constant dropped in rates were only provided by dissolution of grains but experimental dissolution rates were slowed down may be due to the grains surfaces were passivatd by secondary coatings. The overall dissolution rate for micronizer sample was higher compared to hand crushed sample (Fig. 5.3- a & b), it is may be due to more fine and homogeneous fraction of grains are present. And also, the final micronizer dissolution rate (b) is higher than the experimental rates (c) (for hand and micronizer crushed samples), may only because of difference in grains surface coating factor. The average experimental dissolution rates at 50^{o}C for hand and micronizer (Fig. 5.3-b) basaltic glass samples are $1.25x10^{-10}$ mol/sec and $8.144x10^{-11}$ mol/sec respectively.

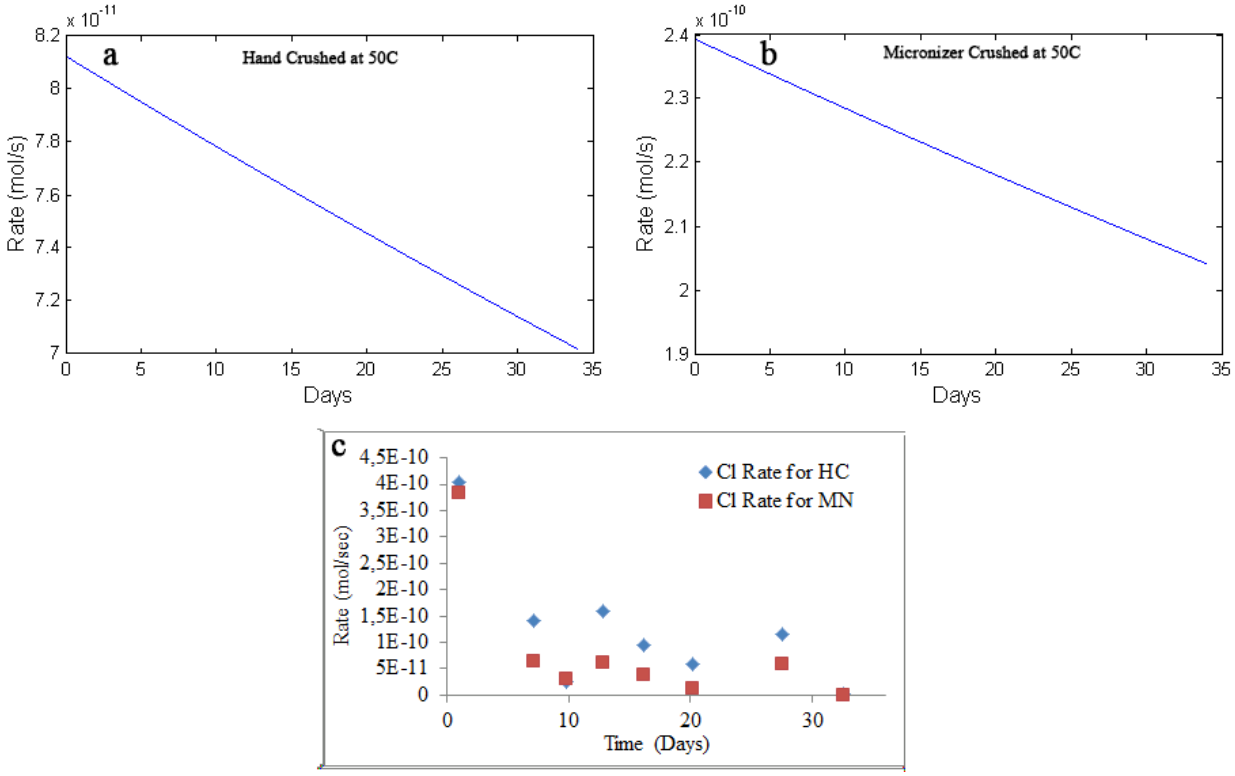

Figure 5.3: Comparison of Matlab (a & b) and experimental (c) dissolution rates of basaltic glass at 50°C. Notice that for the experiment, rates drop by one order of magnitude, whereas the drop is small for the simulated material.

Dissolution Rates at 90°C

Dissolution rates are getting slower after 10 days, it can be explained that, it may be because of the formation of secondary phases on grains surfaces which were hindering the dissolution of basaltic glass. The initial dissolution rates are fast due to rapidly dissolution of fine grains form both samples (hand and micronizer) at two different temperatures. Therefore, the average experimental dissolution rates at 90°C for hand and micronizer basaltic glass samples (Fig. 5.4-b) are 2.409×10^{-10} mol/sec and 6.27×10^{-10} mol/sec respectively.

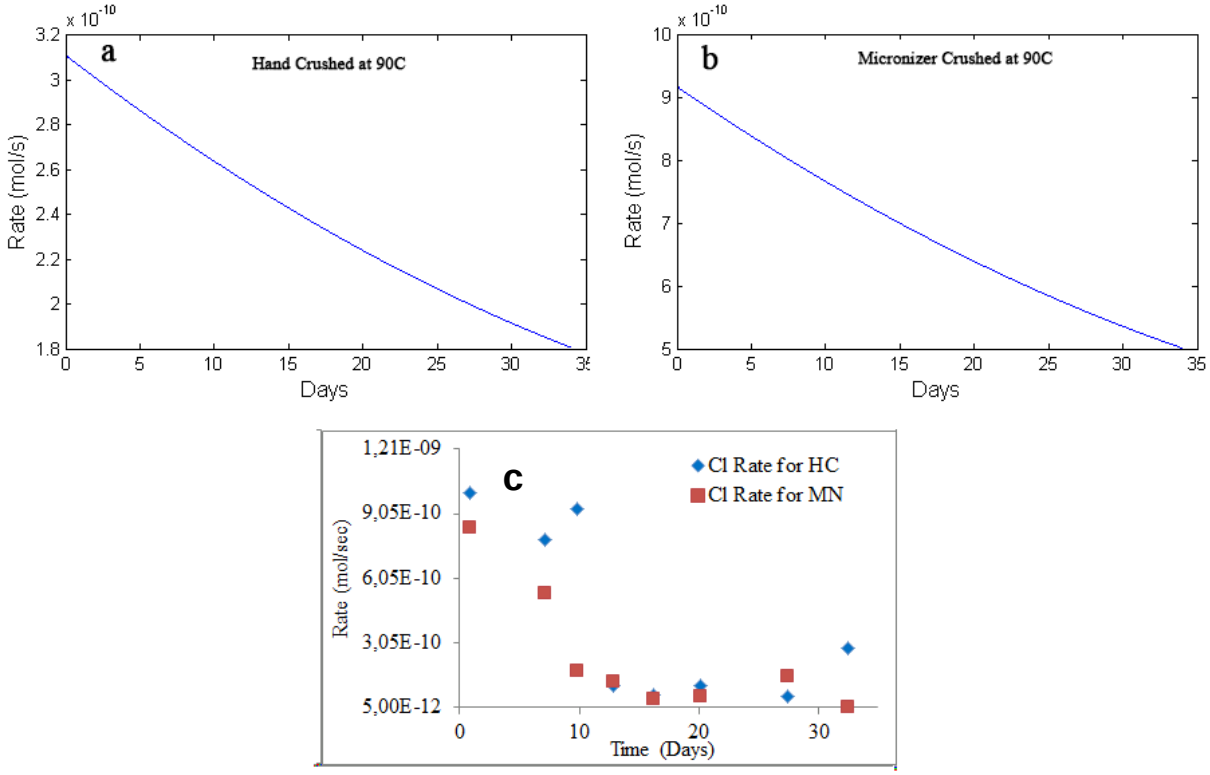

Figure 5.4: Comparison of Matlab (a & b) and experimental (c) dissolution rates of basaltic glass at 90°C.

The simulated rates drop to roughly half after 30 days. The experimental drops much more than to half, so it is not a good match between the simulated and the experimental. Possibly drop in rates are formation of surface coatings, which would make the experiments drop faster than the simulations since simulations are not taking into account surface passivation by coatings. The exchange process enables phosphate to adsorb with the surface of Fe^{3+}, Al oxides and hydroxyl groups (Haygarth and Jarvis, 2002). Form many conducted studies it has been concluded that the dissolution rates of minerals and glasses are to be proportional to their interfacial surface area (e.g. Pačes, 1983; Helgeson et al., 1984; Lasaga, 1984; Siegel and Pfannkuch, 1984; Schott and Oelkers, 1995; Oelkers, 2001; Schott et al., 2009).

5.4 Other Factors Affect Basalt Glass Dissolution Rate

Natural solutions in soils often contain complex forming ligands, which are responsible for to influence dissolution rates at acid conditions (Ullman and Welch, 2002). It is seen that natural glasses are relatively less stable compared to igneous elements at the Earth's surface it is only

because of glass retains more energy from its parent magma than the elements (Gislason and Arnorsson, 1990). So at neutral to alkaline pH environments, the basaltic glass dissolves significantly faster compared to basaltic elements (Daux and Guy, et al., 1997). At regional scales, weathering of basaltic glass supplies dissolved nutrients which are made available to vegetation cover or also it can neutralizes catchment areas which were affected by acid rain. (cf. Navarre-Sitchler and Brantley, 2007).

5.5 Recommendation

1. Particle size affects the rate of dissolution. Large particles take longer to dissolve than smaller particles. Therefore, large particles of a basaltic glass must be broken apart to finer (effective size) enable to dissolve efficiently to provide nutrients (i.e. phosphate, nitrate) throughout year.
2. Pretreatment of basaltic glass grains (like removal of silica structure and chemical treatment of grains etc.) to efficiently supply phosphate and nitrate available for plants.
3. Adjust the soil pH to avoid from the sorption of nutrients in soils.

6.0 Conclusion

In this study, we used basaltic glass from Iceland to see that it has enough capacity to release sufficient amounts of nutrients, especially the phosphate to use it as an alternative to conventional fertilizers. For this purpose, the batch reaction (close system) experiment was used; where hand and micronizer basalt glass crushed samples were reacted at 50^{o}C and 90^{o}C temperatures. The experiments show that dissolution rate of basalt glass is highly connected with grain size distribution and temperature. The initial dissolution rates of nutrients increases during fast dissolution of fine grains but with the passage of time it slows down. Particularly, the dissolution rates of phosphate and nitrate drops soon, it is suggested that faster dissolution of finer grains and strong sorption of these nutrients on grains. The release rate of fluorite is relatively high. The calculated dissolution rates for phosphate and nitrate shows that a basalt glass has enough capacity to use an alternative to conventional fertilizer (e.g., for phosphate). The release rates of nutrients at10^{o}C, suggest that much less two fold and four fold quantity of basaltic glass needed for phosphate (462 kg/ha/year) compared to nitrate (930 kg/ha/year) and potassium (1852 kg/ha/year) based on current normal fertilizer application rates . Basalt glass can be feasible for phosphate compared to nitrate and potassium by crushing it to finer grain size but it will need energy. It's almost 18, 16 and 11 times more required for phosphate, nitrate and potassium respectively compare to normal fertilizers. The grains size diameter range from 0.5 to almost 2 um can eventually last for >1 year to 5 years, if applied in the field with proper grain size distribution. The evidences from elements to Si ratios (Appendix 4.2), from change in concentration of elements from aqueous solutions (Fig. 4.6 & 4.7 and Appendix 4.1) and also from the decrease in dissolution rates (Fig. 4.5) of elements are showing that elements are consuming into formation of phases or just precipitating in the system. Due to thin layer of phase development at 90^{o}C (not formed at 50^{o}C) on grains surfaces, it is difficult to clearly identify with the help of SEM. But the formed phase is amorphous kind of clay. The formed clay phase is probably looks like smectite, and also concluded form the others studies that basaltic glass makes coating with smectite on grains. Complex ligands are often present in the soil solutions, which affect the dissolution rates at acid conditions. In neutral to alkaline pH environments basaltic glass dissolves very rapidly compared to basaltic elements. Thus, dissolution rate of phosphate from basalt glass is quite enough and rate enhances by further crushing to very finer grains, and makes enable to use as a phosphate fertilizer in future.

References

Aagaard P. and H. C. Helgeson. (1982). Thermodynamic and kinetic constraints on reaction rates among elements and aqueous solutions: I. Theoretical considerations. Am. J. Sci. 282, 237–285.

Cahn, M. D., Bouldin, D. R., & Cravo, M. S. (1992). Nitrate sorption in the profile of an acid soil. *Plant and Soil*, *143*(2), 179-183.

Chadwick, O. A., R. T. Gavenda, et al. (2003). "The impact of climate on the biogeochemical functioning of volcanic soils." Chemical Geology **202**(3–4): 195-22

Chester, R. (2009). Marine geochemistry. Wiley-Blackwell.

Cordell, D. (2010). The Story of Phosphorus: Sustainability implications of local phosphorus scarcity for food security. Department of Water and Environmental Studies and Faculty of Arts and Sciences. Linköping, Linköping University PhD: 220.

Cordell, D., J.-O. Drangert, et al. (2009). "The story of phosphorus: Global food security and food for thought." Global Environmental Change 19(2): 292-305.

Daux, V., C. Guy, et al. (1997). "Kinetic aspects of basaltic glass dissolution at 90°C: role of aqueous silicon and aluminium." Chemical Geology **142**(1–2): 109-126.

De Stefano, L., & Llamas, M. R. (2012). Water, Agriculture and the Environment in Spain: Can We Square the Circle?. CRC Press.

DIONEX Corporation. (2005). ICS-1000 Ion Chromatography System.

Dutrow, B. L., Clark, C. M. (2012). "Integrating Research and Education, Geochemical Instrumentation and Analysis, X-ray Powder Diffraction (XRD)."

E. O. Huffman and A. W. Taylor. (1963). Behavior of Water-Soluble Phosphate in Soils, *Journal of Agricultural and Food Chemistry 11* (3), 182-187.

Enk, R. J. van., Acera, L.K., Schuiling, R.D., Ehlert, P., de Wilt, J.G.; van Haren, R.J.F, L. K. Acera. (2011). The phosphate balance: Current developments and future outlook, Innovation Network, ISBN: 978-90-5059-414-1.

FAO. (2008). Efficiency of soil and fertilizer phosphorus use: Reconciling changing concepts of soil phosphorus behavior with agronomic information, Rome: 123.

FIA- International Fertilizer Industry Association. (2009). "Fertilizers, Climate Change and Enhancing Agricultural Productivity Sustainably." 1st Edi, Paris, France.

Fyfe, W. S., B. I. Kronberg, et al. (1978). "Phosphate release from synthetic glasses and inhibition of phosphate fixation on ferric hydroxide." Soil Science and Plant Nutrition 24(4): 455-464.

Gallentine, T.A., Frias . J.E., Al-Jamal, M. (2013). The echnicon Auto Analyzer II, New Mexicon State University, access date: 23-05-2013, from: http://hydrology1.nmsu.edu/teaching/soil698/student_material/AutoAnalyzer/

Gislason S. R., Andre´sdo´ttir A., Sveinbjo¨rnsdo´ttir A. E.,O´ skarsson N., Thordarson Th., Torssander P., Novaˆk N., and Zaˆk K. (1992). Local effects of volcanoes on the hydrosphere: Example from Hekla, southern Iceland. In Water–Rock Interactions, pp. 477–481. Balkema.

Gislason, S. R. and E. H. Oelkers (2003). "Mechanism, rates, and consequences of basaltic glass dissolution: II. An experimental study of the dissolution rates of basaltic glass as a function of pH and temperature." Geochimica et Cosmochimica Acta **67**(20): 3817-3832.

Gislason, S. R. and P. E. Hans (1987). "Meteoric water-basalt interactions. I: A laboratory study." Geochimica et Cosmochimica Acta **51**(10): 2827-2840.

Gong, W. L., Wang, L. M., Ewing, R. C., Vernaz, E., Bates, J. K., & Ebert, W. L. (1998). Analytical electron microscopy study of surface layers formed on the French SON68 nuclear waste glass during vapor hydration at 200° C. *Journal of nuclear materials*, *254*(2), 249-265.

Grambow, B. (1985). A general rate equation for nuclear waste glass corrosion. In Mat. Res. Soc. Symp. Proc (Vol. 44, pp. 15-27).

Gudbrandsson, S., D. Wolff-Boenisch, et al. (2008). "Dissolution rates of crystalline basalt at pH 4 and 10 and 25–75°C." Elementogical Magazine **72**(1): 155-158.

Guomundsson, T., H. Björnsson, et al. (2005). "Elemental composition, fractions and balance of nutrients in an Andic Gleysol under a long-term fertilizer experiment in Iceland." Icelandic Agricultural Science 18: 21-32.

Hawkes, C. & Ruel, M.T., 2007. From Agriculture to Nutrition: Pathways, Synergies and Outcomes. World, (40196), p.1-106.

Haygarth, P. M. and S. C. Jarvis (2002). Agriculture, Hydrology, and Water Quality, Cabi.

Heffer, P. and M. P. Homme (2008). "Outlook for World Fertilizer Demand, Supply, and Supply/Demand Balance." 32: 159-164.

Helgeson, H. C., W. M. Murphy, et al. (1984). "Thermodynamic and kinetic constraints on reaction rates among elements and aqueous solutions. II. Rate constants, effective surface area, and the hydrolysis of feldspar." Geochimica et Cosmochimica Acta **48**(12): 2405-2432.

Hochella, M. F. and J. F. Banfield (1995). "Chemical weathering of silicates in nature; a microscopic perspective with theoretical considerations." Reviews in Elementogy and Geochemistry **31**(1): 353-406.

Hubbert MK. (1956).” Nuclear energy and the fossil fuels”. Drilling and Production Practice, American Petroleum Institute & Shell Development Co., publication no. 95.

IFA-International Fertilizer Industry Association. (2009). "Phosphorus and "peak phosphate": What is the “peak phosphate” theory?" Retrieved 11-03-2013, from: http://www.fertilizer.org/ifa/HomePage/SUSTAINABILITY/Phosphorus-peak-phosphate.

Isherwood, K. and U. Industry (1998). Element fertilizer use and the environment, International Fertilizer Industry Association.

Jasinski, S. M. (2009). Phosphate Rock, Element Commodity Summaries, US Geological Survey, January, 2009, from: http://globalpnetwork.net/facts-figures).

Johnston, A. E. (1997). "Fertilizers and Agriculture: Fifty years of developments and challenges." Fertilizer Society (York, 1997).

Johnston, A. E. (2000), Soil and plant phosphate, International Fertilizer Industry Association (IFA), Paris: 46.

Kauwenburgh, V. (2010). World phosphate reserves & resources, IFDC, Washington D.C, from: http://globalpnetwork.net/facts-figures).

Kronberg, B. I. (1977). The geochemistry of some Brazilian soils and geochemical considerations for agriculture on highly leached soils, PhD Thesis, Thesis, University of Western Ontario (Geology), London, Canada.

LabSource. (2013). Grant Scientific 26L Analogue Water Baths-Jb Aqua 26 Plus, Advantage Business Centre, 132-134 Great Ancoats Street, Manchester, M4 6DE, UK. Access date: 26.03.2013.

Lasaga, A. C., & Kirkpatrick, R. J. (1981). *Kinetics of geochemical processes*(p. 320). Washington DC: Elementogical Society of America.

Lebon, S. L. G. (2009). Volcanic activity and environment: Impacts on agriculture and use of geological data to improve recovery processes University of Iceland.

Lenton, T. M. (2001). "The role of land plants, phosphorus weathering and fire in the rise and regulation of atmospheric oxygen." Global Change Biology **7**(6): 613-629.

Ma, L., W. Q. Ma, et al. (2010). "Modeling Nutrient Flows in the Food Chain of China ." J. Environ. Qual. 39(4): 1279-1289.

McKenzie R. H. and Middleton A. (2013). "Phosphorus Fertilizer Application in Crop Production." Alberta Agriculture and Rural Development, Research and Innovation Division, Agriculture Centre, Lethbridge.

Morgan, N. A. and F. J. Spera (2001). "Glass transition, structural relaxation, and theories of viscosity: a molecular dynamics study of amorphous CaAl2Si2O8." Geochimica et Cosmochimica Acta **65**(21): 4019-4041.

Moulton, K. L., J. West, et al. (2000). "Solute flux and element mass balance approaches to the quantification of plant effects on silicate weathering." American Journal of Science **300**(7): 539-570.

Murphy, W. M., E. H. Oelkers, et al. (1989). "Surface reaction versus diffusion control of element dissolution and growth rates in geochemical processes." Chemical Geology **78**(3–4): 357-380.

Navarre-Sitchler, A. and S. Brantley (2007). "Basalt weathering across scales." Earth and Planetary Science Letters **261**(1–2): 321-334.

Nesbitt, H. W. and G. M. Young (1984). "Prediction of some weathering trends of plutonic and volcanic rocks based on thermodynamic and kinetic considerations." Geochimica et Cosmochimica Acta **48**(7): 1523-1534.

Oelkers, E. H. (2001). "General kinetic description of multioxide silicate element and glass dissolution." Geochimica et Cosmochimica Acta **65**(21): 3703-3719.

Oelkers, E. H., J. Schott, et al. (1994). "The effect of aluminum, pH, and chemical affinity on the rates of aluminosilicate dissolution reactions." Geochimica et Cosmochimica Acta **58**(9): 2011-2024.

OEWRI Quality Assurance Coordinator. (2008). Standard Operating Procedure for: LS 13 320 Laser Diffraction Particle Size Analyzer Operation (Particle Sizer R01.doc), Missouri State University and Ozarks Environmental and Water Resources Institute (OEWRI).

Pačes, T. (1983). "Rate constants of dissolution derived from the measurements of mass balance in hydrological catchments." Geochimica et Cosmochimica Acta **47**(11): 1855-1863.

Pelayo, M., García-Romero, E., Labajo, M. A., & Pérez del Villar, L. (2011). Occurrence of Fe–Mg-rich smectites and corrensite in the Morrón de Mateo bentonite deposit (Cabo de Gata region, Spain): A natural analogue of the bentonite barrier in a radwaste repository. Applied geochemistry, 26(7), 1153-1168.

QUORUM (2013). Quorum Technologies, Q150R S/E/ES Sample Preparation System Instruction Manual. ASHFORD Kent, UK, Quorum Technologies Limited Company. **10621 - Issue 1**.

Sahota Singh, T.S. (2009). Pre-seeding Nitrate Nitrogen Test can save some dollars, Published in Northwest Link, March 2009, Pages 9-10.

Savci, S. (2012). "An Agricultural Pollutant: Chemical Fertilizer", International Journal of Environmental Science and Development, Vol. 3-1.

Schott, J and E. H. Oelkers. (2001). "An experimental study of enstatite dissolution rates as a function of pH, temperature, and aqueous Mg and Si concentration, and the mechanism of pyroxene/pyroxenoid dissolution." Geochimica et Cosmochimica Acta **65**(8): 1219-1231.

Schott, J., & Oelkers, E. H. (1995). Dissolution and crystallization rates of silicate elements as a function of chemical affinity. Pure and applied chemistry,67(6), 903-910.

Schott, J., O. S. Pokrovsky, et al. (2009). "The Link Between Element Dissolution/Precipitation Kinetics and Solution Chemistry." Reviews in Elementogy and Geochemistry **70**(1): 207-258.

Schweitzer, J. (2010). "Radiological and Environmental Management, Scanning Electron Microscope." Retrieved 05.03, 2013, from: http://www.purdue.edu/rem/rs/sem.htm.

Siegel, D. I. and H. O. Pfannkuch (1984). "Silicate dissolution influence on Filson Creek chemistry, northeastern Minnesota." Geological Society of America Bulletin **95**(12): 1446-1453.

Srinivasarao, C., Satyanarayana, T., & Venkateswarlu, B. (2011). Potassium mining in Indian agriculture: Input and output balance. Karnataka Journal of Agricultural Sciences, 24(1).

Swapp, S. (2012). "Integrating Research and Education ,Geochemical Instrumentation and Analysis, Scanning Electron Microscopy (SEM)." Retrieved 05.03, 2013, from http://serc.carleton.edu/research_education/geochemsheets/techniques/SEM.html.

Thermo Fisher Scientific Inc. (2013). Brinkmann/Metrohm SM Titrino, Access Date: 26.03.2013

Tirado, T. and A, Michelle (2012). Phosphorus in agriculture: Problems and solutions. Greenpeace Research Laboratories Technical Report (Review) 02-2012.

Trenkel, M. E. (1997). Controlled-release and stabilized fertilizers in agriculture, International fertilizer industry association Paris.

Trenkel, M. E. (1997). Improving Fertilizer Use Efficiency Controlled-Release and Stabilized Fertilizers in Agriculture. Eusserthal, Germany, International Fertilizer Industry Association.

Ullman, W. J., & Welch, S. A. (2002). Organic ligands and feldspar dissolution.Water–rock interactions, ore deposits, and environmental geochemistry: A tribute to David Crerar. Special publication, 7, 3-35.

United Nations. (2005). "Press Briefing on World Population Trends." Retrieved 11-03-2013, from: http://www.un.org/News/briefings/docs/2005/Brfg_on_Population_050224.doc.htm.

USGS (2009). Element Commodity Summaries - Phosphate Rock, IU.S. Geological Survey, IU.S. Geological Survey, United States Government Printing Office, Washington: 2009, ISBN- 978-1-4113-295-0.

Villalba, G., Liu, Y., Schroder, H. and Ayres, R. U. (2008), Global Phosphorus Flows in the Industrial Economy From a Production Perspective. Journal of Industrial Ecology, 12: 557–569.

Whiting, D., Card, A. and Wilson, C. (2011). Colorado Master Garden Program, Colorado State University Extension.

Wolff-Boenisch, D., S. R. Gislason, et al. (2004). "The dissolution rates of natural glasses as a function of their composition at pH 4 and 10.6, and temperatures from 25 to 74°C." Geochimica et Cosmochimica Acta **68**(23): 4843-4858.

Wolff-Boenisch, D., S. R. Gislason, et al. (2004). "The effect of fluoride on the dissolution rates of natural glasses at pH 4 and 25°C." Geochimica et Cosmochimica Acta **68**(22): 4571-4582.

Wolff-Boenisch, D., S. R. Gislason, et al. (2006). "The effect of crystallinity on dissolution rates and CO2 consumption capacity of silicates." Geochimica et Cosmochimica Acta **70**(4): 858-870.

Yara (2009). ABC Guide to Element Fertilizers: A basic handbook on fertilizers and their use. Bygdøy allé 2, N-0202, Oslo, Norway, Yara International ASA, ISBN 0 85199 385 3, accessed-2013.

3.0 Appendix

3.1 Estimation of Specific Surface Area of Basaltic Glass Grains

Table 3.1.1: Estimation of specific surface area of hand crushed basaltic glass sample with BET method.

Radius (cm) (ri)	**SA(4πr2)** (cm2) (ai)	**Volume** (4/3πr3**)** (cm3) (Vp)	**Dif.** Vol% (Vdiff.i)	**Basalt Vol.** (cm3) (1g/density) (V)	**Frac. Vol.** (cm3) (Vi)	**nr . Of particles per gram** (ni)	**SSA** (cm2/g) (Ai)	**SSA** (m2/g) (Ai)
2E-05	7E-09	6E-14	0.5	0.34	0.00172	3.1E+10	218.8	0.022
4E-05	2E-08	2E-13	1.24	0.34	0.00428	1.9E+10	340.7	0.034
6E-05	5E-08	9E-13	1.63	0.34	0.00562	6.2E+09	280.8	0.028
1E-04	1E-07	4E-12	1.81	0.34	0.00624	1.7E+09	195.6	0.02
0.0002	3E-07	1E-11	2.16	0.34	0.00745	5E+08	146.4	0.015
0.0002	7E-07	6E-11	2.8	0.34	0.00966	1.6E+08	119.1	0.012
0.0004	2E-06	2E-10	3.59	0.34	0.01238	5E+07	95.76	0.01
0.0006	5E-06	1E-09	4.78	0.34	0.01648	1.7E+07	79.96	0.008
0.001	1E-05	4E-09	7.03	0.34	0.02424	6018735	73.79	0.007
0.0016	3E-05	2E-08	9.54	0.34	0.0329	2014252	62.8	0.006
0.0025	8E-05	7E-08	11.6	0.34	0.04	604615	47.9	0.005
0.004	0.0002	3E-07	15	0.34	0.05172	193016	38.86	0.004
0.0064	0.0005	1E-06	17.5	0.34	0.06034	55510.6	28.42	0.003
0.0102	0.0013	4E-06	16	0.34	0.05517	12541.2	16.31	0.002
0.0162	0.0033	2E-05	2.92	0.34	0.01007	565.003	1.867	2E-04
0.0259	0.0084	7E-05	1.79	0.34	0.00617	85.465	0.718	7E-05
0.0412	0.0213	0.0003	0.1	0.34	0.00034	1.17852	0.025	3E-06
							1748	**0.175**

*SSA is the specific surface area, SA is the surface area.

Table 3.1.2: Estimation of specific surface area of microniser crushed basaltic glass sample with BET method.

Radius (cm) (ri)	**SA** (4πr2) (cm2) (ai)	**Volume** (4/3πr3) (cm3) (Vp)	**Dif.** Vol% (Vdiff.i)	**Basalt Vol.** (cm3) (1g/density) (V)	**Frac. Vol.** (cm3) (Vi)	**nr. Of particles per gram** (ni)	**SSA** (cm2/g) (Ai)	**SSA** (m2/g) (Ai)
2.37E-05	7E-09	5.56E-14	1.6	0.34483	0.005517	1E+11	700.14	0.07
3.78E-05	2E-08	2.25E-13	3.95	0.34483	0.013621	6E+10	1085.2	0.109
6.02E-05	5E-08	9.11E-13	5.09	0.34483	0.017552	2E+10	876.86	0.088
9.6E-05	1E-07	3.69E-12	5.58	0.34483	0.019241	5E+09	603.11	0.06
0.000153	3E-07	1.5E-11	7	0.34483	0.024138	2E+09	474.48	0.047

0.000244	7E-07	6.06E-11	10.1	0.34483	0.034828	6E+08	429.46	0.043
0.000389	2E-06	2.45E-10	14.3	0.34483	0.04931	2E+08	381.43	0.038
0.00062	5E-06	9.95E-10	18.7	0.34483	0.064483	6E+07	312.8	0.031
0.000988	1E-05	4.03E-09	19.5	0.34483	0.067241	2E+07	204.69	0.02
0.001576	3E-05	1.63E-08	10.5	0.34483	0.036207	2E+06	69.116	0.007
0.002512	8E-05	6.62E-08	1.96	0.34483	0.006759	102159	8.0934	8E-04
0.004004	0.0002	2.68E-07	0.92	0.34483	0.003172	11838	2.3832	2E-04
0.006385	0.0005	1.09E-06	0.57	0.34483	0.001966	1808.1	0.9258	9E-05
0.010175	0.0013	4.4E-06	0.085	0.34483	0.000293	66.625	0.0866	9E-06
							5148.7	**0.515**

*SSA is the specific surface area, SA is the surface area.

3.2 Determination of Dissolution Rate of Basaltic Glass

The dissolution rate is estimated with the help of equation 1.

$$r = K_1^t.A.a_H^{n1} + K_2^t.A.a_H^{n2} + K_3^t.A.a_H^{n3} \qquad \text{Eq.1}$$

By taking the Log of Equation 1 as,

Log r = $(logK_1^t + n1.\log(H^+) + logK_2^t + n2.\log(H^+) + logK_3^t + n3.\log(H^+)) + logA$

With the help of Figure 1, we can determine the dissolution of basaltic glass.

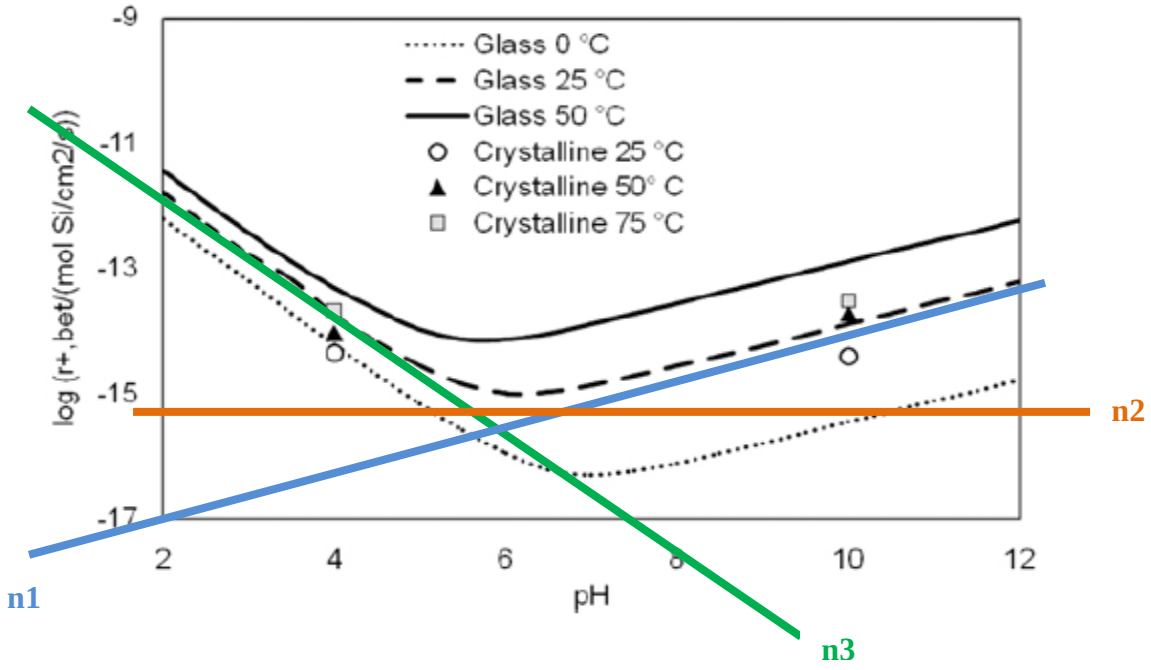

Figure 3.1: Dissolution rates of crystalline basalt in symbols are compared with modeled rates in curves of the basaltic glass adopted from Gudbrandsson and Wolff-Boenisch, et al. (2008).

The slope of the lines can be calculated with Eq. 2 as,

$$n = \frac{\Delta \log r}{\Delta pH} \qquad \text{Eq. 2}$$

And found the following slopes as n1= 0.55, n2 = 0 and n3 = -0.95

To calculate the values of K^{to} used Eq. 3 as;

$$r = K^{to} a_H^{ni} \qquad \text{Eq. 3}$$

Eq. 3 can be written as,

$$\log r = \log K_i^{to} + n_i \log(H^+) \qquad \text{Eq. 4}$$

The values for K_1^{t0}, K_2^{t0} and K_3^{t0} in mol/cm^2/sec are calculated at 25^{o}C and at 2 pH from the given Figure 1 of Appendix 3.2, so;

$K_1^{t0} = 10^{-17.7}$

$K_2^{t0} = 10^{-15}$

$K_3^{t0} = 10^{-10}$

Now calculate the values for K_1^T, K_2^T and K_3^T for 25^o C dissolution rate of basaltic glass slope as;

$$K^t = K^{to} . e^{-(\frac{Ea}{\ln R.T})} \qquad \text{Eq. 5}$$

Determined the values for K_1^T, K_2^T and K_3^T in cm^2/sec at pH=8.5, where Ea is about 32.75 KJ/mol (calculated from pH 7 and 10, where pH=7 having Ea is 30.5 KJ/mol, which is calculated from pH of 4 and 10 and at pH 10 the Ea has value about 35 KJ/mol), and at 25^{o}C which is estimated from Gudbrandsson and Wolff-Boenisch, et al. (2008) are as follows,

$$K_1^T = 10^{-17.7}, \quad K_2^T = 10^{-15}, \quad K_3^T = 10^{-10}$$

Note: the 25^{o}C temperature is the standard temperature, where the values for K^o and K^T remained same.

Now determined the values for K_1^T, K_2^T and K_3^T in mol/cm^2/sec by using pH=8.5 and Ea is about 32.75 KJ but at 50^{o}C as follows,

$$K_1^T = 5.55 * 10^{-18}, \quad K_2^T = 2.782 * 10^{-15}, \quad K_3^T = 2.782 * 10^{-10}$$

Now also determined the values for K_1^T, K_2^T and K_3^T in mol/cm^2/sec by using pH=8.5 and Ea is about 32.75 KJ but at 75^{o}C as follows,

$$K_1^T = 1.33 * 10^{-17}, \quad K_2^T = 6.68 * 10^{-15}, \quad K_3^T = 6.68 * 10^{-10}$$

Finally we estimated the dissolution rate at different temperatures,

Dissolution Rate at 298K (25^{o}C)

Now for slope-1 dissolution rate by using Eq. Log r1 = $logK_1^t + n1.\log\left(H^+\right)$as,

K_1^T	n_1	pH	n_1*pH	a_H^{n1}(=10^{-pH*n1})	$K_1^T * a_H^{n1}$
2.00E-18	-0.45	0	0	1	1.995E-18
2.00E-18	-0.45	-1	0.45	2.818383	5.623E-18
2.00E-18	-0.45	-2	0.9	7.943282	1.585E-17
2.00E-18	-0.45	-3	1.35	22.38721	4.467E-17
2.00E-18	-0.45	-4	1.8	63.09573	1.259E-16
2.00E-18	-0.45	-5	2.25	177.8279	3.548E-16
2.00E-18	-0.45	-6	2.7	501.1872	1E-15
2.00E-18	-0.45	-7	3.15	1412.538	2.818E-15
2.00E-18	-0.45	-8	3.6	3981.072	7.943E-15
2.00E-18	-0.45	-9	4.05	11220.18	2.239E-14
2.00E-18	-0.45	-10	4.5	31622.78	6.31E-14

For slope-2 dissolution rate by using Eq. Log r2 = $logK_2^t + n2.\log\left(H^+\right)$ as,

K_2^T	n_2	pH	n_2*pH	a_H^{n2}(=10^{-pH*n2})	$K_2^T * a_H^{n2}$
1E-15	0	0	0	1	1E-15
1E-15	0	1	0	1	1E-15
1E-15	0	2	0	1	1E-15
1E-15	0	3	0	1	1E-15
1E-15	0	4	0	1	1E-15
1E-15	0	5	0	1	1E-15
1E-15	0	6	0	1	1E-15
1E-15	0	7	0	1	1E-15
1E-15	0	8	0	1	1E-15
1E-15	0	9	0	1	1E-15
1E-15	0	10	0	1	1E-15

For slope-3 dissolution rate by using Eq. Log r3 = $logK_3^t + n3.\log\left(H^+\right)$ as,

K_3^T	n_3	pH	n_3*pH	a_H^{n3} (=10^{-pH*n3})	$K_3^T * a_H^{n3}$
1E-10	0.95	0	0	1	1E-10
1E-10	0.95	-1	-0.95	0.112201845	1.12202E-11
1E-10	0.95	-2	-1.9	0.012589254	1.25893E-12
1E-10	0.95	-3	-2.85	0.001412538	1.41254E-13
1E-10	0.95	-4	-3.8	0.000158489	1.58489E-14
1E-10	0.95	-5	-4.75	1.77828E-05	1.77828E-15
1E-10	0.95	-6	-5.7	1.99526E-06	1.99526E-16
1E-10	0.95	-7	-6.65	2.23872E-07	2.23872E-17
1E-10	0.95	-8	-7.6	2.51189E-08	2.51189E-18
1E-10	0.95	-9	-8.55	2.81838E-09	2.81838E-19
1E-10	0.95	-10	-9.5	3.16228E-10	3.16228E-20

So, overall dissolution rate at 298K is calculated with following equation as,

Log r1 = $logK_1^t + n1.\log(H^+) + logK_2^t + n2.\log(H^+) + logK_3^t + n3.\log(H^+)$

pH	$K_3^T * a_H^{n3}$	$K_2^T * a_H^{n2}$	$K_1^T * a_H^{n1}$	r 1 (mol/cm2/s)	Log r1 (mol/cm2/s)
0	2E-18	1E-15	1E-10	1.00001E-10	-9.999996
1	5.62E-18	1E-15	1.12E-11	1.12212E-11	-10.94996
2	1.58E-17	1E-15	1.26E-12	1.25994E-12	-11.89965
3	4.47E-17	1E-15	1.41E-13	1.42298E-13	-12.8468
4	1.26E-16	1E-15	1.58E-14	1.69748E-14	-13.77019
5	3.55E-16	1E-15	1.78E-15	3.13309E-15	-14.50403
6	1E-15	1E-15	2E-16	2.19953E-15	-14.65767
7	2.82E-15	1E-15	2.24E-17	3.84077E-15	-14.41558
8	7.94E-15	1E-15	2.51E-18	8.94579E-15	-14.04838
9	2.24E-14	1E-15	2.82E-19	2.33875E-14	-13.63102
10	6.31E-14	1E-15	3.16E-20	6.40958E-14	-13.19317

Dissolution Rate at 323K (50^{o}C) and Ea 32750 J/mol

Now for slope-1 dissolution rate by using Eq. Log r1 = $logK_1^t + n1.\log\left(H^+\right)$as,

K_1^T	n_1	pH	n_1*pH	a_H^{n1} (=10^{-pH*n1})	$K_1^T * a_H^{n1}$
5.55E-18	-0.45	0	0	1	5.55E-18
5.55E-18	-0.45	-1	0.45	2.818382931	1.564E-17
5.55E-18	-0.45	-2	0.9	7.943282347	4.409E-17

5.55E-18	-0.45	-3	1.35	22.38721139	1.242E-16
5.55E-18	-0.45	-4	1.8	63.09573445	3.502E-16
5.55E-18	-0.45	-5	2.25	177.827941	9.869E-16
5.55E-18	-0.45	-6	2.7	501.1872336	2.782E-15
5.55E-18	-0.45	-7	3.15	1412.537545	7.84E-15
5.55E-18	-0.45	-8	3.6	3981.071706	2.209E-14
5.55E-18	-0.45	-9	4.05	11220.18454	6.227E-14
5.55E-18	-0.45	-10	4.5	31622.7766	1.755E-13

For slope-2 dissolution rate by using Eq. Log r2 = $logK_2^t + n2.\log\left(H^+\right)$ as,

K_2^T	n_2	pH	n_2*pH	a_H^{n2} (=10^{-pH*n2})	$K_2^T * a_H^{n2}$
2.78E-15	0	0	0	1	2.78E-15
2.78E-15	0	-1	0	1	2.78E-15
2.78E-15	0	-2	0	1	2.78E-15
2.78E-15	0	-3	0	1	2.78E-15
2.78E-15	0	-4	0	1	2.78E-15
2.78E-15	0	-5	0	1	2.78E-15
2.78E-15	0	-6	0	1	2.78E-15
2.78E-15	0	-7	0	1	2.78E-15
2.78E-15	0	-8	0	1	2.78E-15
2.78E-15	0	-9	0	1	2.78E-15
2.78E-15	0	-10	0	1	2.78E-15

For slope-3 dissolution rate by using Eq. Log r3 = $logK_3^t + n3.\log\left(H^+\right)$ as,

K_3^T	n_3	pH	n_3*pH	a_H^{n3} (=10^{-pH*n3})	$K_3^T * a_H^{n3}$
2.782E-10	0.95	0	0	1	2.78E-10
2.782E-10	0.95	-1	-0.95	0.112202	3.12E-11
2.782E-10	0.95	-2	-1.9	0.012589	3.50E-12
2.782E-10	0.95	-3	-2.85	0.001413	3.93E-13
2.782E-10	0.95	-4	-3.8	0.000158	4.41E-14
2.782E-10	0.95	-5	-4.75	1.78E-05	4.95E-15
2.782E-10	0.95	-6	-5.7	2E-06	5.55E-16
2.782E-10	0.95	-7	-6.65	2.24E-07	6.23E-17
2.782E-10	0.95	-8	-7.6	2.51E-08	6.99E-18
2.782E-10	0.95	-9	-8.55	2.82E-09	7.84E-19
2.782E-10	0.95	-10	-9.5	3.16E-10	8.80E-20

So, overall dissolution rate at 323K is calculated with following equation as,

Log r2 = $logK_1^t + n1.\log(H^+) + logK_2^t + n2.\log(H^+) + logK_3^t + n3.\log(H^+)$

pH	K_3^T*a_H^{n3}	K_2^T*a_H^{n2}	K_1^T*a_H^{n1}	r 2 (mol/cm2/s)	Log r3 (mol/cm2/s)
0	5.55E-18	2.78E-15	2.78E-10	2.78203E-10	-9.555639
1	1.56E-17	2.78E-15	3.12E-11	3.12174E-11	-10.5056
2	4.41E-17	2.78E-15	3.50E-12	3.50516E-12	-11.45529
3	1.24E-16	2.78E-15	3.93E-13	3.95874E-13	-12.40244
4	3.5E-16	2.78E-15	4.41E-14	4.72239E-14	-13.32584
5	9.87E-16	2.78E-15	4.95E-15	8.71612E-15	-14.05968
6	2.78E-15	2.78E-15	5.55E-16	6.11867E-15	-14.21334
7	7.84E-15	2.78E-15	6.23E-17	1.06839E-14	-13.97127
8	2.21E-14	2.78E-15	6.99E-18	2.48839E-14	-13.60408
9	6.23E-14	2.78E-15	7.84E-19	6.50548E-14	-13.18672
10	1.76E-13	2.78E-15	8.80E-20	1.78288E-13	-12.74888

Dissolution Rate at 348K (75^{0}C) and Ea 32750 J/mol

Now for slope-1 dissolution rate by using Eq. Log r1 = $logK_1^t + n1.\log\left(H^+\right)$ as,

K_1^T	n_1	pH	n_1*pH	a_H^{n1}(=10^{-pH*n1})	K_1^T*a_H^{n1}
1.33E-17	-0.45	0	0	1	1.33E-17
1.33E-17	-0.45	-1	0.45	2.818382931	3.748E-17
1.33E-17	-0.45	-2	0.9	7.943282347	1.056E-16
1.33E-17	-0.45	-3	1.35	22.38721139	2.977E-16
1.33E-17	-0.45	-4	1.8	63.09573445	8.392E-16
1.33E-17	-0.45	-5	2.25	177.827941	2.365E-15
1.33E-17	-0.45	-6	2.7	501.1872336	6.666E-15
1.33E-17	-0.45	-7	3.15	1412.537545	1.879E-14
1.33E-17	-0.45	-8	3.6	3981.071706	5.295E-14
1.33E-17	-0.45	-9	4.05	11220.18454	1.492E-13
1.33E-17	-0.45	-10	4.5	31622.7766	4.206E-13

For slope-2 dissolution rate by using Eq. Log r2 = $logK_2^t + n2.\log\left(H^+\right)$ as,

K_2^T	n_2	pH	n_2*pH	a_H^{n2}(=10^{-pH*n2})	$K_2^T * a_H^{n2}$
6.68E-15	0	0	0	1	6.68E-15
6.68E-15	0	-1	0	1	6.68E-15
6.68E-15	0	-2	0	1	6.68E-15
6.68E-15	0	-3	0	1	6.68E-15
6.68E-15	0	-4	0	1	6.68E-15
6.68E-15	0	-5	0	1	6.68E-15
6.68E-15	0	-6	0	1	6.68E-15
6.68E-15	0	-7	0	1	6.68E-15
6.68E-15	0	-8	0	1	6.68E-15
6.68E-15	0	-9	0	1	6.68E-15
6.68E-15	0	-10	0	1	6.68E-15

For slope-3 dissolution rate by using Eq. Log r3 = $logK_3^t + n3.\log\left(H^+\right)$ as,

K_3^T	n_3	pH	n_3*pH	a_H^{n3}(=10^{-pH*n3})	$K_3^T * a_H^{n3}$
6.68E-10	0.95	0	0	1	6.68E-10
6.68E-10	0.95	-1	-0.95	0.112202	7.49508E-11
6.68E-10	0.95	-2	-1.9	0.012589	8.40962E-12
6.68E-10	0.95	-3	-2.85	0.001413	9.43575E-13
6.68E-10	0.95	-4	-3.8	0.000158	1.05871E-13
6.68E-10	0.95	-5	-4.75	1.78E-05	1.18789E-14
6.68E-10	0.95	-6	-5.7	2E-06	1.33284E-15
6.68E-10	0.95	-7	-6.65	2.24E-07	1.49547E-16
6.68E-10	0.95	-8	-7.6	2.51E-08	1.67794E-17
6.68E-10	0.95	-9	-8.55	2.82E-09	1.88268E-18
6.68E-10	0.95	-10	-9.5	3.16E-10	2.1124E-19

So overall dissolution rate at 348K is calculated with following equation as,

Log r3 = $logK_1^t + n1.\log(H^+) + logK_2^t + n2.\log(H^+) + logK_3^t + n3.\log(H^+)$

pH	$K_3^T * a_H^{n3}$	$K_2^T * a_H^{n2}$	$K_1^T * a_H^{n1}$	r 3 (mol/cm2/s)	Log r3 (mol/cm2/s)
0	1.33E-17	6.68E-15	6.68E-10	6.68007E-10	-9.175219
1	3.75E-17	6.68E-15	7.5E-11	7.49576E-11	-10.12518
2	1.06E-16	6.68E-15	8.41E-12	8.41641E-12	-11.07487
3	2.98E-16	6.68E-15	9.44E-13	9.50553E-13	-12.02202
4	8.39E-16	6.68E-15	1.06E-13	1.1339E-13	-12.94543

5	2.37E-15	6.68E-15	1.19E-14	2.0924E-14	-13.67935
6	6.67E-15	6.68E-15	1.33E-15	1.46786E-14	-13.83331
7	1.88E-14	6.68E-15	1.5E-16	2.56163E-14	-13.59148
8	5.29E-14	6.68E-15	1.68E-17	5.9645E-14	-13.22443
9	1.49E-13	6.68E-15	1.88E-18	1.5591E-13	-12.80713
10	4.21E-13	6.68E-15	2.11E-19	4.27263E-13	-12.3693

3.2 Estimation of Sampling Time for Required Concentration (ppm) of Silicate in Water

By using the dissolution rate of basaltic glass at 5pH and at 50^{o}C, where logr value is 10^{-13} mol basalt/cm^2/sec or 10^{-9} mol basalt/m^2/sec (Fig. 3.12).

The moles of basaltic glass can be calculated from equation-1 as,

$$m_{bsalat} = R*SSA*M \qquad \text{Eq. 1}$$

Where m_{basalt} the moles of basalt galss, R is the dissolution rate, SSA is the specific surface area and M is the basaltic glass mass used in grams.

Now,

$$m_{bsalat} = 10^{-9} \text{ molbasalt/m2.sec} * 0.175\text{m2/g}*10\text{g}$$

$$m_{bsalat} = 1.75*10^{-9} \text{ mol/sec}$$

Now calculating the moles of basalt per year as,

$$m_{bsalat} = 1.75*10^{-9} \text{ mol/sec} * 3.16*10^{7} \text{ sec/year}$$

$$m_{bsalat} = 0.055 \text{ mol/year}$$

So, now calculating the concentration of silicate in per mol of basalt glass formula given in Gislason and Oelkers (2003). Where the basaltic glass element chemical composition which consistent with $Na_{0.08}Ca_{0.263}Mg_{0.281}Fe_{0.188}Al_{0.358}SiO_{3.32}$, having 1 mol of Si.

$$Csi_{(basalt)} = \text{mbasalt}* 1m_{Si}*M$$

Where M is the molecular weight of Si.

$Csi_{(basalt)}$ = 0.055 mol/year * 1mol Si/mol basalt *28.085g/mol

$Csi_{(basalt)}$ = 1.553 g/year

Now converting g/year to mg/year as,

$Csi_{(basalt)}$ = 1.553 g/year * 1000g/mg

$Csi_{(basalt)}$ = 1553 mg/year

Now estimating the concentration Si in the water sample, as we used 0.3 kg water.

Csi = 1553 (mg/year) / 0.3Kgw

Csi = 5177 ppm/year

Now calculating time required for silicate to reach 200ppm from the dissolution of basaltic glass as,

$T_{(200ppm)}$ = 200(ppm) / 5177(ppm/year) * $3.16*10^7$ (sec/year)

$T_{(200ppm)}$ =120784 sec or

$T_{(200ppm)}$ =339.107 hours or

$T_{(200ppm)}$ =14.129 days

4.0 Appendix

4.1 Ion Chromatography Analysis of Solution Species

Aqueous concentration of elements was measured from batch reactions for hand and micronizer crushed basalt glass materials with the help of Ion Chromatography System (ICS). (A) and (B) graphs are showing change in concentration (ΔC) for hand and micronizer crushed glass powders when reacted at 50°C, and similarly, (C) and (D) graphs are representing ΔC for hand and micronizer crushed glass powders when reacted at 90°C.

4.1.1 Anions Aqueous Concentration

1. Cl

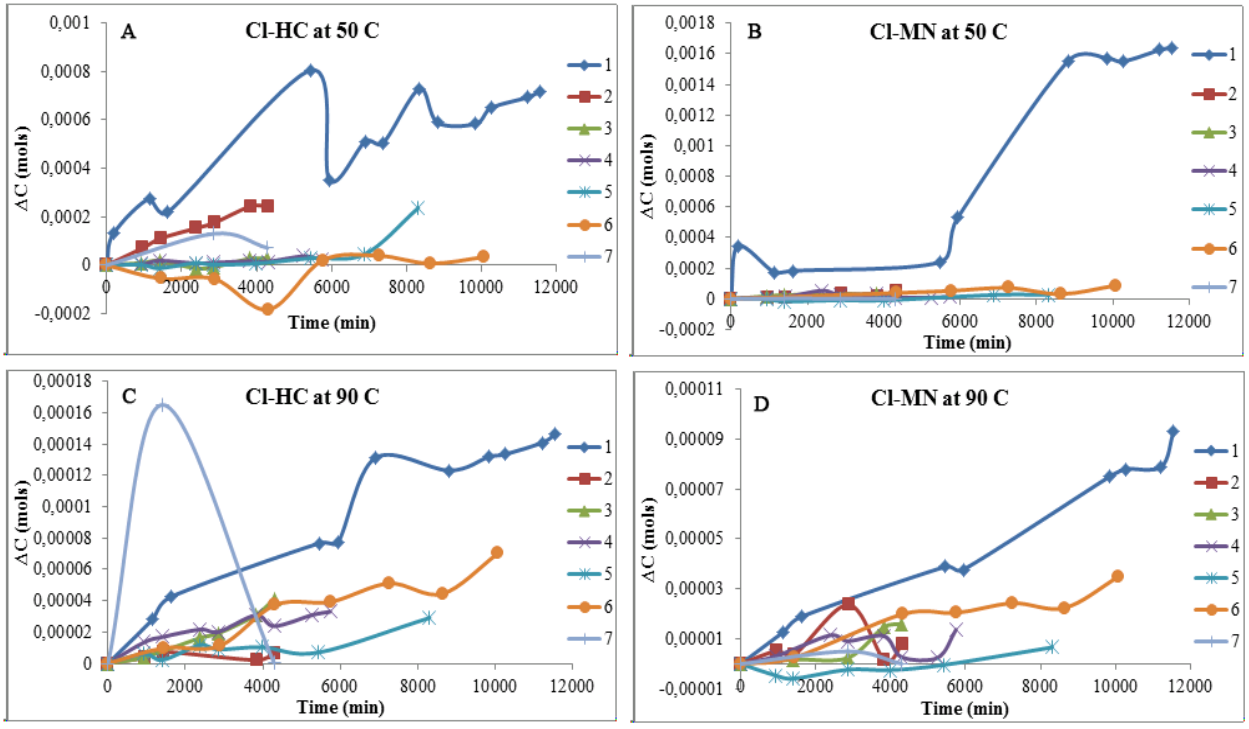

2. PO_4

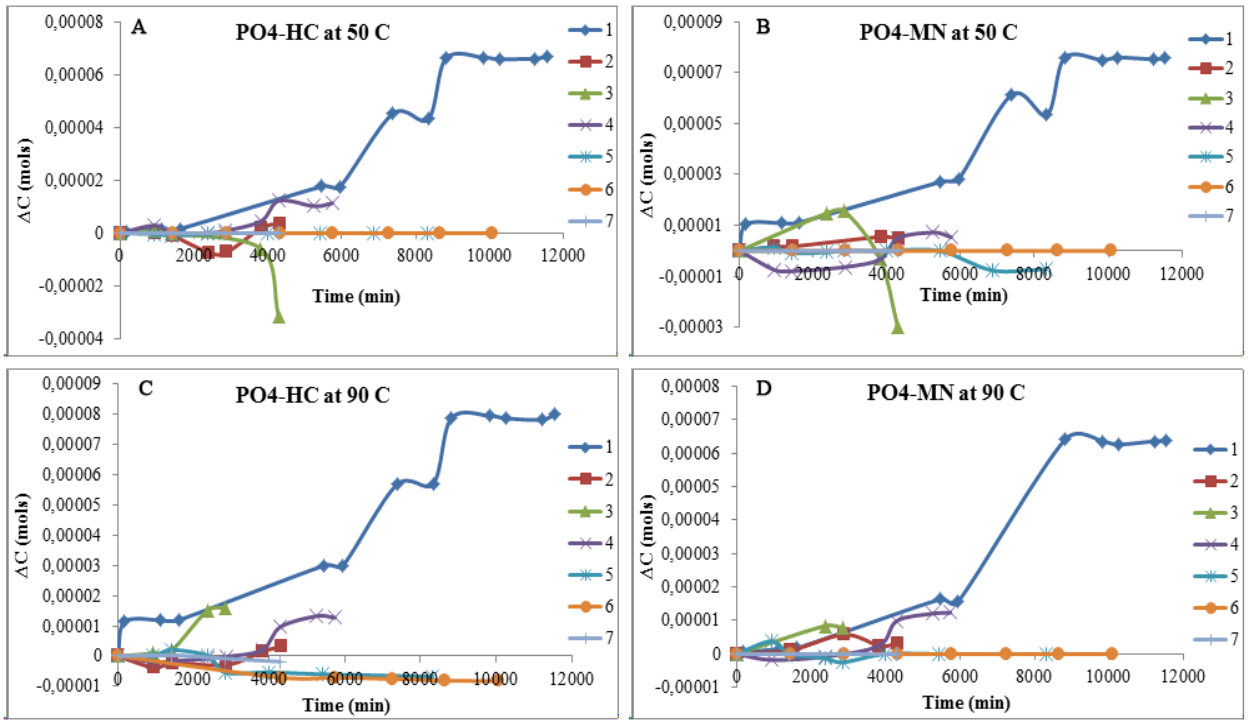
A
PO4-HC at 50 C
B
PO4-MN at 50 C
C
PO4-HC at 90 C
D
PO4-MN at 90 C
ΔC (mols)
Time (min)
1
2
3
4
5
6
7

3. SiO_2

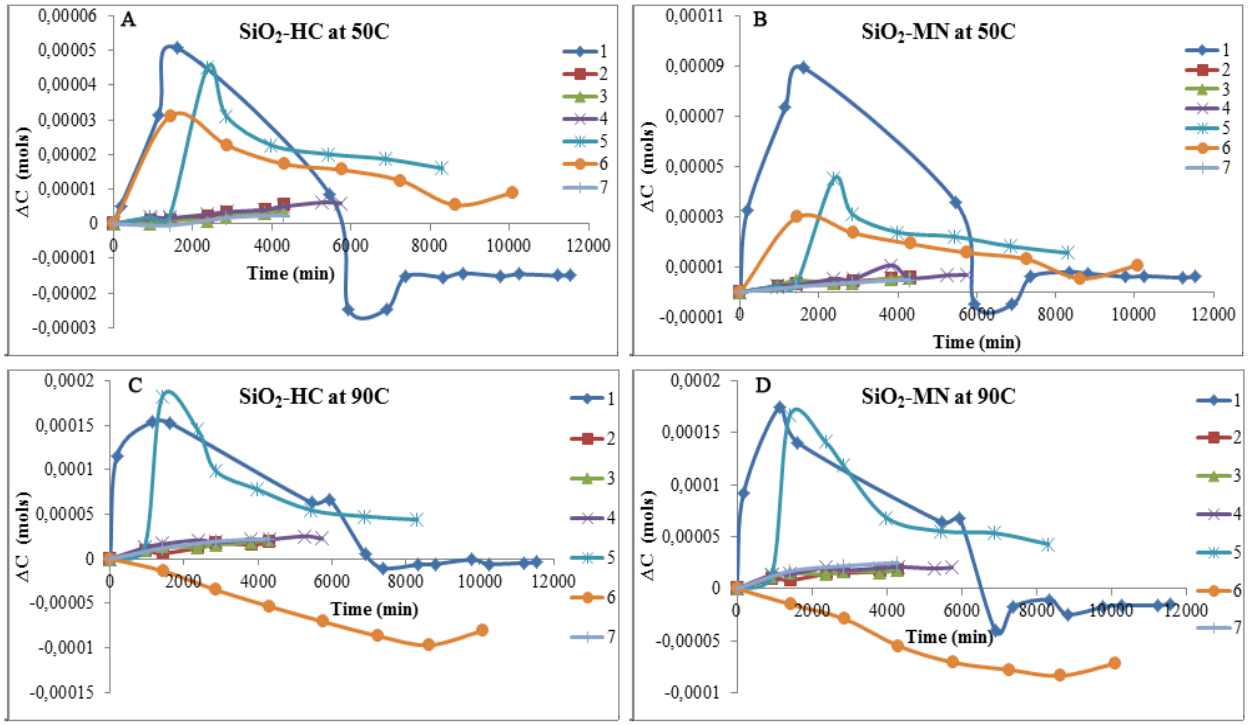
A
SiO2-HC at 50C
B
SiO2-MN at 50C
C
SiO2-HC at 90C
D
SiO2-MN at 90C
ΔC (mols)
Time (min)
1
2
3
4
5
6
7

4. NO_3

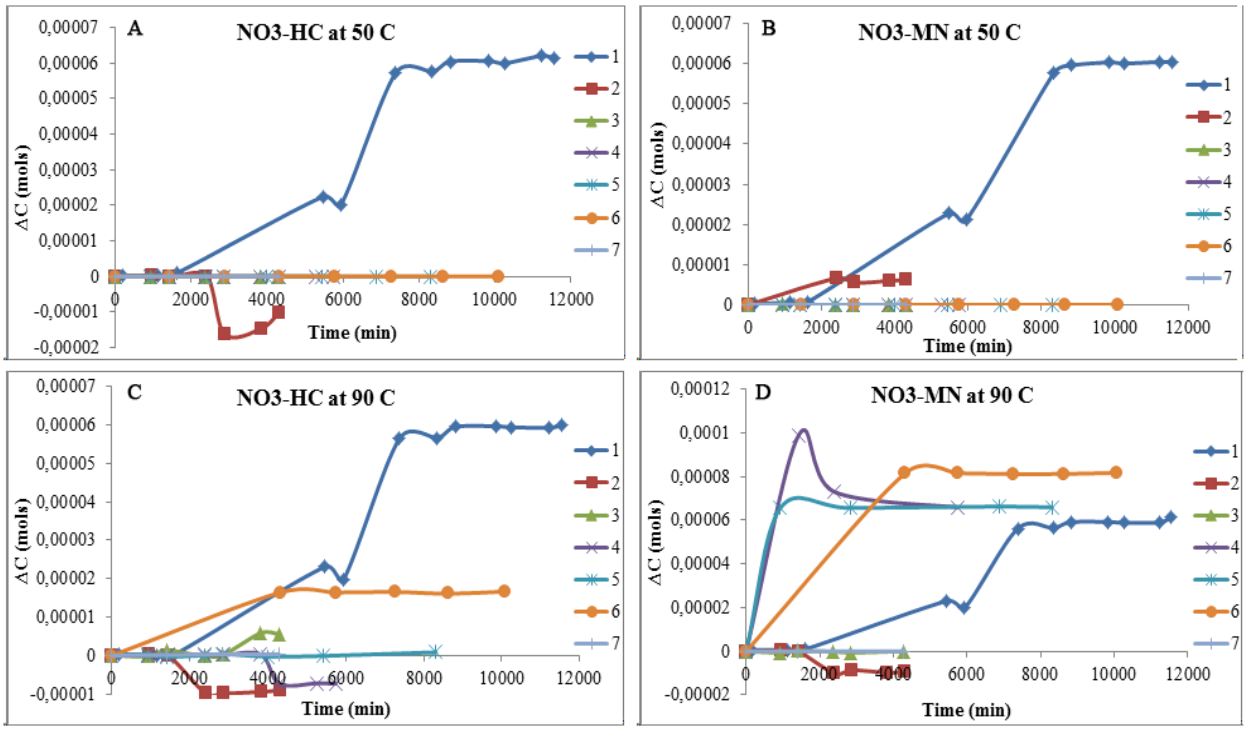
A
NO3-HC at 50 C
B
NO3-MN at 50 C
C
NO3-HC at 90 C
D
NO3-MN at 90 C
ΔC (mols)
Time (min)
1
2
3
4
5
6
7

5. F

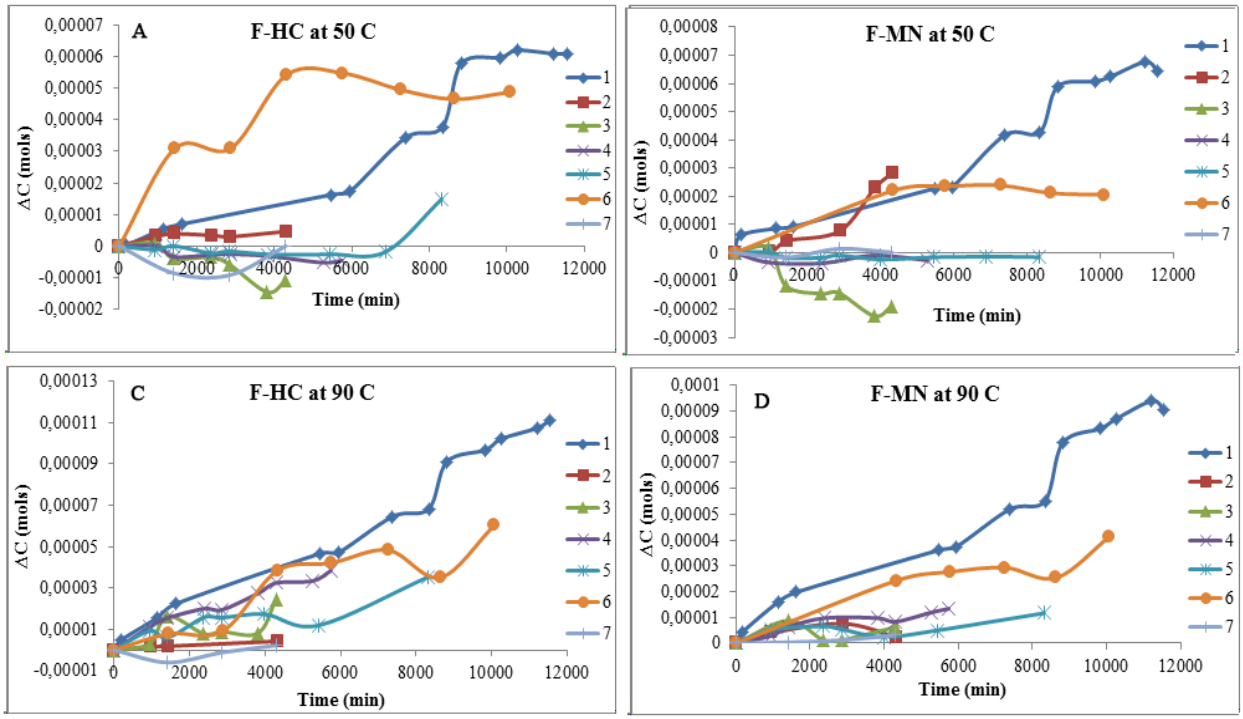
A
F-HC at 50 C
F-MN at 50 C
C
F-HC at 90 C
D
F-MN at 90 C
ΔC (mols)
Time (min)
1
2
3
4
5
6
7

6. SO_4

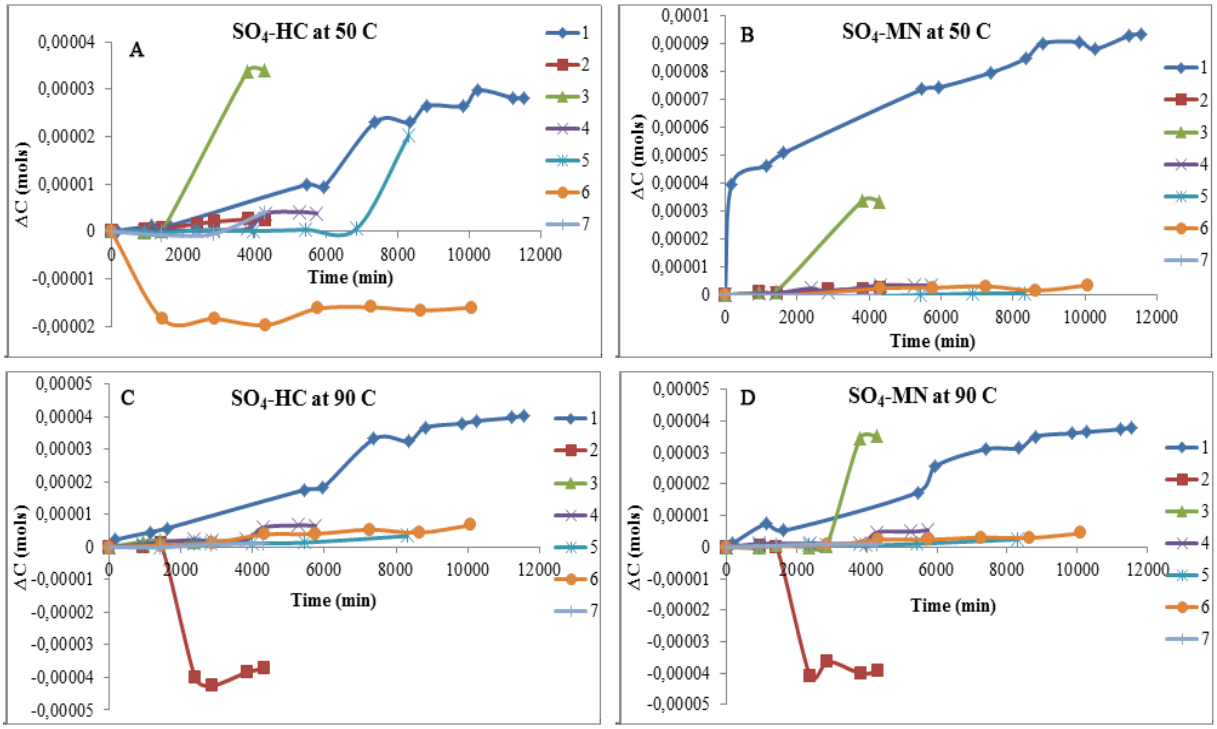
A
SO4-HC at 50 C
B
SO4-MN at 50 C
C
SO4-HC at 90 C
D
SO4-MN at 90 C
ΔC (mols)
Time (min)
1
2
3
4
5
6
7

7. Br

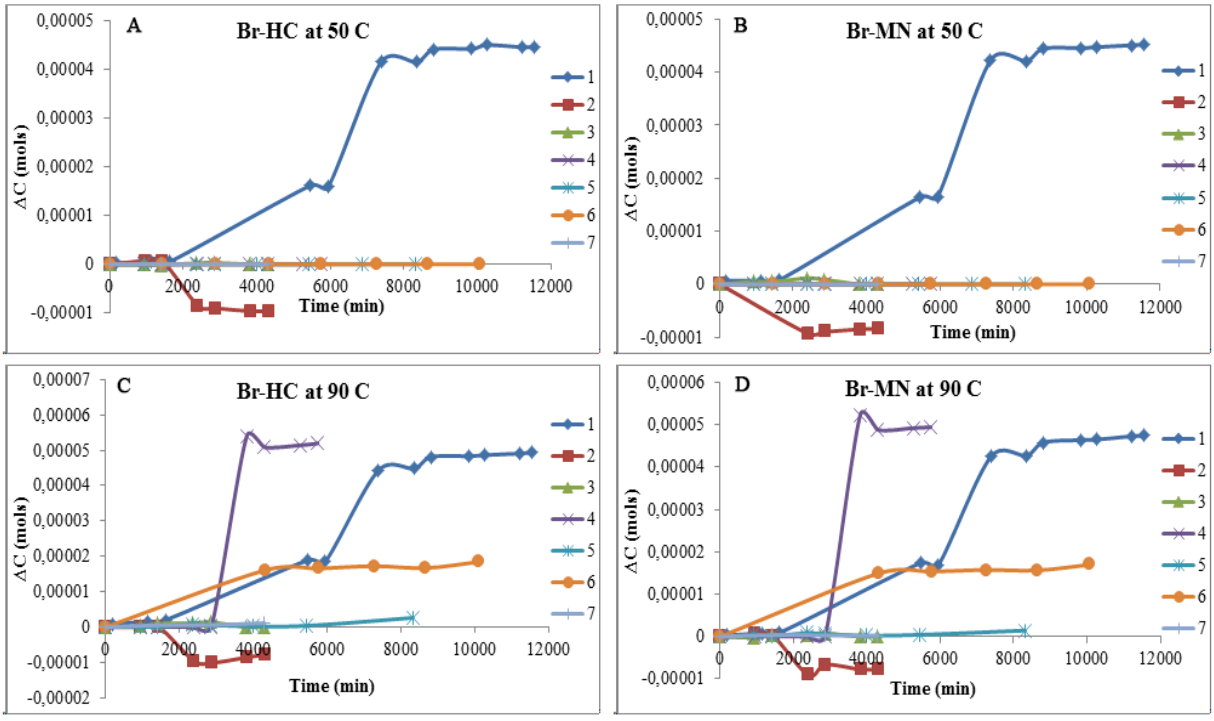
A
Br-HC at 50 C
B
Br-MN at 50 C
C
Br-HC at 90 C
D
Br-MN at 90 C
ΔC (mols)
Time (min)
1
2
3
4
5
6
7

4.1.2 Cations Aqueous Concentration

8. Na

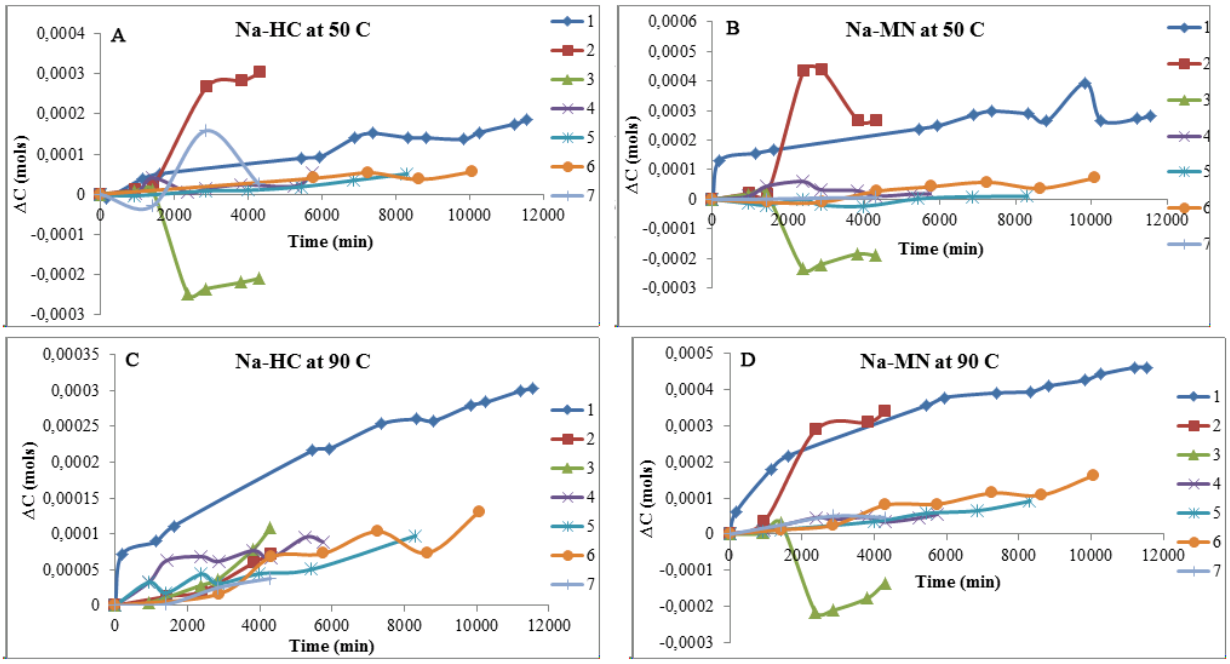

9. K

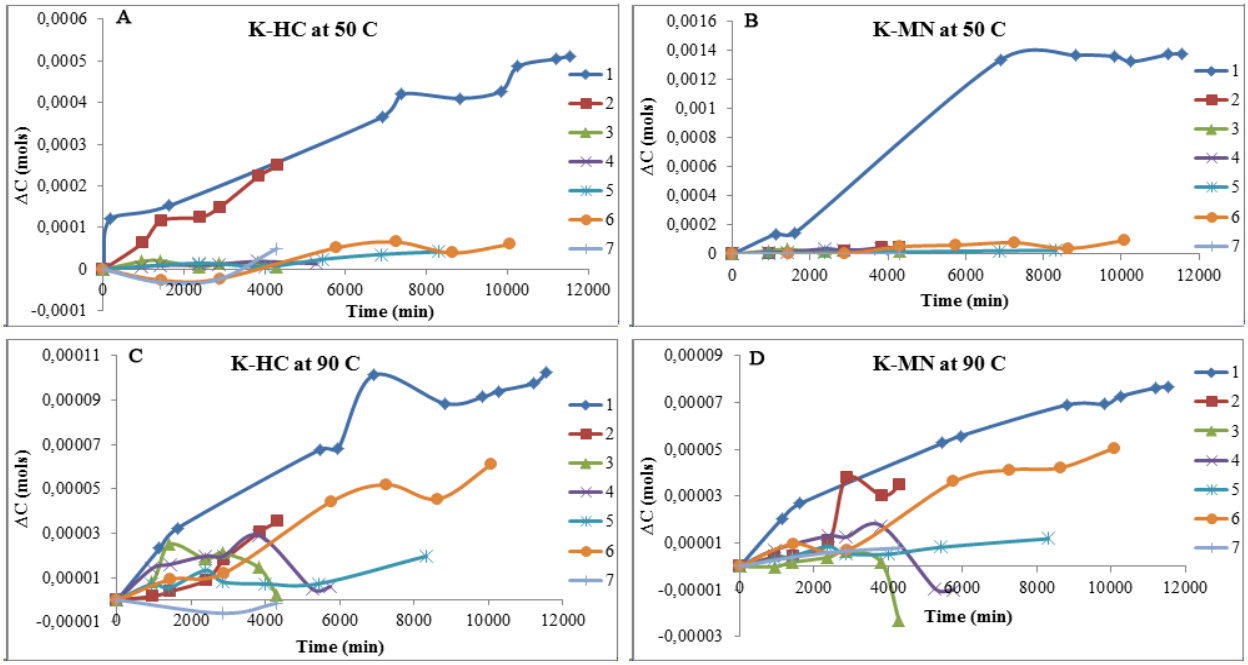

10. Mg

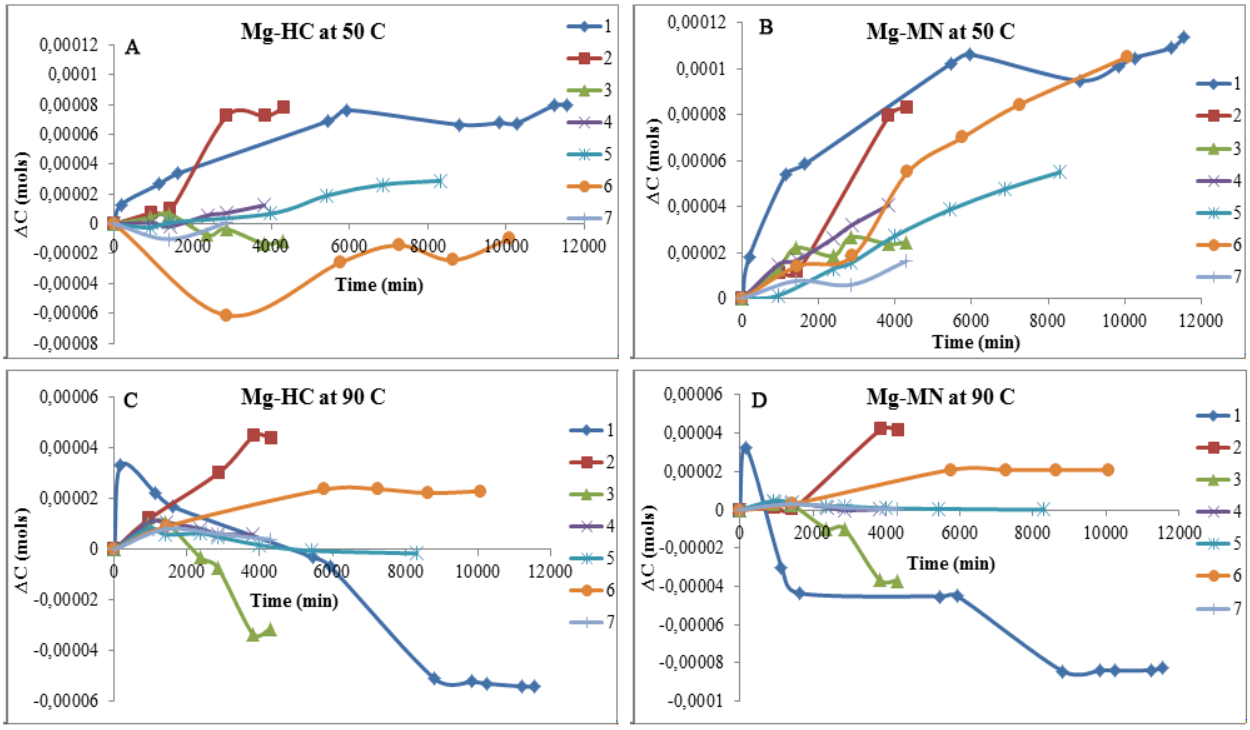
A
Mg-HC at 50 C
B
Mg-MN at 50 C
C
Mg-HC at 90 C
D
Mg-MN at 90 C
ΔC (mols)
Time (min)
1
2
3
4
5
6
7

11. Ca

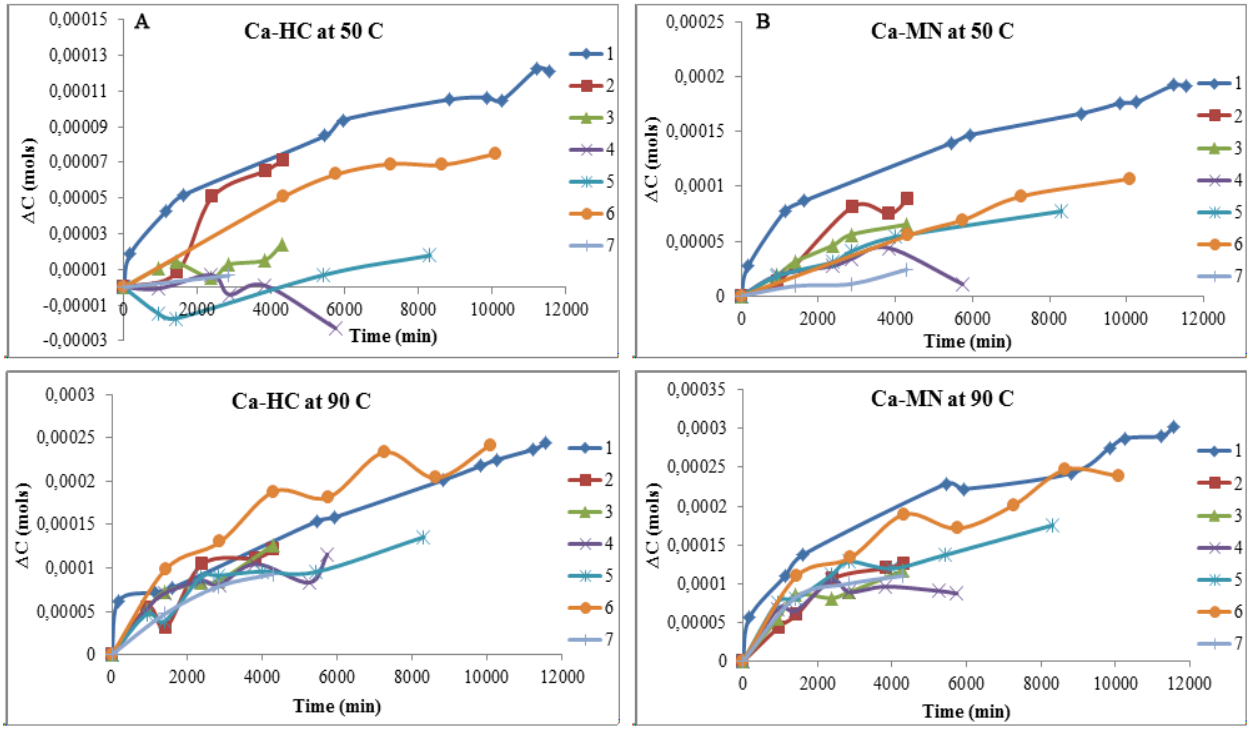
A
Ca-HC at 50 C
B
Ca-MN at 50 C
Ca-HC at 90 C
Ca-MN at 90 C
ΔC (mols)
Time (min)
1
2
3
4
5
6
7

4.2 EDS Analysis

4.4.1.1 Un-reacted Basaltic Glass

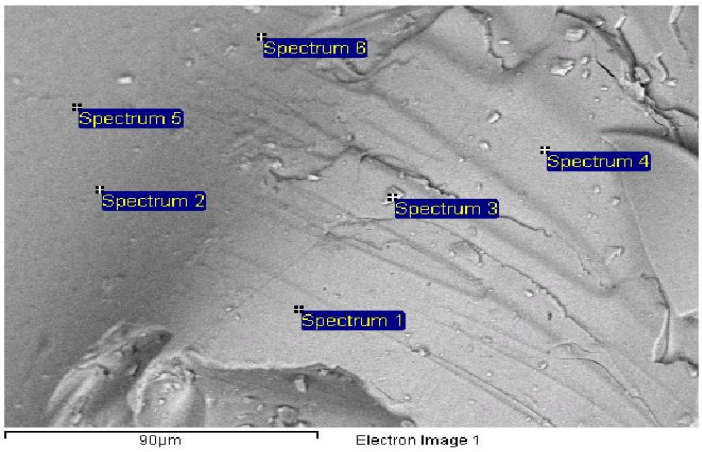

Figure 4.6: Image shows the selection of sites on the unreacted basaltic glass for EDS analysis.

Table 4.1: Element to Si ratios for different EDS spectrums of un-reacted basaltic glass.

	Spectrum 1	**Spectrum 2**	**Spectrum 3**	**Spectrum 4**	**Spectrum 5**	**Spectrum 6**
Si	1,00	1,00	1,00	1,00	1,00	1,00
C	0,48	0,50	0,50	0,56	0,47	0,41
O	0,93	0,63	0,64	0,97	0,83	0,84
Na	0,93	0,63	0,64	0,97	0,83	0,84
Mg	0,15	0,13	0,13	0,13	0,17	0,16
Al	0,27	0,30	0,32	0,29	0,31	0,29
Ca	0,34	0,47	0,53	0,38	0,43	0,40
Ti	0,04	0,04	0,06	0,06	0,06	0,04
Fe	0,38	0,52	0,57	0,42	0,43	0,38

4.4.1.2 Reacted Basaltic Glass

Randomly selected the treated basaltic glass grains from both hand crushed and micronizer crushed samples at 90^{o}C experiment for EDS analysis. Those experiment were conducted at 50^{o}C, was just ignored for the EDS analysis, it is only because of did not seen any phases formation on the grains surfaces (Figures 4.213 and 4.14 in phases identification section).

A. Hand Crushed Basaltic Glass Experiment Conducted at 90°C

a. Hand Crushed grain 1

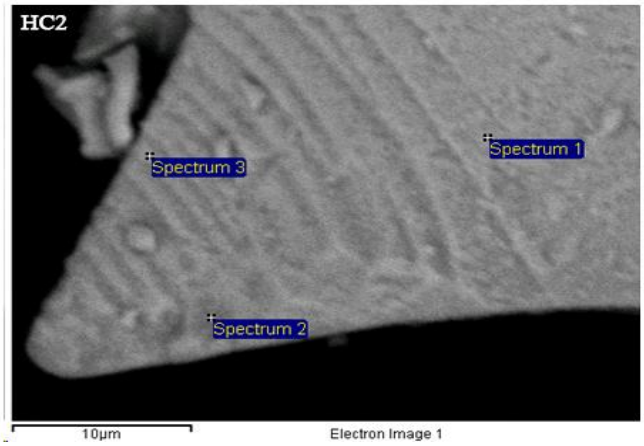

Figure 4.7: Image shows the selected sites for EDS analysis on hand crushed grain 1 treated at 90°C.

Table 4.2: Element to Si ratios of EDS spectrums of reacted hand crushed basaltic glass grain 1 at 90°C.

	Spectrum 1	Spectrum 2	Spectrum 3
Si	1,00	1,00	1,00
C	2,23	2,62	2,47
O	1,08	1,52	1,56
Mg	0,17	0,19	0,18
Al	0,29	0,32	0,30
Ca	0,35	0,37	0,40
Fe	0,38	0,32	0,31

b. Hand Crushed grain 2

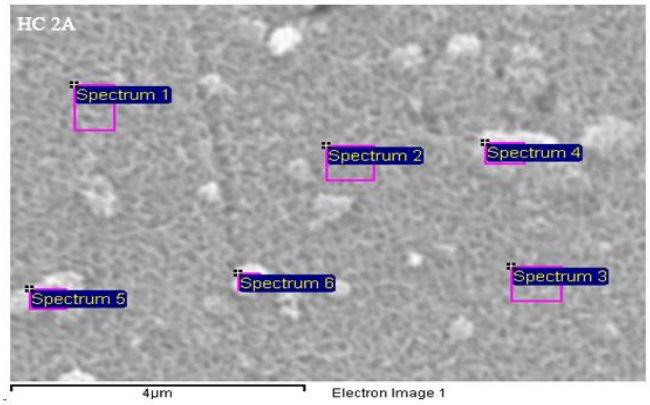

Figure 4.8: Image shows the selected sites for EDS analysis on hand crushed grain 2 treated at 90°C.

Table 4.3: Element to Si ratios of EDS spectrums of reacted hand crushed basaltic glass grain 2 at 90°C.

	Spectrum 1	Spectrum 2	Spectrum 3	Spectrum 4	Spectrum 5	Spectrum 6
Si	1,00	1,00	1,00	1,00	1,00	1,00
C	0,50	1,02	0,57	0,79	0,62	0,70
O	0,27	0,31	0,28	0,53	0,56	0,33

Mg	0,14	0,15	0,14	0,15	0,16	0,13
Al	0,25	0,25	0,29	0,29	0,26	0,22
Ca	0,40	0,39	0,41	0,46	0,45	0,41
Fe	0,55	0,60	0,53	0,32	0,43	0,42

c. Hand Crushed grain 3

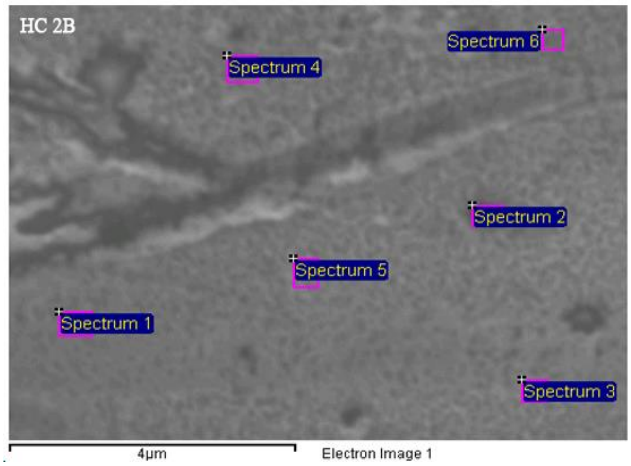

Figure 4.9: Image shows the selected sites for EDS analysis on hand crushed grain 3 treated at 90^{o}C.

Table 4.4: Element to Si ratios of EDS spectrums of reacted hand crushed basaltic glass grain 3 at 90^{o}C.

	Spectrum 1	**Spectrum 2**	**Spectrum 3**	**Spectrum 4**	**Spectrum 5**	**Spectrum 6**
Si	1,00	1,00	1,00	1,00	1,00	1,00
C	0,87	1,05	1,05	0,81	0,86	0,75
O	0,59	0,46	0,39	0,26	0,38	0,32
Mg	0,16	0,10	0,13	0,13	0,14	0,12
Al	0,25	0,30	0,23	0,31	0,25	0,26
Ca	0,44	0,47	0,50	0,56	0,47	0,45
Ti	0,10	0,05	0,07	0,11	0,07	0,03
Fe	0,48	0,60	0,59	0,93	0,52	0,57

B. Micronizer Crushed Basatltic Glass Experiment at 90C

a. Micronizer Crushed grain 1

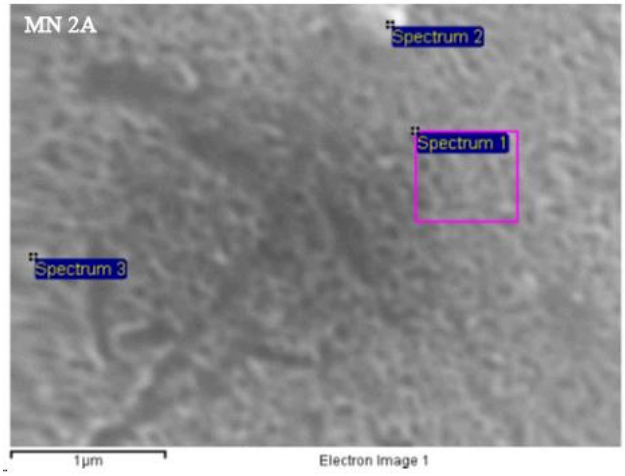

Figure 4.10: Image shows the selected sites for EDS analysis on micronizer crushed grain 1 treated at 90°C.

Table 4.5: Element to Si ratios of EDS spectrums of reacted Micronizer crushed basaltic glass grain 1 at 90°C.

	Spectrum 1	Spectrum 2	Spectrum 3
Si	1,00	1,00	1,00
C	0,35	0,48	0,39
O	0,99	0,98	0,98
Na	0,04	0,05	0,04
Mg	0,18	0,16	0,17
Al	0,27	0,31	0,30
Ca	0,42	0,39	0,47
Ti	0,06	0,04	0,08
Fe	0,38	0,31	0,50

b. Micronizer Crushed grain 2

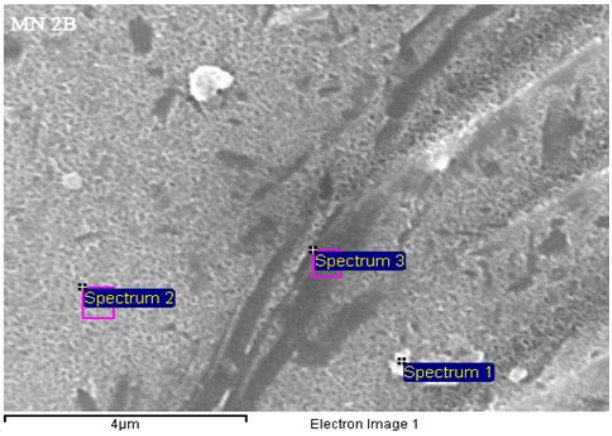

Figure 4.11: Selected sites for EDS analysis on micronizer crush grain 2 treated at 90°C.

Table 4.6: Element to Si ratios of EDS spectrums of reacted Micronizer crushed basaltic glass grain 2 at 90°C.

	Spectrum 1	Spectrum 2	Spectrum 3
Si	1,00	1,00	1,00
C	0,68	0,45	0,51
O	1,08	1,07	1,12
Mg	0,19	0,19	0,18
Al	0,30	0,31	0,28
Ca	0,37	0,38	0,41
Fe	0,42	0,29	0,36

c. Micronizer Crushed grain 3

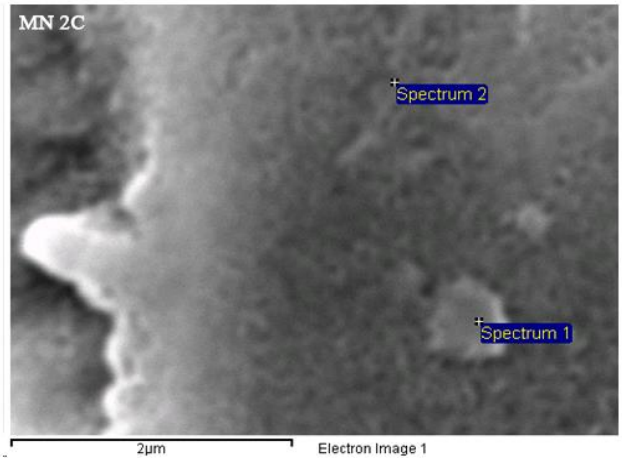

Figure 4.12: Image shows the selected sites for EDS analysis on micronizer crushed grain 3 treated at 90^{o}C.

Table 4.7: Element to Si ratios of EDS spectrums of reacted micronizer crushed basaltic glass grain 3 at 90^{o}C.

	Spectrum 1	**Spectrum 2**
Si	1,00	1,00
C	0,96	0,95
O	1,11	1,24
Na	0,03	0,05
Mg	0,18	0,19
Al	0,31	0,28
Ca	0,38	0,39
Ti	0,05	0,05
Fe	0,35	0,35